ABSTRACT

Title of Dissertation: MICROBIAL-INDUCED CORROSION IN OIL PIPELINES

Azadeh Farzaneh, Doctor of Philosophy, 2020

Dissertation directed by: Professor Mohamad Al-Sheikhly, Department of Materials Science and Engineering

Crude oil pipeline failure due to corrosion processes is a global issue with detrimental effects on the environment and economy. More than 10,000 oil spills occur in the United States alone, each year. These oil spills are so prevalent that they have become the rule rather than being a 1-time incident. Many of these oil spills happen as a result of pipeline failure due to corrosion. Microbial-Induced Corrosion (MIC) accounts for 20% of the total number of pipeline corrosion incidents. Therefore, the mechanisms involved and especially in the case of microbial corrosion must be studied and elucidated.

Sulfate-Reducing Bacteria (SRB) are the main culprits of MIC. The first suggested mechanism in 1930's related high corrosion rates in buried pipelines to SRB hydrogen utilization and depolarization of the cathodic area on the metal surface. Despite its numerous flaws, it remained the most widely accepted mechanism of MIC. In 2004, a new mechanism called direct electron uptake was suggested for MIC. It related corrosivity of bacteria to direct electron uptake from metallic iron. This mechanism is not fully understood hitherto. Only a few bacteria have been isolated so far that demonstrated direct electron uptake capabilities. Most of the research has been focused on these few isolates. However, if direct-electron uptake is the main MIC mechanism, other SRB strains should possess similar capabilities. This work investigated the possibility of direct electron uptake as the main MIC mechanism for SRB D. bastinii, which has not been studied before, and D. vulgaris, an organotrophic SRB. Both are common bacteria existing in crude oil pipelines.

Studies including electrochemical measurements, immersion corrosion testing, metal surface monitoring via scanning electron microscope revealed direct-electron uptake capabilities for both strains. SRB strains were tested under 18 different environmental conditions. Extremely high cathodic current densities were observed in SRB cultures confirming electron transfer from the iron surface to bacteria cells. Finally, based on the large experimental dataset provided in this work, an artificial neural network model was developed to predict MIC. This model demonstrates high correlation coefficients comparable or higher than existing models for general corrosion prediction in the literature.

Revealing the predominant mechanisms of MIC along with modeling capabilities enables us to design appropriate measures to eradicate pipe failure due to MIC. Additionally the investigated direct electron uptake ability of the specific SRB strains studied can be used in microbial fuel cells for enhancing the efficiency of biocathodes.

MICROBIAL-INDUCED CORROSION IN OIL PIPELINES

by

Azadeh Farzaneh

Dissertation submitted to the Faculty of the Graduate School of the
University of Maryland, College Park, in partial fulfillment
of the requirements for the degree of
Doctor of Philosophy
2020

Advisory Committee:
Professor Mohamad Al-Sheikhly, Chair
Professor Lourdes Salamanca-Riba
Professor Sreeramamurthy Ankem
Professor Gary Pertmer
Dr. Joseph Robertson

Dedicated to Parvaneh & Abolhasan, my beloved grandparents.

Acknowledgement

First of all, I want to thank my advisor, Dr. Mohamad Al-Sheikhly, whom without his support this work was not possible. I joined his group from civil engineering department. He continuously supported and encouraged me during these 3 years of my PhD studies. It has been an upheaval path, I had to change my major in midst of my studies, and he strongly supported me and believed in me. His leadership, kind heart, an immense knowledge guided me throughout this whole path. He was so caring for our research group that we always felt like we are part of his family. Our concerns, concerned him, and our achievements made him happy.

I want to thank Dr. Salamanca-Riba, for being part of my committee. I had my first material science course with her. I have learned a lot during her course thanks to her unrivaled teaching and her time devotion to her students.

I want thank my other committee members Dr. Ankem, Dr. Pertmer, and Dr. Robertson.

I want to thank Dr. Josell, who opened the door to interesting world of solid state physics and nanostructure of materials. His lectures were always stimulating and enjoyable.

I want to thank Dr. Kjellerup, who was the inspiration behind this study. I have learned scientific approach, diligence and independent thinking from her. I sometimes had to use the equipment in their lab for culturing my anaerobes. I appreciate her permission to use their lab equipment.

I want to thank Dr. Takeuchi, who is the utmost gentleman, always treated me kindly and patiently resolved all the registration, administration issues during my PhD studies.

I want to thank my lab mate, Dr. Travis Dietz, who always was an exemplary senior for me. I tried to follow his steps and learned a lot from him. I want to thank my other lab

mates who offered sincere friendship throughout these years Dr. Zois Tsinas, Dr. Najlaa Hassan, Kevin Mecadon, Salimeh Gharazi, and Lorelis Gonzalez.

I want thank my very dear friends, Ali Asadabadi, who, his intelligence always amazes me. Who never ever failed to help me, and is an inspiring, extremely kind, super talented human being. I greatly thank my friend, Aref Darzi, who opened the doors to the amazing world of Rumi to me and saved my sanity during dissertation writing. I was always impressed by his intellectuality and domain of knowledge. Thanks to my dear friend Shahrzad Saffari for her unique friendships, for her kind heart, Marjan & Mostafa for their welcoming and warm hearts.

At the end, I want to thank my dear family Behnaz, who battled cancer bravely and it's a shame I wasn't there for her, Forouhar, Arezou, and Farhad.

List of Figures

List of Tables

List of Abbreviation

MIC	Microbial-Induced Corrosion
SRB	Sulfate Reducing Bacteria
FHWA	Federal Highway Administration
GDP	Growth National Income
CS	Carbon Steel
PIG	Pipeline Inspection Gauge
EPS	Extracellular Polymeric Substance
EET	Extracellular Electron Transfer
EMIC	Electrical Microbial-Induced Corrosion
CMIC	Chemical Microbial Induced Corrosion
FAD	Flavin Adenine Dinucleotide
BUG	Benthic Unattended Generators
IRB	Iron-reducing Bacteria
NRB	Nitrate-Reducing Bacteria
ATCC	Amerocan Type Culture Collection
FTIR	Fourier Transform Infrared Spectroscopy
MCT	Mercury Cadmium Telluride
ATR	Attenuated Total Reflectance
ASTM	American Society for Testing and Materials
E_{corr}	Corrosion potential
i_{corr}	Corrosion current density

β_a	Anodic Tafel constant
β_c	Cathodic Tafel constant
LPR	Linear Polarization Resistance
Mpy	Mills per year
SEM	Scanning Electron Microscopy
EDS	Energy Dispersive Spectroscopy
CDP	Cathodic Depolarization
FMN	Flavin Mononucleotide
V	D. Vulgaris
B	D. Bastinii
LF	Lactate-Free
LFR	Lactate-Free plus Riboflavin
Fl_{ox}	Flavoquinone
$Fl^{\cdot-}_{rad}$	Flavosemiquinone Radical
Fl^{2-}_{red}	Flavohyroquinone
DET	Direct Electron Transfers
Ea	Activation Energy
Rp	Polarization Resistance
sulfcons	Sulfate Consumption
MLR	Multivariate Linear Regression
LMLR	Linear Multivariate Linear Regression
Q-Q	Quantile-Quantile
AIK	Akaike Information Criterion
RSS	Residuals Sum Squared
R	Correlation Coefficient

ANN	Artificial Neural Network
SCC	Stress Corrosion Cracking
MLP	Multi-Layer Perceptron
ReLU	Rectifier activation function
MSE	Mean Squared Error
TV	Total Variation
UV	Unexplained Variation
EV	Explained Variation
MAE	Mean Absolute Error
RMSE	Root Mean Squared Error
RMSLE	Root Mean Squared Logarithmic Error

Chapter 1 - Introduction

1.1 Economic importance and possible pathways of Microbial-Induced Corrosion

Corrosion of iron is a pervasive problem across the globe. It costs industry, infrastructure, and manufacturing billions of dollars annually. According to a study by federal highway administration (FHWA), the annual cost of corrosion in U.S. is 3.1% of Gross Domestic Product (GDP) [1].

Corrosion is an electrochemical process that happens in presence of water and oxygen. Cathodic site on iron is oxidized and anodic site is reduced in the presence of an electrolyte. Oxygen and water are the two main components in the corrosion process. However, if oxygen is eliminated this electrochemical process becomes biologically influenced. This type of corrosion is known as microbiologically influenced corrosion (MIC). 20% of the corrosion in metals is due to MIC [2].

MIC is a major concern in oil and gas industry. Carbon steel is the primary material used in oil and gas industry [3]. Carbon steel pipes are vulnerable to different types of corrosion. Koch et al. (2001) estimated the cost of the corrosion in oil and gas industry at $13.4 billion annually, $2 billion of which directly related to MIC [1]. Cost of repair and maintenance of pipelines in the UK in 1956 estimated to be around $20 million and most of it was related to MIC [4]. In 2006 a pipeline failure in Alaska discharged 267,00 gallons into environment. The failure was due to MIC.

In order to facilitate oil extraction and maintain high pressure, water is added into the pipeline stream. Sometimes more than 25% water is added to maintain the pressure. This water is

deoxygenated to reduce electrochemical corrosion inside the pipelines. Water can be supplied from three different sources; fresh aquifer, seawater, and recovered water from oil that can be reused. In some areas seawater is injected into pipelines due to scarcity of fresh water. This water is the source for sulfur and microorganisms like Sulfate Reducing Bacteria (SRB). Sulfate reducing bacteria are known to be the main culprits of MIC [5][6].

SRB are obligate anaerobic bacteria that are ubiquitous in the environment. They can grow in a variety of niches. Inside the pipelines, due to harsh environment, they form biofilm for survival. Once SRB is established in the pipeline and biofilm is formed, it is very hard to remove them. The Interactions of SRB and resulting biofilm with surfaces of metal induces local the corrosion in the form of pitting. These microorganisms induce corrosion through direct and indirect mechanisms. As an indirect mechanism, H_2S is produced as a result of bacterial metabolism. H_2S is a very corrosive agent. Several direct mechanisms are suggested in the literature for Sulfate reducers. The first suggested mechanism in 1930's related high corrosion rates in buried pipelines to bacterial hydrogen utilization and depolarization of the cathodic area on metal surface. This theory debut many controversies. The experimental data did not confirm the proposed chemical reactions. In 2004, a new mechanism was proposed. It related corrosivity of bacteria to direct electron uptake from metallic iron. In the meanwhile, other mechanisms were suggested for MIC including: catalytic effect of FeS layer, corrosive phosphorous compounds production by SRB, interactions of biofilm and metallic surface, etc. Experimental evidence for direct electron transfer has been recently introduce for one SRB species and a methanogenic archaea. This mechanism is not fully understood hitherto. Only a few isolates have been found so far that demonstrate direct electron uptake capabilities. Most of the research has been done on these few isolates.

There are several preventative (e.g. coating) or remedial (e.g. Pipeline Inspection Gauge (pigs), biocides) approaches for MIC, however there are limits to their effectiveness. Biocides cannot penetrate and remove the biofilms. Physical approaches like cleaning pigs are very

expensive since a whole section of the pipe should be shut down to run the pig, which stops the production for couple of hours. Coating is another approach, which is not feasible to apply inside the pipelines, besides any delamination and deficiency in the coating increases the potential difference and exacerbates corrosion. MIC is generally localized and hard to monitor, thus it is important that preventive measures are taken to reduce the risks. In this study we inspect MIC mechanism to provide a better understanding of this phenomena.

Two SRB strains, D.bastinii and D. vulgaris, have been studied in this PhD work. It should be noted that D.bastinii had not been studied before at all. Also, D. vulgaris had not been investigated for direct- electron uptake based MIC mechanism. Dinh et al. first provided the experimental proof of this mechanism in 2004 [27]. Since then, researchers tried to follow similar approaches of Dinh et al. in order to isolate strains with similar capabilities [32][31][7]. Other researchers tried to re-investigate the same strains that Dinh et al used, in order to further comprehend the newly proposed MIC pathway of direct electron mechanisms [19, 28, 29, 34]. However, this new mechanism was not investigated for formerly known SRB species found in oil pipelines. There was only one study, however, showed that Desulfovibrio vulgaris survived for more than 43 days under organic electron donor starvation [3]. In other words, in the absence of the organic electron donors, these bacteria survived through utilizing electrons from the Fe. Those authors of this paper suggested that the bacteria survived through iron's utilization as an electron source. However evidence of direct electron uptake by the bacteria was not provided in this study. In this PhD work, D. bastinii, a corrosive SRB isolated from oil pipelines, was cultured and the corrosion process and its results were studied to further investigate the direct electron uptake process for SRB. Also, in this PhD work, the role of Strain D. vulgaris in the corrosion processes, was investigated with electrochemical techniques.

Finally, there has been no work focused on building models for MIC and the models generated in this work can both help in gaining a better understanding of the mechanism and its contributing factors and provide a guidance for preventative measures.

1.2 Objective

This PhD work aims to investigate the possibility of the direct electron uptake as the main MIC mechanism for SRB, D. bastinii and D. vulgaris. The mechanism and the corrosion rate of carbon steel coupons were investigated in the presence and absence of organic electron donors. In all experiments in this work, carbon steel coupons were exposed to SRB cells in aqueous media. Bacterial metabolism was monitored by measurements of sulfate consumption in the cultures. Corrosion products were analyzed using FTIR. Electrochemical experiments including linear polarization, potentiodynamic scan, corrosion potential monitoring were performed to elucidate the electron transfer mechanism, and the reactions that take place on the surface of CS coupons. Finally, data obtained from the experiments was analyzed and used to build predictive model(s) of MIC.

The main focus of this dissertation is twofold. First, is to elucidate the theory of direct electron uptake as the main mechanism for bacterial-induced corrosion of D. batinii and D. vulgaris. Second, data collected from corrosion experiments were analyzed and appropriate predictive model(s) has been developed to predict MIC rates based on various influencing parameters such as temperature, exposure time, sulfate consumption rate, pH, media type, and bacteria type.

Numerous microorganisms are involved in MIC. Studying all these microorganisms is out of scope of a single PhD dissertation. Thus, two sulfate reducing species, D. bastinii and D. vulgaris, that are notorious for inducing corrosion, especially in oil and gas industry, are selected. Also, these bacteria are the best candidates to complete one of the main focuses of this research, which is to study MIC mechanisms and in particular, the newest discovered process of direct electron update.

Furthermore, the controlled influencing parameters (e.g. sulfate consumption rate, pH, H_2S accumulation, etc.) are logged as inputs and the results of the corrosion process (e.g.

corrosion rate) are collected as outputs. These data were analyzed for correlation patterns and predictive (machine learning) models were developed to model the data.

This dissertation aimed at studying direct electron uptake mechanism in corrosion and developing MIC predictive models and will provide answers to the following important questions:

1. Can D. bastinii & D. vulgaris demonstrate direct electron uptake capabilities?
2. Can D. bastinii survive organic electron donor starvation in the media?
3. Can electrochemical techniques provide proof of direct-electron uptake by D. vulgaris and D. bastinii?
4. Can a pattern be devised based on environmental conditions to predict MIC?

1.3 Approach

In order to effectively prevent MIC from taking place, its mechanisms should be elucidated. This thesis aims to provide deeper explanation for MIC mechanisms. Hence, microbial iron corrosion was investigated through monitoring bacterial activities, and performing real-time analysis. The approach of this PhD work can be outlined as follows:

1. Evaluating corrosion rate by mass loss and electrochemical techniques
2. Analyzing corrosion products by FTIR
3. Applying electrochemical tests for experimental proof of direct-electron uptake
4. Monitoring microbial activity by measuring the decrease of sulfate content as a function of time and temperature
5. Correlating corrosion rate with bacterial activity under various physical and chemical experimental conditions.
6. Developing a regression model based on the experimental results
7. Developing a neural network model based on the experimental results

Chapter 2 - Literature Review

2.1 - Abiotic metal corrosion

Corrosion is defined as deterioration of metal due to its interaction with the environment [8]. In the absence of moisture or an electrolyte, metal stays stable infinitely. However, when it comes in contact with moisture, charge-transfer reactions lead to metal instability [9]. Therefore abiotic corrosion is an electrochemical process. Electrons flow from anodic sites to cathodic sites. Presence of an aqueous solution (electrolyte) is needed to carry electrons. Hence, the anodic current produced due to the electron transfer is equivalent to the corrosion rate [10]. Therefore, corrosion happens at the interface of metal and electrolyte.

The corrosion process can be initiated with an electrochemical cell, where oxidation happens at the anodic site and reduction happens at the cathodic site. Cathodic reaction depends on two main factors; (1) the dissolved oxygen content and (2) the pH of the solution. Cathodic reaction can happen through Eq. 2.2 and Eq. 2.3 [11]. In absence of oxygen and in an acidic solution, due to proton availability, Eq. 2.4 is the overall reaction. At high oxygen partial pressure and neutral pH, Eq. 2.5 is the overall reaction.

As long as anodic and cathodic sites are close, they can switch interchangeably due to variation in ion contents, diffusion of various compounds, etc. This variation leads to a uniform corrosion. Otherwise localized corrosion happens.

$Fe \rightarrow Fe^{2+} + 2e$ (Anodic Reaction) **Eq. 2.1**

$2H^+ + 2e \rightarrow H_2$ **Eq. 2.2**

$\frac{1}{2}O_2 + 2H^+ + 2e \rightarrow H_2O$ **Eq. 2.3**

$Fe + 2H^+ \rightarrow Fe^{2+} + H_2$ **Eq. 2.4**

$Fe + \frac{1}{2}O_2 + 2H^+ \rightarrow Fe^{2+} + H_2O$ **Eq. 2.5**

2.2 - Aerobic Microbial Corrosion

Microbial corrosion under aerobic conditions, is a combination of chemical and microbial processes. It should be noted that during aerobic microbial corrosion, the whole process is not completely aerobic. Oxygen is limited in depth of the aerobic biofilm. This limitation on oxygen diffusion in the structure of the biofilm, provides the niche for anaerobic microbes to flourish and contribute to corrosion process along with aerobic bacteria. The aerobic biofilm also induces corrosion.

Pseudomonas species are highly associated with aerobic corrosion. These species are slime-forming bacteria and they are prevalent in seawater [12]. Pseudomonas quickly colonize on the surface of the metal and form a biofilm. Differential oxygen concentration cells are formed due to metabolic activity of microorganisms in the biofilm. These concentration cells obliterate the passive film on the surface of the metal and induce pitting and crevice corrosions [13]. These differential concentration cells can also lead to the formation of tubercles on the surface of the metal [14]. According to suggested mechanism for this process, oxygen deficient areas become anodic sites where iron dissolution happens (Anodic reaction Eq. 2.6). Electrons released from anodic reaction react with oxygen and water and form hydroxyl anions (Cathodic reaction Eq. 2.7). This reaction induces localize pH increase. As a result of this pH increase, Fe^{2+} ions precipitate in the form of iron hydroxide (Tubercle formation Eq. 2.8) [14] [15]. These iron hydroxide form a prominence on the surface of the metal. Schematic of this process is depicted in Figure 2.1. It can be visualized in this figure that anodic reaction happens inside the tubercle while cathodic reaction occurs outside the tubercle. In other words, in this process anodic site is surrounded by cathodic sites. Released iron ions from anodic reaction precipitate due to pH increase in anodic sites.

$$Fe \rightarrow Fe^{2+} + 2e$$ **Anodic reaction** Eq. 2.6

$$O_2 + 2H_2O + 4e \rightarrow 4OH^-$$ **Cathodic reaction** Eq. 2.7

$$2Fe^{2+} + \frac{1}{2}O_2 + 5H_2O \rightarrow 2Fe(OH)_3 + 4H^+$$ **Tubercle formation** Eq. 2.8

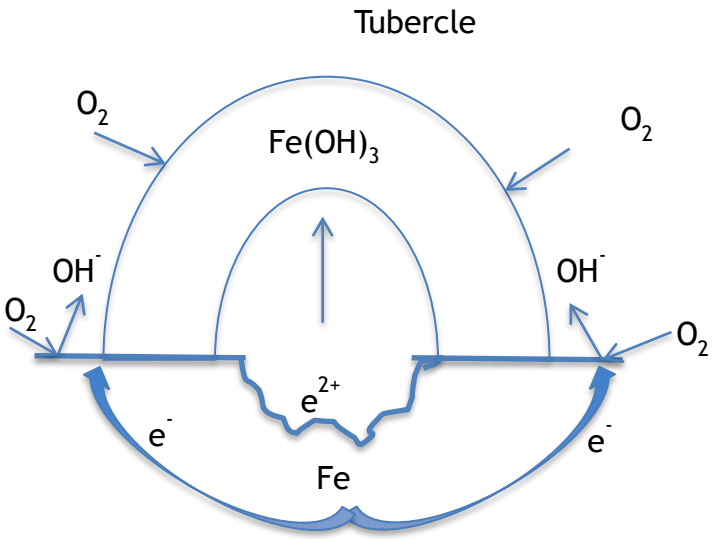

Figure 2.1-Differential aeration cell formed by oxygen depletion under a microbial film

Another group of aerobic bacteria induces corrosion by acid production. Prominent members of this group is genus Thiobacillus. These species oxidize thiosulfate and elemental sulfur leading to the production of sulfuric acid [16]. The produced H_2SO_4 as a result of Thiobacillus activity, plays an important role in carbon steel and concrete corrosion [17]. Their coexistence with SRB can exacerbate MIC. They can also generate sulfate species required for SRB metabolism (Eq. 2.9) [17]. Figure 2.2 represents suggested mechanism in the literature on how sulfide-oxidizers and sulfate-reducers induce corrosion. According to this figure, Thiobacillus ferrooxidans (a common representative of genus Thiobacillus) oxidizes the iron sulfides (formed due to SRB metabolic activity) in presence of oxygen as terminal electron acceptor and generates energy and releases acid and sulfate species. Symbiotic coexistence of SRB and sulfide-oxidizing bacteria exacerbates MIC in this way according to Figure 2.2: Sulfurization of metal happens due to reaction of H_2S, produced by SRB, and metal. Formation of FeS_x layer is exothermic and chemical energy is stored in the iron sulfide layer. Thiobacili

then utilize this energy and provide organic chemical energy by secreting an organic layer. This organic layer contains polysaccharides, phospholipid, and other compounds. This organic energy can be used by SRB to again produce more H_2S and continue the cycle. Thiobacili can also use Fe^{2+} as an energy source near the surface and transfer the electrons to oxygen. As another parallel reaction thiobacili produces sulfate ions by oxidizing the iron sulfide layer.

$$FeS_2 + 15O_2 + 2H_2O \rightarrow 2Fe_2(SO_4)_3 + 2H_2SO_4 \qquad \text{Eq. 2.9}$$

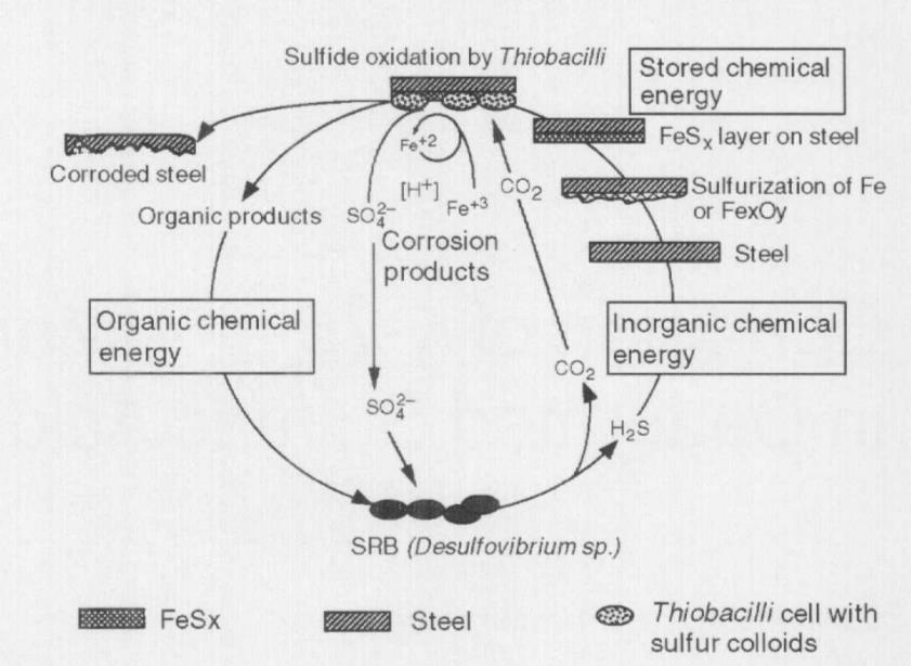

Figure 2.2- SRB and Thiobacilli MIC cycle suggested by [17].

Another aerobic group of bacteria contributing to MIC is iron bacteria. Iron bacteria are aerobic microorganisms that oxidize ferrous ions through their metabolic activity [18][19]. This, results in extracellular deposition of ferric hydroxide. Iron bacteria induce corrosion through crevice corrosion mechanism [20]. They partition metal surface into multiple small oxygen-free zones (anodic sites) surrounded by cathodic sites [21]. This pathway is similar to tubercle formation on the surface of metal. Iron bacteria form differential oxygen concentration cells and induce corrosion. Subsequently, the produced amorphous iron hydroxides deposited on the surface also impede the penetration of biocides in the carbon steel crude oil pipelines and let the

corrosion process to carry on [22]. This form of corrosion frequently happens at oil refineries, especially in reservoirs where there is access to oxygen [23]. Genus Gallionella is one of the widely studied iron bacteria in corrosion area[24].

Fungi are amongst other microorganisms that their activity can induce corrosion. Fungi produce organic acids like citric acid and oxalic acid [25]. These acids dissolve iron and magnesium ions and promote corrosion. Aspergillus and Penicillium are amongst fungi species that induce MIC in presence of hydrocarbons due to their carbon-assimilating capabilities [26]. Besides fungi, many microbial genera biodegrade hydrocarbons. Decomposition of hydrocarbon requires molecular oxygen. Therefore, most of hydrocarbon-utilizer microbes are aerobes [27]. Fungi are extremely desiccant-resistant, so they can survive arid conditions by forming spores and start growing as soon as water is available [27].

Algae can also induce corrosion in oxic environments. They are photosynthetic organisms. These organisms produce oxygen during the day and consume it during the night. This cycle can trigger formation of regions with different oxygen concentrations and enhance corrosion [28].

Algae also enhance MIC by secretion of organic acids like glycolic acid [29]. This acid secretion depends on oxygen availability, light absorption, and presence of biocarbonate anions. Acid production also decrease pH and promote further iron dissolution, since algae photosynthesis requires sunlight, this type of corrosion does not occur in light lacking environments.

2.3 - Anaerobic microbial corrosion

Sulfate-reducing bacteria are known to play the central role in anaerobic microbial corrosion [5]. Other anaerobic microorganism also part in inducing corrosion either by their metabolic activity or by curating suitable conditions for SRB to thrive. Pitting corrosion is characteristic of SRB-induced corrosion on steels [5]. SRB even contribute to aerobic corrosion

by germinating under deposits and debris, tubercles, or slimes where oxygen is consumed by other microorganisms like iron-oxidizing bacteria. SRB have been subject of study over the last centaury, however their corrosion inducing mechanisms are not fully understood.

2.4 - Anaerobic corrosion by SRB

2.4.1 What are SRB?

SRB are ubiquitous in marine and terrestrial environments that contain SO_4^{2-}. They are typically abundant in subsurface seawater and sediments that lack oxygen and are high in sulfate concentration (28 mM in seawater) [30]. SRB can gain energy either by oxidizing organic compounds or SO_4^{2-} reduction with H_2 (dissimilatory sulfate reduction). Lactate and pyruvate are common electron donors for the species.

SRB are strict anaerobes, although some sulfate reducers may tolerate oxygen at very low concentration. SRB are categorized into four phylogenic groups based on analysis of 16S rRNA gene sequence: Gram-negative mesophilic SRB, Gram-positive spore forming SRB, thermophilic bacterial SRB, and thermophilic archaeal SRB [31]. The mesophilic SRB are the largest and most studied group having 20 genera including Desulfuvibrio, desulfobacterium, desulfobacter, etc. Desulfotomaculum is the dominant genus in gram-positive spore forming SRB [31]. Due to their spore forming ability, they can survive longer in the presence of oxygen. Thermophilic SRB are generally thriving in temperatures higher than 60°C. Two well-known species in this group are Thermodesulfobacterium commune and Thermodesulfovibrio yellowstonii [32].

2.4.2 Hydrogenase in SRB

Sulfate reducers, especially Desulfovibrio species, have the ability to utilize H_2. Enzyme hydrogenase is responsible for the metabolism of molecular hydrogen following the reaction [33]:

$$H_2 \rightleftharpoons 2H^+ + 2e^-$$

This enzyme is found in many microorganisms like methanogenic archaea, nitrogen-fixing bacteria, sulfate-reducing bacteria. There are three different metal containing hydrogenases associated to SRB: Fe, NiFe and NiFeSe [34]. FeNi hydrogenase found to be more prevalent than the other two in SRB [35]. This enzyme is mostly present peripheral membrane than the membrane. In dissimilatory sulfate reduction, molecular hydrogen is oxidized by hydrogenase in the periplasm. Obtained electrons are transported via cytochrome c_3, a periplasmic low potential cytochrome, to the cytoplasmic membrane where sulfate reduction happens (Figure 2.3) [36][37]. The reductases in the cytoplasm facilitate sulfate reduction reaction in the cell. This process can be summarized in the following reaction:

$$4H_2 + SO_4^{2-} + 2H^+ \longrightarrow H_2S + 4H_2O$$

H_2 can also be produced as a result of catabolism in cytoplasm. This can be due to presence of hydrogenases in the cytoplasm.

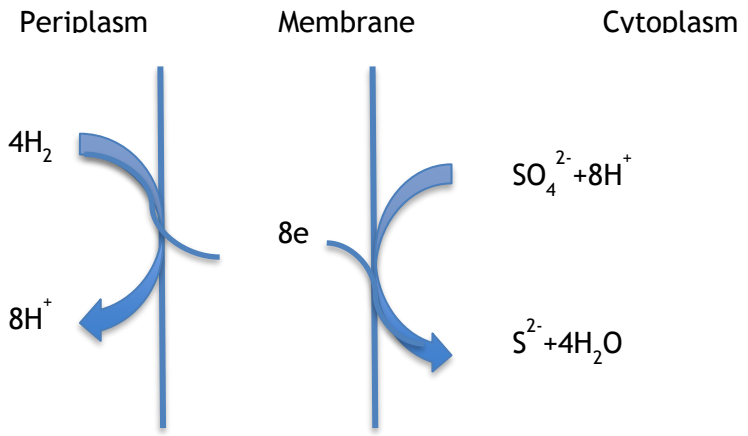

Figure 2.3- vectorial electron transport in dissimilatory sulfate reduction in Desulfovibrio [Badzjong & Thauer, 1980)

2.4.3 MIC mechanisms by SRB

2.4.3.1 Cathodic Depolarization:

Evidence of biological corrosion was first observed by Gaines in 1910. He observed high sulfur content and organic matter in the rusts collected from steel conduits [38]. He related the underground corrosion and rapid destruction of buried iron structure to carbon/sulphur fixing

activities of bacteria. It was not until 1934 that Wolzogen Kuhr & van der Vlugt identified the SRB as the main players in buried pipeline corrosion. They proposed the classical theory or the cathodic depolarization [39]. According to their theory, hydrogen depolarizes the cathode (cathodic polarization) based on Eq. 2.10 & Eq. 2.11. This hydrogen formation on the surface of the metal reduces the potential difference between anode and cathode and impedes corrosion. In an aerobic corrosion the atomic oxygen O acts as a depolarizer and breaks this film ($2H + O \rightarrow H_2O$). In anaerobic solution, sulfate oxygen from biogenic sulfate reduction plays the role of O in aerobic conditions (Eq. 2.12). This theory has several debatable issues. First, hydrogen reduction is the rate-limiting reaction and hydrogen desorption does not affect the kinetics of hydrogen evolution. Second, the ratio of iron to iron sulfide should be 4:1 according to the overall reaction. However, the ratio was close to 1 in the experiments. Several studies confirmed the classical theory with electrochemical techniques during the 1960s [40][41]. However, the common mistake in these studies was the presence of organic electron donor besides iron. Lactate and H_2 can both be electron donors for SRB, besides lactate consumption induces more chemical corrosion due to the presence of sulfides [42]. The classical theory had a lithotrophy-based concept [43]. Costello in his experiments showed that acceleration of cathodic reaction in presence of SRB is more likely due to the presence of sulfide species rather than hydrogen utilization of the bacteria [44]. He mainly related the corrosiveness of SRB to the formation of H_2S. In a similar study, hydrogen-grown SRB used to investigate their ability of cathodic depolarization. Polarization curves showed depolarization of the cathode after introduction of the SRB. However, the results were inconclusive to determine what fraction of hydrogen utilization is due to SRB and what fraction is due to the presence of sulfides [45].

$$2H_2O \rightarrow 2H^{\cdot} + 2OH' \qquad \text{Eq. 2.10}$$

$$Fe + 2H^{\cdot} \rightarrow Fe^{\cdot\cdot} + 2H \qquad \text{Eq. 2.11}$$

$$H_2SO_4 + 8H \rightarrow H_2S + 4H_2O \qquad \text{Eq. 2.12}$$

$$Fe^{\cdot\cdot} + 6(OH)' \rightarrow \ 3Fe(OH)_2$$ Eq. 2.13

Overall reaction: Eq. 2.14

$$4Fe + H_2SO_4 + 2H_2O \rightarrow 3Fe(OH)_2 + FeS$$

2.4.3.2 Effect of biogenic sulfides:

Several H_2S mechanisms have been suggested in the literature. Corrosion mechanism by abiotic H_2S is different from biogenic H_2S. Abiotic H_2S provides protons for the cathodic reaction and accelerates corrosion process. However, biologically produced H_2S does not contribute to acidity of the solution. On the contrary, it increases the pH. SRB does not produce H_2S directly. They produce HS^- through their sulfate respiration. This HS^- combines with the protons in the solution, which leads to the increase of the pH [46]. The distribution of abiotic and biogenic H_2S is also different in the aqueous solutions. Concentration of bacterial cells in the biofilm on the surface is much higher than planktonic cells. Thus, concentration of biogenic H_2S is much higher on the surface of the coupon. While, in abiotic, H_2S is distributed in the bulk solution.

H_2S is a strong cathodic reactant. It reacts with metallic iron rapidly and produces FeS ($H_2S + Fe \rightarrow FeS + H_2$, ΔG°= -72.5 kJ (mol Fe^0)$^{-1}$) . This reaction is thermodynamically more favorable than H_2O reaction with water:

$$H_2O + Fe^0 \rightarrow H_2 + FeO \qquad \Delta G^0 = \text{-}14.3$$ Eq. 2.15

kJ/mol Fe

$$H_2O + Fe^0 \rightarrow H_2 + Fe(OH)_2 \quad \Delta G^0 = \text{-}15.6$$ Eq. 2.16

kJ/mol Fe

2.4.3.3 Effect of Biofilm:

There is no doubt in the detrimental effect of biofilm on corrosion. Biofilms are comprised of cells, metabolites, extracellular polymeric substance (EPS), and other dissolved ions

and substances. EPS is a matrix of polysaccharides, proteins, and nucleic acids [37]. Conditions under the biofilm differ from the bulk. This includes formation of concentration cells, localized low pH areas, and trapped bacterial metabolites. This localization induces different potential cells and induce pitting corrosion. EPS produced by SRB can also be corrosive by itself without cells being present [47]. Chan et al. (2002) suggested EPS binding to metal ions could be the preliminary mechanism of enhanced corrosion by biofilm.

2.4.3.4 Effect of Corrosive Metabolites:

Another MIC mechanism is the corrosive metabolites. This indirect mechanism can induce pH reduction by bacteria's metabolite. It can also lead to creation of different concentration cells on the surface of the metal, affecting the protective film on metal surface. For instance, Acid Producing Bacteria (APB) secrete organic acid during fermentation that contributes to the corrosion [48]. For instance, Thiobacillus is a genus of bacteria that form sulfuric acid by oxidizing sulfur species [49]. MIC happens in a consortium of bacteria. Thus, the interactions of bacteria, for instance SRB and APB, may influence the corrosion process.

2.4.3.5 Direct Electron Uptake:

Direct uptake of electron from metal is another mechanism that can explain high corrosion rates in the presence of bacteria and has been the center of attention in the last decade. Dinh et al. (2004) were the first researchers providing experimental evidence for this mechanism [50]. They isolated new marine SRB strains that possessed extracellular electron transfer (EET) ability. This mechanism is known as electrical microbiologically influenced corrosion (EMIC) [51]. In this mechanism, SRB takes up electron directly or indirectly from metallic iron. The direct process can be through proteins in the outer membrane or filaments, while the indirect mechanism is through mediator compounds [52]. Mediators can be exogenous or endogenous. Zhang et al. (2015) investigated the indirect mechanism by addition of riboflavin and FAD (flavin adenine dinucleotide) as electron mediators in the solution [53]. They used non-hydrogen

utilizing bacteria and inspected high corrosion rates in presence of electron mediators. In another study, one SRB strain and one H_2-scavenging strain were grown in lithotrophic conditions, and it was shown that the latter strain did not induce corrosion in spite of its hydrogen consumption [42]. So far, a few strains were identified by scientists with capability of direct electron uptake from metallic iron [51][54][55]. Thus, more studies are necessary to shed light on this peculiar capability of SRB.

Metallic iron is a recent form of iron on earth from evolution standpoint. That's why SRB capability to corrode and destruct metallic iron is unanticipated. This trait can originate from the corroding anthropological metals [51]. It can also originates from the interaction of bacteria by which they exchange electrons by means of metabolites [56]. This trait of microorganism is of high importance in biogeoelectrical areas to develop fuel cells. Benthic unattended generators (BUG) are one of the latest discoveries in microbial fuel cell area. BUGs work based on direct electron transfer between microbes and metal. Thus they can be placed in remote locations like bottom of the ocean, buried in sediments to generate eco-friendly power [56].

In summary, MIC is a complex process involving different groups of bacteria. MIC can be a combination of chemically microbial induced corrosion (CMIC) and EMIC. For instance if the corrosion is merely chemical, exclusion of organic nutrients can solve the problem, however if it is EMIC, this solution does not work since the bacteria can obtain their nutrient from metallic iron. Determining to what degree each mechanism is responsible helps applying right techniques to prevent it.

2.5 - Anaerobic corrosion by methanogenic archaea

Methanogens (methanogenic archaea) produce methane as part of their metabolic activity. The main methanogenesis pathway is the reduction of CO_2 in presence of H_2 as electron donor (Eq. 2.17). They are physiologically obligate anaerobes. They inhabit in anoxic sediments, lakes, paddy fields, animal digestion system, sewages, etc. Methanogens are divided into three

groups based on the substrate they utilize to produce methane. These three substrates are; CO_2-type substrates, methylated, and acetotrophic substrates [37]. CO_2-type substrates include CO_2, formate ($HCOO^-$) and CO. Methanogens utilizing these substrates are called hydrogenotrophic. They combine with H_2 or other alcohols to form CH_4. Methylated substrates include methanol (CH_3OH), methylamine ($CH_3NH_3^+$), dimethylamine ($(CH_3)_2NH_2^+$), trimethylamine ($(CH_3)_3NH^+$), .methylmercaptan (CH_3SH), and dimethylsulfide ($(CH_3)_2S$). Methanogens producing methane by consuming these substrates are called methylotrophic. Methanol reduction reaction by methylotrphs is presented in Eq. 2.18. And finally acetotrophic substrates include acetate (CH_3COO^-) and pyruvate (CH_3COCOO^-) [37]. Utilizers of these compounds are called acetotrophic. The reaction leading to methane formation from acetate is presented in Eq. 2.19.

$$4H_2 + CO_2 \rightarrow CH_4 + H_2O \quad \text{Eq. 2.17}$$

$$CH_3OH + H_2 \rightarrow CH_4 + H_2O \quad \text{Eq. 2.18}$$

$$CH_3COO^- + H^+ \rightarrow CO_2 + CH_4 \quad \text{Eq. 2.19}$$

It has been believed for a long time that MIC is linked to the activity of hydrogenotrophic bacteria. It was mentioned earlier that according to the cathodic depolarization theory, hydrogen utilization happens at cathode by bacteria to accelerate corrosion. All methanogenesis pathways, as mentioned in previous section, can proceed by methanogens hydrogen utilization. However it was shown that hydrogen desorption on the surface of the metal is not the rate-limiting reaction in MIC [57]. In another study, it was demonstrated that hydrogen utilization of a hydrogenotrophic methanogen does not induce iron reduction [58]. Therefore biogenic hydrogen-utilization cannot be a potential methanogenic-induced corrosion pathway.

By isolation of a new methanogen strain in less than 2 decades ago, it was demonstrated that this strain can use steel as the sole electron donor [50]. After this pioneering study, this capability was confirmed by other researchers [7, 54, 59, 60]. Therefore, methanogens can induce MIC by direct electron uptake from the metal. Uchimaya et al. (2010) showed iron-corroding ability in a novel methanogen isolated from crude oil storage sludge. This strain was cultured

with iron as the only electron donor. Observed growth rate and iron dissolution rate in the cultures supported direct electron uptake in methanogen-mediated corrosion [54].

Methanogens can contribute to MIC indirectly. SRB can live syntrophically with methanogens, i.e. they can use SRB metabolites as energy source [61]. Therefore they provide a more suitable environment for SRB to grow by consuming SRB harmful metabolites like HS^{-}.

2.6 - Anaerobic corrosion by acetogenic bacteria

Acetogens are strictly anaerobic bacteria. The main product of their metabolism is acetate. They reduce CO_2 to acetate via acetyl-CoA pathway [37]. According to this pathway CO_2 is reduced in two different ways. It is reduced to carbonyl group, and methyl group of acetate. These two, combine to form acetyl-CoA [37]. The overall reaction is shown in Eq. 2.20.

$$4H_2 + H^+ + 2HCO_3^- \rightarrow CH_3COO^- + 4H_2O \qquad \text{Eq. 2.20}$$

Participation of acetogens in MIC has not been under scrutiny until Mand et al. (2014) suggested acetogens can incur MIC by catalyzing the reaction in Eq. 2.21 [62]. Possibility of MIC by acetogens was earlier suggested, however no evidence was provided [63]. In a more recent study, a newly isolated acetogen demonstrated acetogenesis-dependent MIC through direct electron uptake from Fe^0 [55]. The acetogenic culture in this study showed significantly higher corrosion rate than abiotic system in presence of Fe^0 as the sole electron donor.

$$4Fe^0 + 6HCO_3^- + 5H^+ \rightarrow CH_3COO^- + 4FeCO_3 + 4H_2O \qquad \text{Eq. 2.21}$$

Acetogens can also induce MIC indirectly. Acetate can be used by SRB as an energy source. Therefore, acetogenesis can provide the substrate for SRB to grow on. Acetate is also a carbon source for hydrogenotrphic methanogens. In nutrient-deficient environments acetogens come into play and provide acetate by transforming bicarbonate to acetate. It was shown that co-cultures of D. vulgaris and Acetobacterium woodii are more corrosive than the single culture of each [62]. Inducing MIC through symbiotic relationship of SRB and acetogens were formerly shown [64][65].

2.7 - Anaerobic corrosion by iron-reducing bacteria

Iron-reducing bacteria (IRB) reduce ferric ion (Fe^{3+}) for cellular growth. Iron respiration in these microorganisms happen either through electron transport chain or by fermentation accompanied by Fe^{3+} as an auxiliary electron acceptor [66]. Facultative anaerobes usually use the first pathway. These facultative IRB can consume the oxygen and then switch to Fe^{3+} reduction. This provides ecological niches for SRB to grow. Most strict anaerobes take advantage of the second pathway. Fermentation process in these organisms usually involves an organic compound as terminal electron acceptor [67]. Ferric ion in this case enhances the growth conditions. Iron-reducers convert ferric ion to ferrous ion, which is more soluble. The amount of converted ferric ion is highly dependent on the type and availability of organic matter. Therefore organic matter play a role in iron dissolution, and consequently corrosion by IRB [68]. A study on Pseudomonas isolated from an oil pipeline showed that this strain enhances MIC by dissolving the protective Fe (III) compounds on the surface of the metal and exposing metal surface to any harsh environment [69]. These IRB colonized on the surface and inhibited formation of crystalline coating layer on the metal surface.

On the other hand, the exact role of IRB on MIC is not fully understood. Some researches have shown that IRB can have an inhibitory effect on MIC. One inhibitory mechanism suggests that in static environments, reduced Ferrous ion (Fe^{2+}) act as a barrier for oxygen diffusion in the bulk fluid. They are oxidized in the bulk fluid and then reduced again by IRB. This process retard corrosion by protecting metal surface from further oxidation [70].

2.8 - Other forms of corrosion in oil pipelines

Different types of corrosion (categorized based on appearance) occur in oil pipelines including pitting corrosion, crevice corrosion, erosion corrosion, stress corrosion, galvanic corrosion, etc. In this section frequent forms of corrosion, besides MIC are discussed. Sometimes

corrosion cannot be attributed to one form of corrosion and a combination of different types happen in one spot.

2.8.1 Pitting corrosion

Pitting corrosion is a localized attack on the surface of the metal in form of holes. This is one of the most notorious types of corrosion. It is hard to detect due to small amount of weight loss and small size of pits that are usually covered with corrosion products [8]. These small holes can grow and coalesce and perforate the material finally leading to failure.

Pitting initiates with attack on the passive film formed on the surface of the metal. Aggressive anionic species like chloride ions play a key role in pitting corrosion. Chloride anions, which are abundant in seawater systems, are anion of strong acid and they have high diffusivity [71]. These anions can induce film breakdown through the pores in the film. Metal dissolution happens in the pit. Formation of metal anions produces extra positive charge in the pit. Chloride ions migrate into the pit to balance the charges. pH decreases in the pit due to the cation hydrolysis according to Eq. 2.22 [71]. This acidic environment promotes further penetration of the metal. Pit growth can also be a mass-transfer-controlled process depending on the rate that ions diffuse out or into the pit. When the pit is saturated with metallic salt, a salt film precipitates at the bottom of the pit. Thus pit growth is under control of ions transport across this film [72].

$$Me^{2+} + 2H_2O \rightarrow Me(OH)^{+} + H^{+} + H_2O \rightarrow Me(OH)_2 + 2H^{+} \qquad \text{Eq. 2.22}$$

Pitting can also be described from a defect stand point. Aggressive anions can be adsorbed into the anion vacancies at the film/solution interface. This occupation of anion vacancies, generates a flux of cation vacancies at the metal/passive film interface. These cation vacancies can migrate to the metal/ solution interface and combine and form a hole in the passive film [72].

2.8.2 Erosion corrosion

Water is injected into the pipeline stream for enhancement of the oil extraction and for maintaining high pressure in the pipelines. This water contains sand particles that induce erosion corrosion in the pipes. These fine particles induce local shear heating at impact. Beneath the impacted region a work-hardened zone forms due to the high kinetic energy of particles. When the surface is covered with platelets and work-hardened zone reaches a stable state, erosion corrosion continues at a steady rate [73]. Initial stages of platelet formation are depicted in Figure 2.4.

In the case of formation of passive layer like iron hydroxide on the surface of the metal, the surface is considered brittle and erosion pathway changes. The deformation becomes plastic and cracks are formed. Mechanism of the erosion corrosion on brittle surface is presented in Figure 2.5. In this type of erosion corrosion, elastic deformation does not occur. Part of the passive layer is delaminated at impact. According to Figure 2.5, at the time of impact cracks are formed in the interface of brittle passive layer and metal. These cracks are both planar and in radial direction. The brittle layer cannot deform elastically to dissipate the energy gained through impact. After the erodent particle rebounds these crack lead to final knock off of the surface [74].

High turbulent flow can also remove the passive layer. This will expose fresh metal surface and induce further corrosion. Critical flow rates in pipeline that induce erosion corrosion can be calculated based on Eq. 2.25 [75]. In this equation, U_e is the flow rate in ft/s. C_{API} is 450 for pipelines injected with seawater and ρ_m is liquid density in lb/ft^3. However this equation overestimates in case of carbon steel [76]. This is a very simplistic model. A more detailed model was later suggested that named Koutecky-Levich which is beyond the scope of this work to discuss. A viable solution to combat erosion corrosion is application of organic coatings. Which are cheaper than selecting erosion-resistant alloys. However, these coatings are endanger of delamination by sand particles in the flow.

$$U_e = \frac{C_{API}}{\rho_m}$$ Eq. 2.23

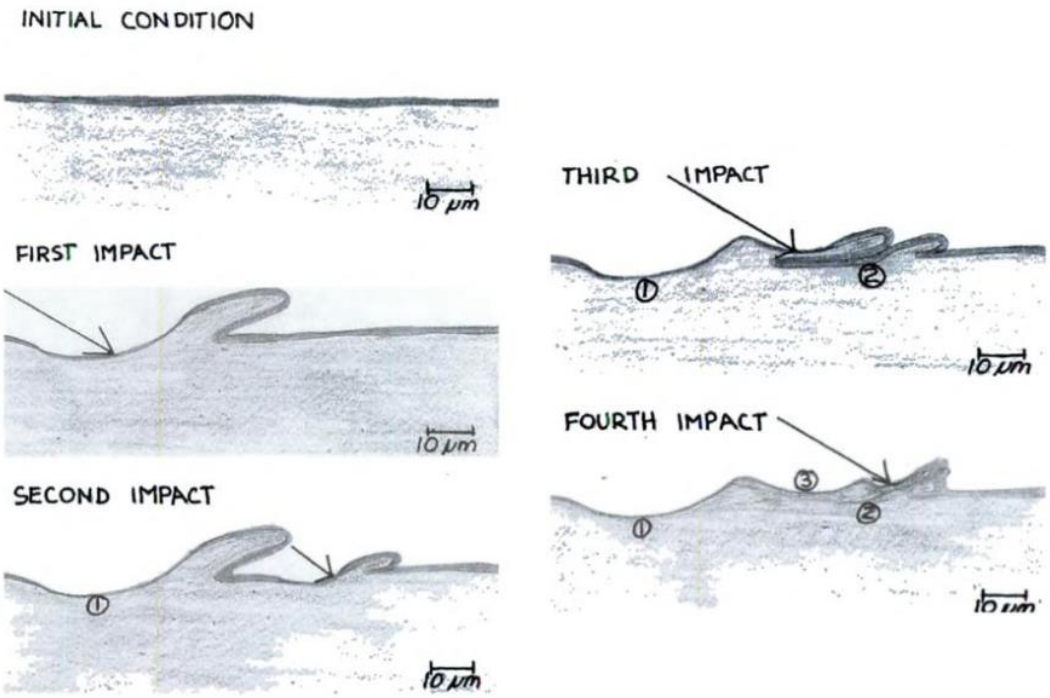

Figure 2.4- erosion corrosion mechanism in ductile materials. Different stages of erosion corrosion by particles on a ductile surface are depicted. Due to ductility surface deforms rather than cracking after impact with particles[73].

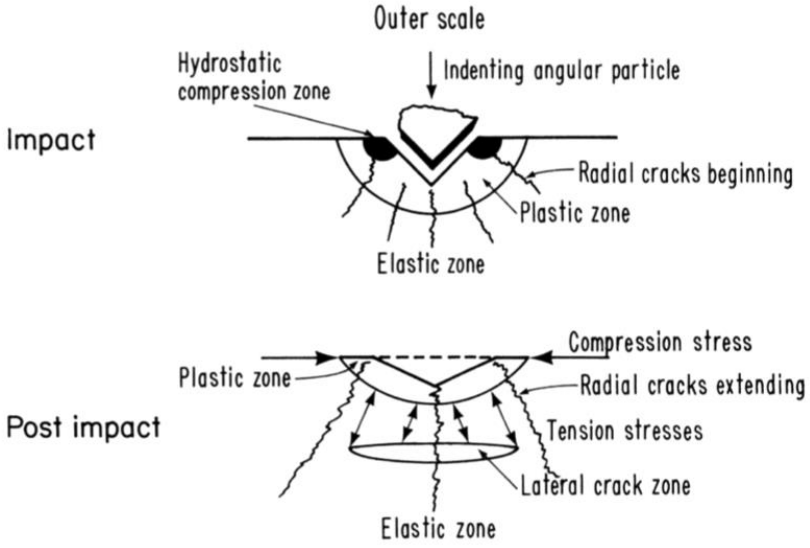

Figure 2.5- erosion corrosion mechanism on brittle surface. No elastic deformation happens. At the time of impact the protrusions on the surface detach and expose fresh metal surface to corrosion [73].

2.9 - MIC mitigative measures

2.9.1 Biocides

A very common approach in oilfields to inhibit SRB activity is the application of biocides. Effective biocides application depends on biocide concentration, frequency of application, knowledge on targeted microorganisms, and monitoring biocide concentration [77]. Biocides can be categorized as oxidizing and non-oxidizing. Oxidizing includes inorganic compounds like ozone, chlorine, and non-oxidizing includes organic compounds like glutaraldehyde and formaldehyde [78]. Non-oxidizing biocides are known to be more effective due to their longer persistency in pipelines and independency of pH [79]. A combination of both biocides can be used for a better control of microbial populations in the pipelines.

There are limitations on biocides application due to their toxicity. These biocides are finally released into the environment and affect plants and animal life. Therefore it should be guaranteed that they are biodegradable and are in low concentrations. The efficacy of biocides has been matter of question in certain conditions, for instance biocides cannot penetrate the biofilms, or they are effective only in certain pH ranges. After frequent injection of biocides, microbes become resistant to these chemicals [80]. Therefore, their application should be done based on knowledge of the pipeline niche.

2.9.2 Nitrate treatment

An environmental-friendly approach to take MIC under control is the injection of nitrate/nitrite into oil pipelines. Unlike biocides and chemical applications, this approach does not impose health or toxicity risks on the environment. Nitrate injection alternates microbial community from SRB-dominated to nitrate-reducing bacteria (NRB)-dominated. NRB compete with SRB on organic electron donor [81]. Addition of NO_3^-/NO_2^- can inhibit MIC through following mechanisms; Outcompetition of SRB by NRB for common electron donors, inhibition of SRB by nitrate-reducing sulfide-oxidizing bacteria (NR-SOB) metabolites like nitrite or

nitrous oxide, SRB switching from sulfate reduction to nitrate reduction, Suppression of H_2S via NR-SOB H_2S oxidation with nitrate [82–84]. Nitrate reduction is more favorable than sulfate reduction according to Eq. 2.24-Eq. 2.25 [85].

$$5CH_3CO_2^- + 8NO_3^- + 3H^+ \rightarrow 10HCO_3^- + 4N_2 + 4H_2O \quad \text{Eq. 2.24}$$

$$\Delta G^{\circ\prime} = -495\ kJ\ /(mol\ NO_3^-)$$

$$CH_3CO_2^- + SO_4^{2-} \rightarrow 2HCO_3^- + HS^- \quad \text{Eq. 2.25}$$

$$\Delta G^{\circ\prime} = -47\ kJ\ /(mol\ SO_4^{2-})$$

Nitrate treatment was performed in injection water on oil platform in the North Sea. Due to this treatment, activity of SRB was significantly suppressed and corrosion rate dropped more than 70% after 32 months [86]. Addition of nitrate in produced water in a Canadian oil field, reduced sulfides in the brine more than 50% [87]. Schwermer at al. (2008) showed that microbial corrosion was decreased in lieu of nitrate addition in water injection system of an oilfield in North Sea [84]. In a model column study, it was shown nitrate addition to samples did not reduce weight loss in samples [88]. Authors suspected this was due to low concentration of added nitrate and NRB population was not stimulated. Overall, it has been shown by multiple studies that nitrate is effective in sulfide suppression in oilfields [89–93][86]. In summary, this method, proven to be effective in inhibiting MIC, especially in North Sea oilfields [86].

2.9.3 Mechanical cleaning

Mechanical cleaning in oil pipelines is done via special equipment called ‘pig’ (Figure 2.6). It stands for pipeline inspection gauge. Pigs were initially developed for application in oil pipelines; however, their applications were extended into fluid products and process industries over the course of time. Pigs are devices inserted into pipelines to remove debris, corrosion products, and microbial deposits from pipelines. Pigs travel within the pipeline by means of flow. Different types of pigs are used in oil and gas industry like mandrel pigs, multi diameter, solid cast pigs, etc.

Pigs can also be used for monitoring and inspection of pipelines in addition to the cleaning purposes. They can be equipped with cameras, ultrasonic transducers, magnets, etc. to monitor diameter variation and possible alterations on pipes surfaces. As previously mentioned that biofilms are resistant to biocides and chemical penetration. Therefore mechanical cleaning is the only way to remove those entities. Pigs have disadvantages as well. They can be trapped into pipelines. They can be trapped due to deposits pile up ahead of the pig, the flow bypassing the pig, jack-knife of the pig [94]. These trapped pigs block the flow and sometimes it is hard to locate them. Subsequently, the line needs to be shut down to remove the pig, which is costly and time-consuming.

Figure 2.6- Two pigging devices used in oil pipelines (http://www.tdwilliamson.com/solutions/pipeline-pigging/pipeline-pigs/cleaning-pigs).

Chapter 3 - Experimental Procedure

3.1 - Coupon Materials and culture vials

Mild carbon steel is the main material used for crude oil pipelines. C1018 mild carbon steel was opted for corrosion coupons. The chemical composition of the carbon steel coupons are listed in Table 3.1.

Strains Desulfovibrio bastinii (ATCC BAA-903) and Desulfovibrio vulgaris (ATCC 7757) were purchased from American Type Culture Collection (ATCC). Desulfovibrio microorganisms are the species responsible for anaerobic corrosion. These strains was previously isolated from the production water of an oil pipeline.

Table 3.1The chemical composition of carbon steel coupons.

Element	C	Cu	Mn	Si	P	S	Cr	Ni	Mo	Fe
Wt.%	0.16	0.16	0.755	0.17	0.013	0.02	0.048	0.078	0.014	balanced

3.2 - Culture Condition and Growth

D. bastinii is cultivated on Modified Baar's medium (ATCC 1250 media) containing $MgSO_4$ (2 g/L), sodium citrate (5g/L), $CaSO_4.2H_2O$ (1 g/L), NH_4Cl (1 g/L), NaCl (25 g/L), K_2HPO_4 (0.5 g/L), sodium lactate (3.5 g/L), and yeast extract (1g/L). D. vulgaris is cultivated in the same medium excluding NaCl (ATCC 1249 media). The pH of the medium components were adjusted to 7.5 by addition of NaOH and HCl. Resazurine was added to the medium (4 mg/L) as redox indicator. Media were prepared in 3 separate components. Components were autoclaved separately. If nutrients in the media are dissolved and prepared in one component, some compounds might react and produce harmful compounds for the cells. It was believed that autoclave is harmful for some species for a long time, however it was the chemical reactions that taking place at higher temperatures amongst nutrients that harmed some species. The dissolved

O_2 was removed from the medium by purging nitrogen. Depending on medium volume N_2 bubbling duration was adjusted. In the next step, cysteine solution was added (100 mg/L) to remove the remaining oxygen. After bubbling, medium was transferred to sterile serum bottles under N_2 pressure with extra precautions.

The cells were initially cultured in anaerobic chamber under 0.0% O_2 and a constant flow of N_2. After transferring the cultures from original vials to stoppered tube, they were transferred to incubator in an anaerobic jar. The cultures were allowed to grow at 35°C for 48 h to reach exponential phase, or early stationary phase. For the growing process, all samples were placed in rubber-stoppered tubes. Transfers were performed by nitrogen-flushed sterile syringes.

For each strain, 3 different media were prepared. First media was the original cultivation media; ATCC 1250 media for D. bastinii and ATCC 1249 media for D. vulgaris. In the 2nd media lactate was eliminated; 1250-LF for D. bastinii and 1249-LF for D. vulgaris. For the last media, besides the elimination of lactate, riboflavin was added (10 ppm); 1250-LFR for D. bastinii and 1249-LFR for D. vulgaris.

3.3 - Immersion Corrosion Experiment Setup

The carbon steel coupons were placed in 100% ethyl alcohol for 30 minutes under UV light. This was done for the following two purposes; first, is to ensure the removal of anti-corrosive products on the surface of coupons. Coupons were wrapped in an anticorrosive paper at the time of arrival to prevent the oxidation of the metal during storage time. Second, is to fully sterilize the coupons. Modified Baar's medium is a suitable environment for many cells to grow, thus all steps should be done under sterilized conditions to inhibit the growth of any unwanted species.

Coupons were hung in serum bottles while a 2/3 of the coupon was immersed in culture medium. Picture of serum bottles setup at the beginning and end of immersion tests are shown in Figure 3.1 and Figure 3.2. This process is done under N_2 flow. 0.2 ml 0.5% cysteine is added to

scavenge any remaining O_2 after placing the coupons. After complete exclusion of O_2, 0.5 mL of fresh culture was added to each serum bottle. Samples were then transferred to incubator, and were left to stay at 35°C overnight. During immersion period, the sulfate concentrations were quantified on a daily basis.

Figure 3.1- Serum bottles containing carbon steel coupons for at the beginning of immersion corrosion tests.

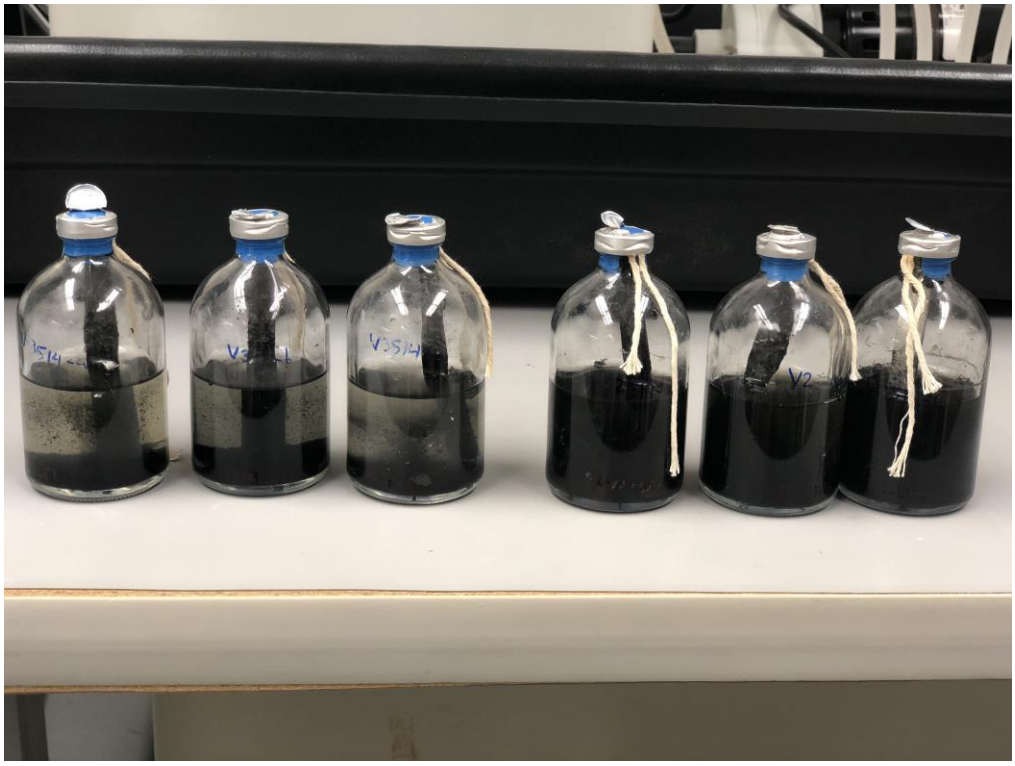

Figure 3.2- Serum bottles containing carbon steel coupons for at the end of immersion corrosion tests.

3.3.1 Sulfate Quantification Procedure

Sulfate in the cultures was quantified via turbidimetric method. The sulfate ions (SO_4^{-2}) detection range of this method is 1-40 mg/L. $BaCl_2$ is used as the reagent in this method. Sulfate ions are converted to barium sulfate during the reaction with the reagent (Eq. 3.1). This reaction disturbs the solution and the turbidity can be measured at a specific wavelength with a spectrophotometer (420 nm). Steps of the designed procedure are summarized in the following section.

$$Ba^{2+}(aq) + SO_4^{2-}(aq) \leftrightarrow BaSO_4(s) \qquad \text{Eq. 3.1}$$

1. A 0.4 ml aliquot was taken from each sample. To ensure exclusion of any corrosion particles, samples were filtered with 0.2 µm syringe filter. The corrosion products are highly absorbent and they affect the readings from spectrophotometer, therefore any FeS or Fe associated particle should be removed prior to testing.

2. A conditioning reagent was prepared according as follow. 30 ml concentrated HCl was added to 300 ml DI water. 75 gr of NaCl dissolved in DI water and was mixed with 100 ml 95% isopropyl alcohol and 50 mL glycerol. DI water was added to reach a final volume of 500 ml.
3. 5 mL of conditioning reagent was added to 100 m- volumetric flask. Sample aliquot was added to 100 mL volumetric flask.
4. 0.1 g of $BaCl_2$ was added to the flask.
5. Flask was stirred via a vortexer immediately after addition of the reagent. It was vortexed for exactly 1 minute. $BaCl_2$ reacts spontaneously with the solution. Thus the steps must be followed quickly and in a timed manner. Any delays can lead to erroneous reads due to $BaSO_4$ precipitation.
6. After mixing, 1.5 mL aliquot from the flask is transferred to a clean cuvette. The cuvette is placed in the spectrophotometer.
7. 8 reads are performed for each sample at 30-second intervals. Readings are made at 420 nm wavelength.
8. Maximum read amongst these 8 reads is selected to reflect the sulfate concentration in the sample.

To determine the sulfate concentration, a series of sulfate standards were prepared. To prepare sulfate standard stock solution, 1.479 g Na_2SO_4 dissolved in 1 L DI water (1 mL= 1 mg SO_4^{2-}). This stock solution then was diluted 10 times. Each day a set of 5 standards was measured along with samples. Standards were measured in between samples to avoid systematic errors in readings.

3.4 - Corrosion Rate & Corrosion Products Analysis

After coupons were withdrawn from serum bottles, corrosion rate was calculated via gravimetric methods. The powdered attained from the coupons is investigated via Fourier

Transform Infrared spectroscopy (FTIR). A Nicolet Nexus 670 FTIR equipped with a liquid nitrogen cooled mercury cadmium telluride (MCT) detector has been used. Background was collected every 30 minutes and prior to testing. ATR module was cleaned with organic solvent before placing each sample. The surface of the coupons was also inspected under SEM. Before SEM monitoring, cells were fixed following a 5-step protocol.

3.4.1 Gravimetric Method

Corrosion rate was calculated based on mass loss as a function of time, in the gravimetric method. Coupons weights were measured before immersion. After coupons were taken out of the test media, they were cleaned before final weighting. Coupons were cleaned according to ASTM G1-03[95]. Based on this ASTM standard coupons were sonicated in distilled water for 5 minutes. Then they were transferred to Clarke's solution for 10 minutes (Clarke solution= 500 ml concentrated HCL+ 500 ml DI H_2O + 3.5 g hexamethylenetetramine). This step was followed by another 5 minutes of sonication. Electrolytic cleaning was performed if corrosion products still remained on the surface. Then coupons were left to dry in a desiccator. Then they were weighted. Corrosion rate was calculated based on the following equation:

$$Corrosion\ rate\ (mpy) = \frac{3.45 \times 10^6 \times \Delta m}{d \times t \times A}$$

where: Δm= mass difference (g), d= metal density (g/cm^3), t= immersion duration (hr.), and A= cross sectional area of exposure (cm^2).

3.5 - Electrochemical Experiments

A Specific anaerobic electrochemical cell was designed for the purpose of this study. Conventional cells does not allow for O_2 exclusion. The cell is shown in Figure 3.3. This design is completely air-tight. The cell was filled with the media in the anaerobic chamber. Electrochemical tests shed light on the corrosion kinetics, and the reactions that are taking place

on the surface of metal. Four electrochemical tests were performed; Tafel scan, linear polarization resistance, potentiodynamic sweep, and corrosion potential monitoring.

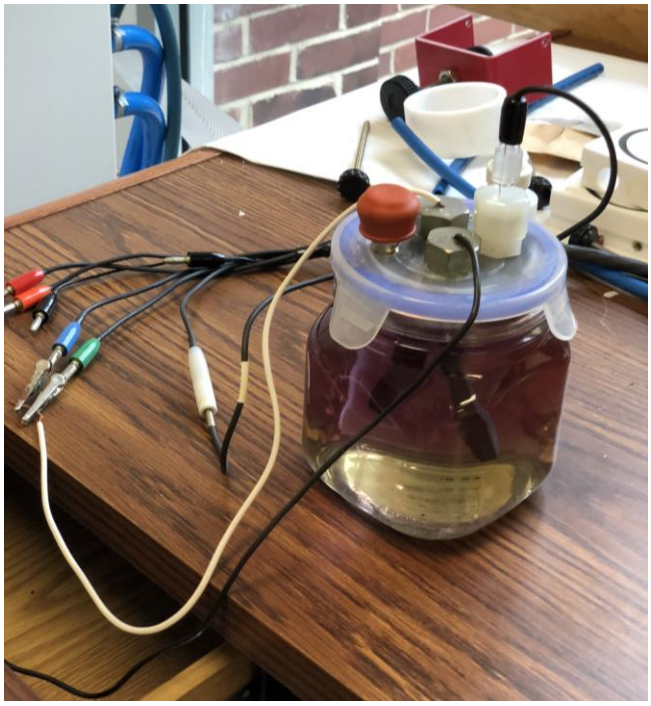

Figure 3.3- Anaerobic electrochemical cell used in this work

3.5.1 Tafel Scan

The purpose of this test is to extract Tafel constants. In a corroding system, two main reactions are present; one is the corroding metal M (Eq. 3.2), and the other one is the reduction of species Z^+ in the solution (Eq. 3.3)[96].

$$M^+ + e^- \leftrightarrow M \qquad \text{Eq. 3.2}$$

$$Z^+ + e^- \leftrightarrow Z \qquad \text{Eq. 3.3}$$

Consider $i_{R,M}$ and $i_{O,M}$ as metal reduction current, and metal oxidation current, respectively. Also consider the same thing for species Z, $i_{R,Z}$ and $i_{O,Z}$. At the steady-state condition, the total rate of oxidation and reduction is equal (Eq. 3.4). At corrosion potential (E_{CORR}), the measured current is zero. When an external voltage applied in a way that corrosion potential is sufficiently removed from equilibrium, reduction rate of M ($i_{R,M}$) and oxidation rate of Z ($i_{O,Z}$) become insignificant [97]. Therefore, the corrosion rate would be equal to the oxidation

rate of M ($i_{O,M}$), or reduction rate of Z ($i_{R,Z}$). This current can be measured according to Eq. 3.5. Relationships between current and potential in the ongoing reaction in this system are illustrated in Figure 3.4.

$$i_{O,M} + i_{O,Z} = i_{R,M} + i_{R,Z} \qquad \text{Eq. 3.4}$$

$$i_{Measured} = i_{O,M} - i_{R,Z} \qquad \text{Eq. 3.5}$$

Thus Tafel constants can be obtained from following equations (where η is the overvoltage):

$$\eta = \beta_{Anodic} log \frac{i_{O,M}}{i_{CORR}} \qquad \text{Eq. 3.6}$$

$$\eta = -\beta_{Cathodic} log \frac{i_{R,Z}}{i_{CORR}} \qquad \text{Eq. 3.7}$$

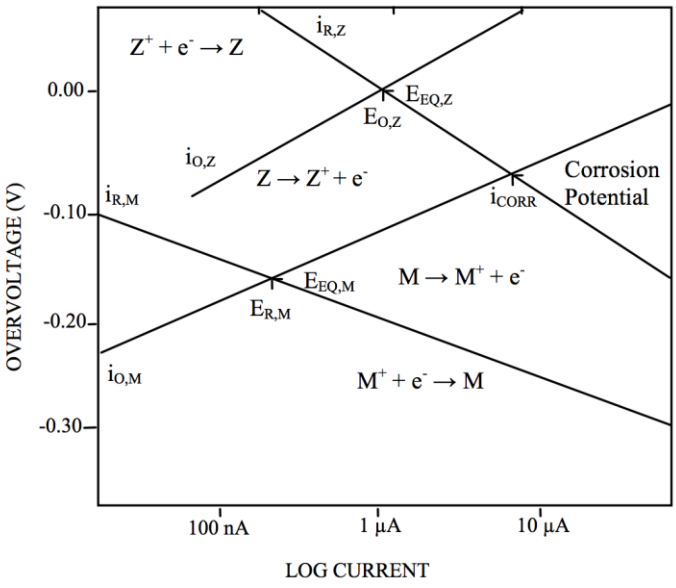

Figure 3.4-Overvoltage vs. current for a corroding system (taken from www.princetonappliedresearch.com)

In this study, samples were polarized about 250 mV anodically (positive-going potential) and cathodically (negative-going potential) about the corrosion potential (E_{CORR}). The scan rate was 0.167 mV/s.

3.5.2 Linear Polarization Resistance

Polarization resistance curves are obtained through a potential scan ± 20 mV about E_{CORR}. Slope of the potential vs. current plot attained from these experiments, is known as polarization resistance (R_p). R_p is inversely proportional to i_{CORR}. The relationship is demonstrated in Eq. 3.8. Corrosion rate can be obtained from the corrosion current according to Eq. 3.9.

$$i_{CORR} = \frac{\beta_A \beta_C}{2.3(\beta_A + \beta_C)} \frac{1}{R_P} \qquad \text{Eq. 3.8}$$

$$Corrosion\ rate\ (mpy) = \frac{0.13\ I_{CORR}(E.W.)}{d} \qquad \text{Eq. 3.9}$$

β_A ,β_C = Anodic and cathodic Tafel constants, i_{CORR} = corrosion current in µA, E.W. = equivalent weight of the corroding species, g., d = density of the corroding species, g/cm^2, I_{CORR}= corrosion current density µA/cm^2.

Tafel constants were obtained from the preparatory Tafel scan. Polarization resistance tests are performed starting from -40mV to 40 mV about E_{CORR} at a rate of 0.167 mV/sec.

3.5.3 Cathodic Potentiodynamic Sweep

Samples were also polarized cathodically (in the negative direction) for 40 mV. It was performed n the same way as the polarization resistance scans were conducted , except for the sample which was not polarized in the positive direction.

3.5.4 Corrosion Potential Monitoring

Open circuit potential of the carbon steel coupon was monitored daily for a continuous 1 hour. Gamry potentiostat was used to monitor the E_{corr} evolution by time.

3.6 - SEM Fixation and Visualization

Samples were fixed following a glutaraldehyde fixation protocol after they were taken out of the test media. Samples were placed in 2% glutaraldehyde and 0.1 M phosphate buffer for 2 hour on the bench and then were kept in the fridge overnight at 4˚C. Draining process was

performed in ethanol series for 2 days (50%, 70%, 85%, 95%, 100%). Summary of the steps are as follows:

1. 1 hour and 30 minutes at -20°C in 50% ethanol
2. 1 hour and 30 minutes at -20°C in 70% ethanol
3. 1 hour at 4°C in 85% ethanol
4. 1 hour at 4°C in 95% ethanol
5. Overnight at 4°C in 95% ethanol
6. 1 hour at 4°C in 100% ethanol
7. Overnight at 4°C in 100% ethanol
8. 2 hours at room temperature in 100% ethanol

When the draining steps were completed, samples were placed in a desiccator to achieve complete dryness. Then they were taken to SEM for visualization and imaging tests. Imaging was done under 15K accelerating voltage. Probe current was alternated to get the best image possible from 50-70 μA. EDS analysis were performed along with SEM. Some of the imaging were done in low pressure mode.

Chapter 4 - Microbial-induced corrosion on C1018 carbon steel by D. vulgaris

4.1 - Background and motivation

D. vulgaris is a common SRB strain that has been extensively studied so far. It was generally believed that SRB induce corrosion by consuming hydrogen formed on the surface of the metal, based on the cathodic depolarization theory (CDP) [98]. For the mechanism of the cathodic depolarization, the following anodic, cathodic and water dissociation reactions were suggested:

Anodic dissolution: $4Fe \rightarrow 4Fe^{2+} + 8e^{-}$ **Eq. 4.1**

Water dissociation: $8H_2O \rightarrow 8H^{+} + 8OH^{-}$ **Eq. 4.2**

Cathodic reaction: $8H^{+} + 8e^{-} \rightarrow 8H_{adsorbed}$ **Eq. 4.3**

Cathodic depolarization: $8H_{adsorbed} + {SO_4}^{2-} \rightarrow 4H_2O + S^{2-}$ **Eq. 4.4**

Overall reaction: **Eq. 4.5**

$$4Fe + H_2SO_4 + 2H_2O \rightarrow 3Fe(OH)_2 + FeS$$

However, this theory has faced serious flaws. In the last decade, a new mechanism was proposed to fill in the gaps for the previous suggested mechanisms. A few strains, recently have been isolated, and have demonstrated capability to oxidized metallic iron (Fe^0) directly [50]. Metallic iron utilization by SRB is depicted in Figure 4.1. Electrons are directly transferred across cell walls via proteins in the cell membrane like c-type cytochrome [99]. According to this figure, SRB utilize metal electrons by aid of proteins in their cell wall. These electrons can either be used by sulfate reduction system in SRB or they can be used by enzyme hydrogenases. This discovery has led to a new proposed mechanism for MIC called direct electron uptake theory. According to direct-electron uptake theory, hydrogen does not have to be the intermediate for the electron transfer. If we assume that this is the predominant mechanism, one would expect that other SRB

strains inducing MIC, possess similar capabilities of direct electron uptake. However not many studies have been conducted on other common SRB strains. In this work, D. vulgaris is selected as a common SRB. Organic electron donors play the key role in determination of MIC mechanism therefore this strain is tested in presence and absence of organic electron donor. The corrosion rates of metal samples as a function of time, temperature, and different media were studied. Carbon-steel sample powders were analyzed by FTIR after the coupons were taken out of the aqueous solutions. In another setup, D. vulgaris was subjected to various electrochemical tests under starvation conditions. This chapter discusses the results from these experiments, and proposed mechanisms.

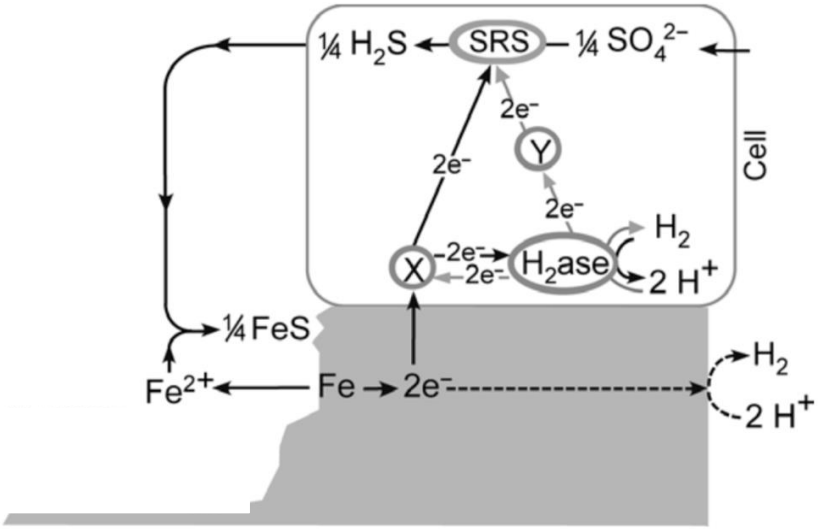

Figure 4.1- Schematic of direct electron uptake by SRB adapted from Hang (2003). Direct electron transfer happens via cell bound proteins (X). These electrons are yielded to sulfate reduction system (SRS) of SRB. H_2 evolution via enzyme hydrogenases happens as a side reaction. There could be other carriers (Y) that utilize this electrons for SRS.

4.2 - Experimental set-up

The following three different media were prepared for D. vulgaris:

1. The first media was the original growth media (ATCC 1249 media). Since this is the original media, whenever the name of the media is not mentioned in the graphs and texts

throughout this chapter, it means ATCC 1249 media was used or it will be referred as 1249.

2. The second media was designed to study the starvation conditions. In the second media, lactate was eliminated from ATCC 1249 media. This media is referred as LF (lactate-free) throughout this section. Lactate was eliminated from the media to create organic electron donor scarcity. Citrate can be utilized by SRB as a potential electron donor source. However its utilization is only possible in a microbial microcosm where other cells convert citrate to acetate or formate. Hence it can be used by SRB[100]. Citrate is added to the medium to prevent FeS particles to precipitate [101].
3. The third media was designed to study one specific pathway in direct electron uptake mechanism. One of the pathways for direct-electron uptake mechanism is the electron transfer through mediator compounds. These compounds act as electron shuttles. They are oxidized inside the cell. Then, they are diffused out of the cell, where they are reduced by taking up electrons directly from the metallic iron. Vitamins can act as these mediator compounds. In order to study this mechanism riboflavin was added to LF media. This media is referred as LFR (lactate-free plus riboflavin) throughout this section. Riboflavin is the precursor of flavin mononucleotide (FMN), and flavin adenine dinucleotide (FAD), which are coenzymes participating in electron transfer reaction inside cell membrane [102]. They are reduced when they accept $2e^-$+ $2H^+$ and they are oxidized as they pass on the $2e^-$ (Figure 4.2) [37].

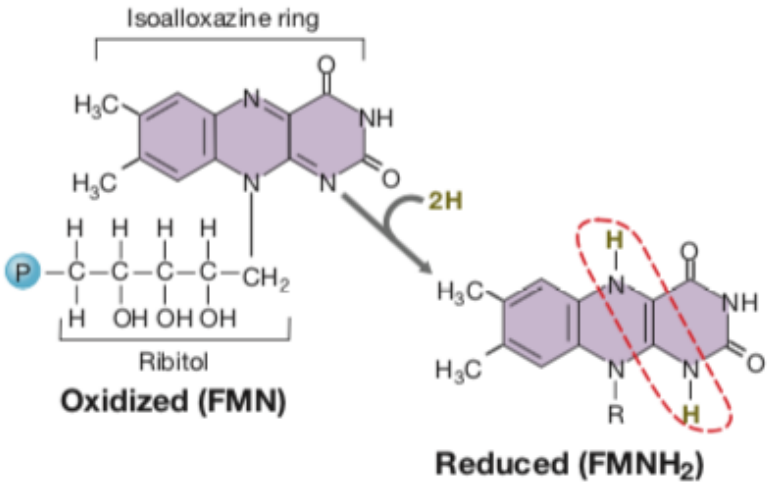

Figure 4.2- FMN structure. The dashed section shows the oxidation-reduction site for electron transfer [37]

Besides those tests performed in 1249, 1249-LF, and 1249-LFR media, a series of additional tests were conducted on samples without SRB incubation. These are called control tests. The control tests were performed on ATCC 1250 Media. This media is the incubation one for D. bastinii, which is another strain studied in this work. Components in this media are exactly the same as ATCC 1249 media except for NaCl. The ATCC 1250 media contains NaCl, since D. bastinii is a halophilic strain. In the absence of SRB cells, corrosion rate is not expected to be different in these two media, since all the used salts are completely dissolved and ionized, and do not precipitate out of the solutions during the experiments. In addition to sterile tests, as control experiments, D. vulgaris was grown in 1249, 1249-LF, and 1249-LFR media in the absence of carbon steel coupons. This last set up determines whether SRB can survive in absence of both organic electron donors and iron or not.

Two different immersion periods were chosen for the corrosion tests. These two time frames were chosen based on preliminary experiments. Preliminary tests were performed to find the optimum initial sulfate concentration. It should be mentioned that although the bacterial can survive high sulfate concentration, however, their reactions with the sulfate give rise to the formation of H_2S. The bacteria cannot survive high H_2S concentration. The preliminary experiments had showed that the added sulfate in the designed media bottles is mostly consumed

within the first four days of culture growth and cells start to die after that. Thus, it can be said that, in the first 5 days metabolic activity was very high and it depreciated slowly after that. Therefore, 7 days and 14 days were selected as immersion periods. During the seven days, bacteria were still in exponential phase. Cells started dying gradually after the 5th or 6th day. These results clearly demonstrate that how corrosion rate evolves and continues even after the cells death. Besides, it can be inferred whether SRB survive longer periods of starvation.

Experiments were performed at three temperatures (25°C, 35˚C and 45°C). 35°C was chosen because it is the incubation temperature for both D. bastinii and D. vulgaris. This is the optimal temperature for these strains. It is expected that their metabolic activities reach their maximum potential at this temperature. 25°C was chosen to study the corrosion at a non-optimal temperature for SRB growth. After completion of these tests at two temperatures (25°C and 35°C), another temperature was added (45°C) to draw a more comprehensive conclusion and gather more data for the modeling section.

These experiments were conducted under different conditions (Media, time, temperature), which comprise of 18 unique environmental conditions. Each environmental condition was repeated 3 times to attain statistical significance.

4.2.1.1 Sampling nominal process

In the next sections, samples were named with five digits. First capital letter digit refers to the SRB strain in that sample, i.e. V refers to D. vulgaris and B refers to D. bastinii. The second two digits refer to temperature. And the final two digits refer to duration of the experiment, i.e. 07 and 14 for seven days and fourteen days, respectively. Sulfate concentration, mass loss, and corrosion rate plots were averaged for three samples in 14-day category. They were averaged for 6 samples in 7-day category (14-day samples and 7-day samples were averaged together during first 7 days). Individual samples (repeated experiments) were named with –a, -b, -

c. Sterile tests are identified as control; the remaining naming agenda for sterile samples are similar to incubated samples.

4.3 - Results

4.3.1 Corrosion results in media 1249

During immersion corrosion experiments, the sulfate content was quantified on a daily basis. Sulfate quantification graph for D. vulgaris in media 1249 is shown in Figure 4.3. More than 70% of the sulfate was consumed within the first 3 days. Cells metabolic activity maximized at day 2. Then, the sulfate reduction (sulfate consumption) followed a distinctively slow rate (sulfate consumption slope reaches almost zero). Similar behavior was observed in all three temperatures. Average values are depicted in Figure 4.3. All individual samples had the same trend. It can be seen from the error bars in the figure that there was not much deviation amongst samples. These results suggest that the temperature did not have a significant effect on metabolic activity of D. vulgaris in media 1249.

Figure 4.4 shows the changes in the corrosion rate as a function of time. Corrosion rates for sterile samples at 25 and 35°C are included in this graph as control.

Relatively higher corrosion rates were observed in the first period (7 days). This is because D. vulgaris reaches exponential growth phase after 3-4 days according to preliminary tests and the SRB population diminishes after that due to depletion of sulfate in the media. Therefore the corrosion rate did not rise significantly in the second week. This can also be interpreted from sulfate consumption graphs. Based on Figure 4.3, cells consumed most of the sulfate in the media within the first couple of days. Since these experiments were conducted under anaerobic conditions, hence, the main corrosion pathway is biocorrosion by SRB. It is expected that less active cells result in less corrosion. These results demonstrate the important relationship between the bacterial activity and the metal corrosion. Sulfate reduction stopped after

day 3-5, or significantly slowed down. This initial 3 days seem to be the peak of the corrosion rate period. When sulfate reduction stopped the rate of increase in mass loss almost ceased too.

As expected, the corrosion rate has a direct relationship with the temperature in this media. However, this conclusion is only based for 25°C -45°C range and should not be extrapolated to other temperatures, since D. vulgaris does not survive at very high temperatures.

Figure 4.5 shows mass loss vs. time for samples at various temperatures. Mass loss in all samples increased with time as expected, even though the corrosion rate decreased. Control samples also had significantly lower mass loss. In this graph it can be seen that there is an ascending trend for mass loss based on increasing temperatures.

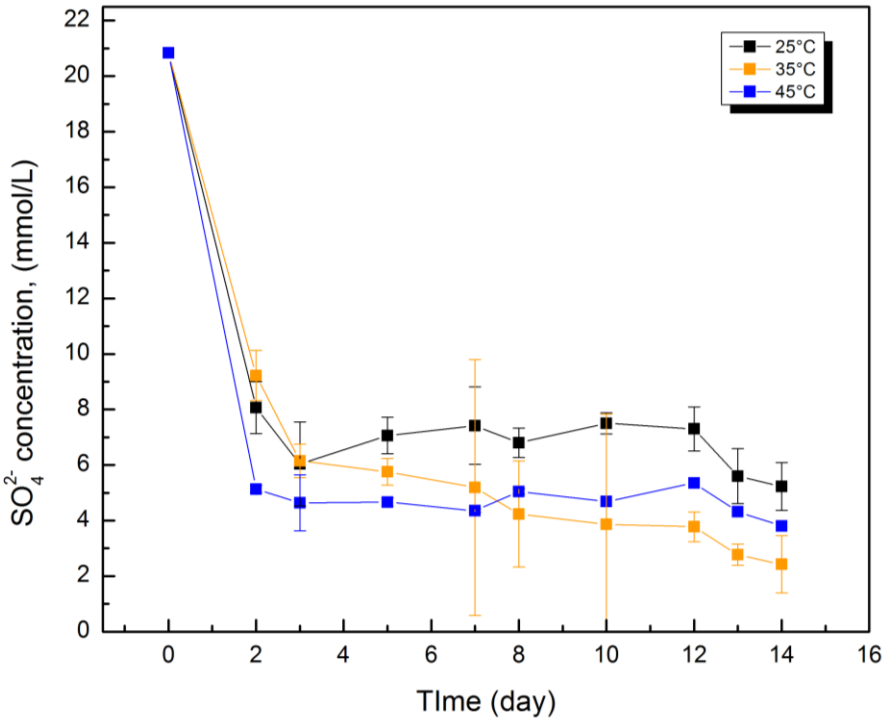

Figure 4.3- Average sulfate concentration vs. time for D. vulgaris in 1249 media

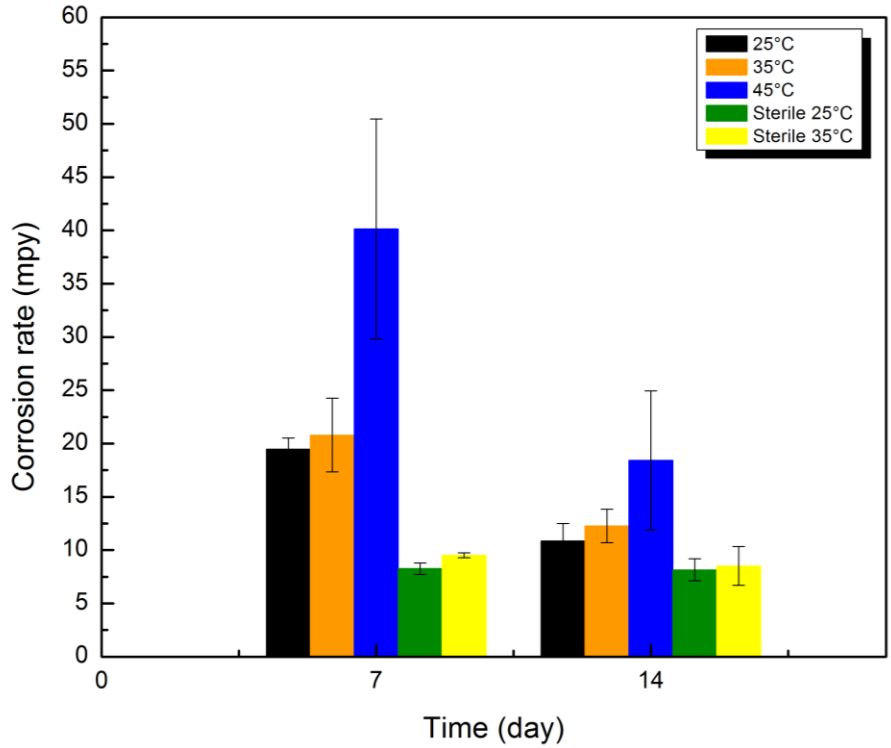

Figure 4.4- Average corrosion rate vs. time for D. vulgaris in 1249 media

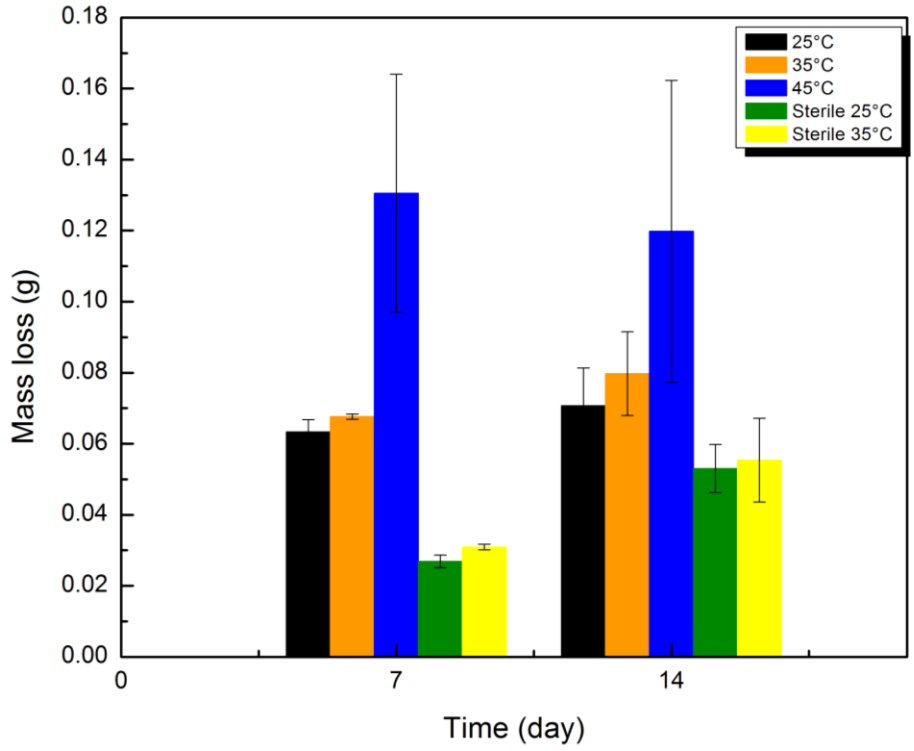

Figure 4.5- Average mass loss vs. time for D. vulgaris in 1249 media

4.3.2 Corrosion results in media 1249-LF

The decrease of the sulfate concentration as a function of time in 1249-LF (lactate free) did not follow a similar pattern to media 1249. It can be noticed from Figure 4.6 that the sulfate-concentration plot as a function of time had a step-like shape with more than one break point at 35°C. There was a high sulfate consumption rate in the first two days. Then the rate slowed down significantly and peaked again after 4 days. Then the rate slowed down again (This can also be visualized from individual samples included in appendix). It seems that the exclusion of organic electron donor suppressed SRB population partially, however it did not impede growth of SRB. The SRB population was affected by exclusion of organic electron donor and there was a reduction in activity of SRB. However a portion of population survived and remained active by switching to Fe utilization. Xu and Gu conducted a series of starvation experiments on D. vulgaris and observed that with exclusion of lactate, there was reduction in SRB cell counts. In spite of sessile population loss, authors observed that the corrosion rate increased in the starved samples in comparison to non-starved ones [103]. They related the increase in corrosion rate to SRB utilizing metallic iron. This conclusion was further corroborated by work of Dou et al. (2019) where they tested organic electron donor starvation on SRB on Cu coupons. They observed a decrease in the corrosion rate in the starvation experiments conducted on D. vulgaris. D. vulgaris did not survive in the absence of both Fe and organic electron donor in their experiments. And the MIC rate on the Cu coupons decreased [104]. This suggests that the survival of SRB in absence of organic electron donor is dependent on Fe.

Two distinctive sulfate consumption periods were also subjected to kinetic studies to gain further insights into the reactions happening in LF media. The sulfate consumption graph at 35˚C exhibits two distinctive slopes. The first slope is relatively small followed by a much faster consumption rate. Therefore log of sulfate concentration were plotted vs. time (Figure 4.7). The linear slopes in $\ln[SO_4^{2-}]$ vs. time graph shows that consumption rate of the $[SO_4^{2-}]$ follows a

Pseudo-first-order. Similarly, the data shows there are two distinctive first order reactions with clear different half-lives. It should be mentioned that these two first order decays may be pseudo, and the ultimate second order decay can be calculated by dividing the determined observed pseudo first order reaction rate constant over the initial $[SO_4^{2-}]$ concentration. The consumption rates do not fit second order as $1/[SO_4^{2-}]$ as a function of time. The higher slope can be attributed to SRB utilization of iron electrons that leads to more sulfate consumption by SRB. In this media SRB needs to be very close to metal surface to utilize electrons from iron because these electrons are not soluble in the media. After the SRB form the biofilm they start utilizing iron electrons, hence more sulfate is used by the sulfate reduction system in SRB. Therefore, the first small slope is before SRB establish biofilm on the surface of the metal. It takes at least 3 days for D. vulgaris to establish a mature biofilm [105]. After biofilm formation the sulfate consumption rate increases and that's why a distinctive higher slope is observed in Figure 4.7.

As mentioned before, temperature plays an important role in this media. It was observed that in media 1249, cells kept growing at the same rate at all temperatures. However, in 1249-LF media, cells do not seem to prosper much at non-optimal temperatures (25°C & 45°C). There is a minimal bacterial activity at 45°C, and negligible activity at 25°C. The ideal condition for SRB is at 35˚C in 1249 media. Cells still keep growing with a delay in 1249-LF media at 35°C. However, at the other two temperatures (25°C & 45°C) less SRB activity is observed.

Corrosion rate in this media is depicted in Figure 4.8. Samples at 35°C had higher corrosion rates than samples at the two other temperatures. Corrosion rate of 25°C samples barely exceeded 16 mpy, while 35°C samples corrosion rate reached up to 26 mpy. Corrosion rate at 45°C, samples were close with ones at 35°C samples in spite of less growth. This can be explained by the fact that the kinetics of reactions increases at higher temperatures. An interesting pattern in the corrosion rate graph was that, corrosion rate during 7 days and 14 days was almost

the same at each temperature. This result is evaluated in the next section, based on sulfate consumption curve and mass loss data.

Mass loss graphs for samples are illustrated in Figure 4.9. Mass loss in 1249-LF during the second 7-day increases (in 1249 media it was observed that there was not much increase in mass loss in the second period). Mass loss for samples at different temperatures increased almost linearly with time i.e., after 14 days of exposure, the mass loss approximately doubles with doubling of time. This is due to the evenly distribution of cell active population over the 14-day period. For sample V35-b, for instance, almost similar mass was lost during the first and second 7-day period (Individual mass loss of samples are included in the appendix). This agrees fairly well with the sulfate concentration plot (Individual sulfate content graph is added in the appendix). Figure 4.6 showed that SRB were active during the whole 14-day period. Samples at 25°C had lower corrosion rate than 35°C samples. The corresponding sulfate concentration curve showed lower SRB activity at 25˚C than 35˚C. In the case of 1249 media cells were mostly active during the first 7 days rather than the whole 14-day period, therefore there was a slight drop in corrosion rate for longer exposure time.

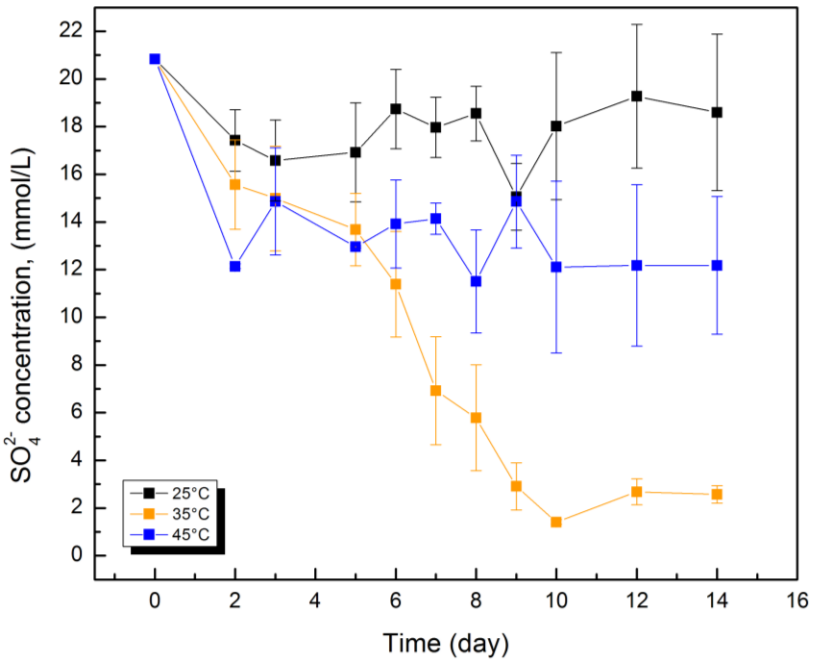

Figure 4.6- Average sulfate concentration for D. vulgaris in 1249-LF media

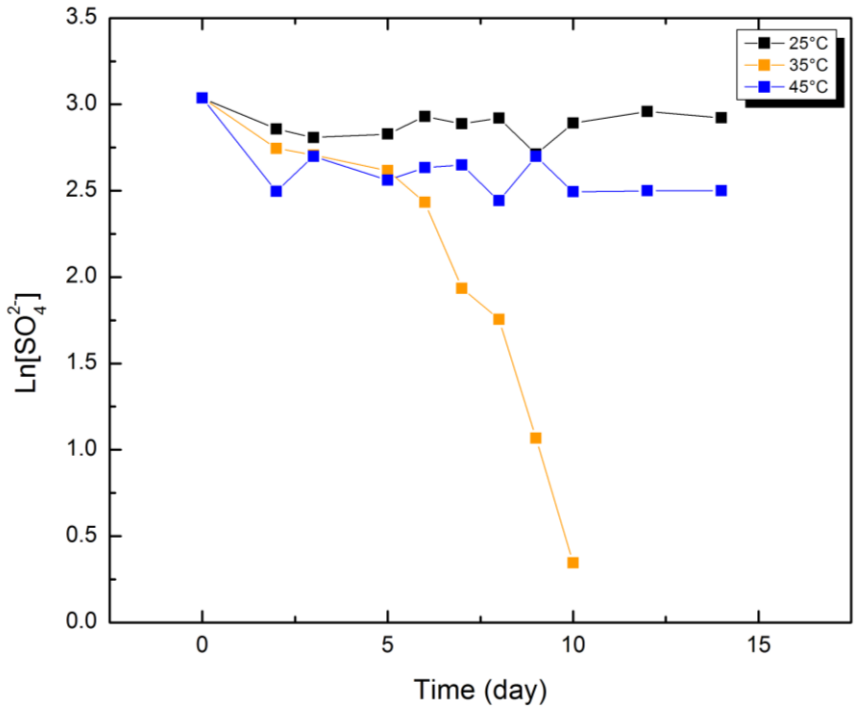

Figure 4.7- logarithmic concentration of sulfate vs. time for D. vulgaris

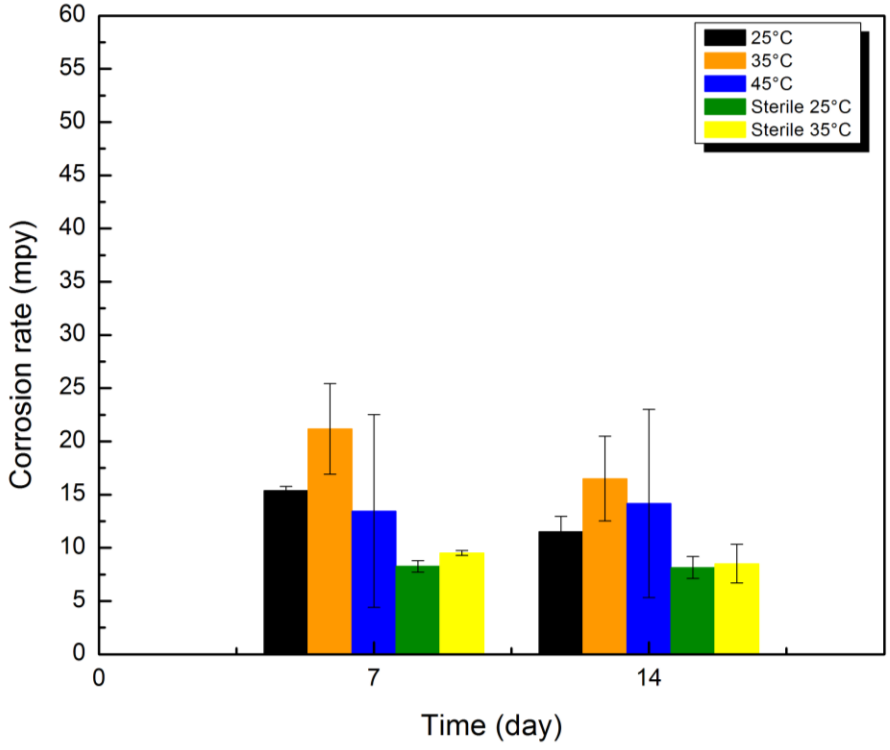

Figure 4.8- Average corrosion rate vs. time for D. vulgaris in 1249-LF media

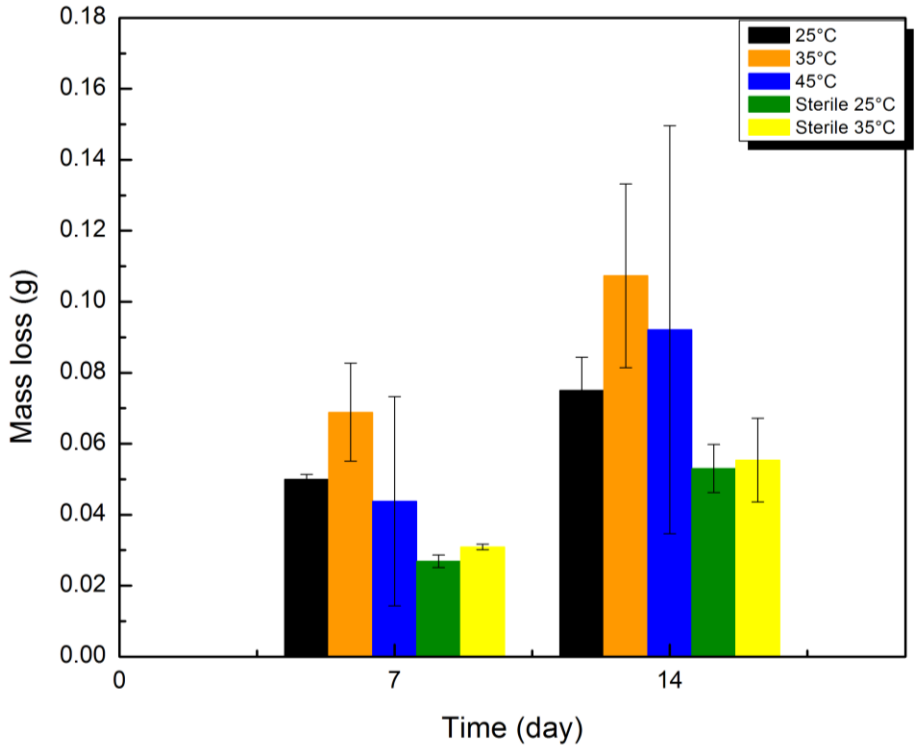

Figure 4.9- Average mass loss vs. time for D. vulgaris in 1249-LF media

4.3.3 Corrosion results in media 1249-LFR

Sulfate consumption curves in 1249-LFR media were similar to those in 1249-LF media. There was no instant sulfate consumption at the beginning of the incubation in 1249-LFR media (Figure 4.10). Samples at 45°C showed little SRB activity, while samples at 25 °C showed negligible activity. SRB activity can be compared at these two temperatures by analyzing the sulfate consumption rates. In the first two days, sulfate was consumed at a rate of 8 mmol/L/day at 45°C while the rate was only 0.7-1.8 g/L/day in the 25°C samples. Meanwhile sulfate consumption rate was almost zero during the first 3 days at 35°C. It peaks up after this delay, and sulfate consumption continues to take place till day 10. One thing to notice is the relatively large error bars for 14-day samples at 35°C. Based on the individual sulfate concentration curves at 35°C, sample V3514-b had a steady declining consumption rate (a very slow rate, 0.35 mmol/L/day), while samples V3514-a and V3514-c had a step-like curve with higher

consumption rates at each step, about 1 mmol/L/day at each step. This leads to higher error bars for V3514 curve (individual sulfate concentration curves are included in the appendix).

These results suggest that in spite of the absence of organic electron donors, the SRB growth did not stop. Differences in sulfate consumption rates depend on survival strategies taken by the bacteria. If the cells do not switch to taking up electrons directly from the metal, there is no alternative source of electrons in the media. In the absence of oxygen, electron diffusion from the metal into the bulk solution is a very slow process. Thus, the only viable option for cells to grow is to utilize the electrons from the metal. Riboflavin was added to this media as potential electron mediators. Flavins, which are the derivative of riboflavin, have three oxidation states: fully oxidized flavoquinone (Fl_{ox}), flavosemiquinone radical ($Fl^{\cdot -}_{rad}$), and two-electron-reduced flavohydroquinone (Fl^{2-}_{red}) [37][106–108]. Schematic of electron/proton transfer pathways by flavins is presented in Figure 4.13. This figure demonstrates sensitivity of the flavin redox reactions on pH values. There are more than 45 pathways for these redox reactions according to this figure. Therefore detecting the pathway is beyond scope of this study. However by investigating pH values in further sections, potential pathways can be identified. These compounds shuttle electrons from interior cell to external terminal electron acceptors. The mechanisms of electron shuttling by bacteria has not been fully understood. First evidence of the riboflavin role as an electron shuttle was demonstrated for Shewanella species [109]. These species secret riboflavin to reduce insoluble Fe(III) minerals in absence of oxygen as electron acceptor to provide required energy for growth. However it is not known how riboflavin accelerate Fe(III) oxides [110]. The mechanism of these compounds effectiveness is complex. Many factors contribute to the efficiency of these compounds including temperature, pH, solubility of targeted electron donors, etc. [111]. SRB strains did not show capability of excreting these compounds by themselves, however in a consortia of a microorganisms they can take advantage of mediator compounds secreted from other species. Corrosion rate from this media (Figure 4.11) shows that riboflavin was mostly effective at higher temperature. Corrosion rate

decreases after 14 days in this media at all temperatures, however the decrease at 45˚C is less significant than the other two temperatures. Dos Santos et al. showed that riboflavin efficiency of mediator compounds including flavins increases with temperature [112]. This could explain higher biocorrosion at 45˚C. Addition of flavin shuttles in this media did not enhance corrosion at 25˚C and 35˚C. As explained before, this can be related to complex factors affecting riboflavin efficiency. Besides, studies show that most bacterial cell walls are imper.meable to external riboflavin [113]

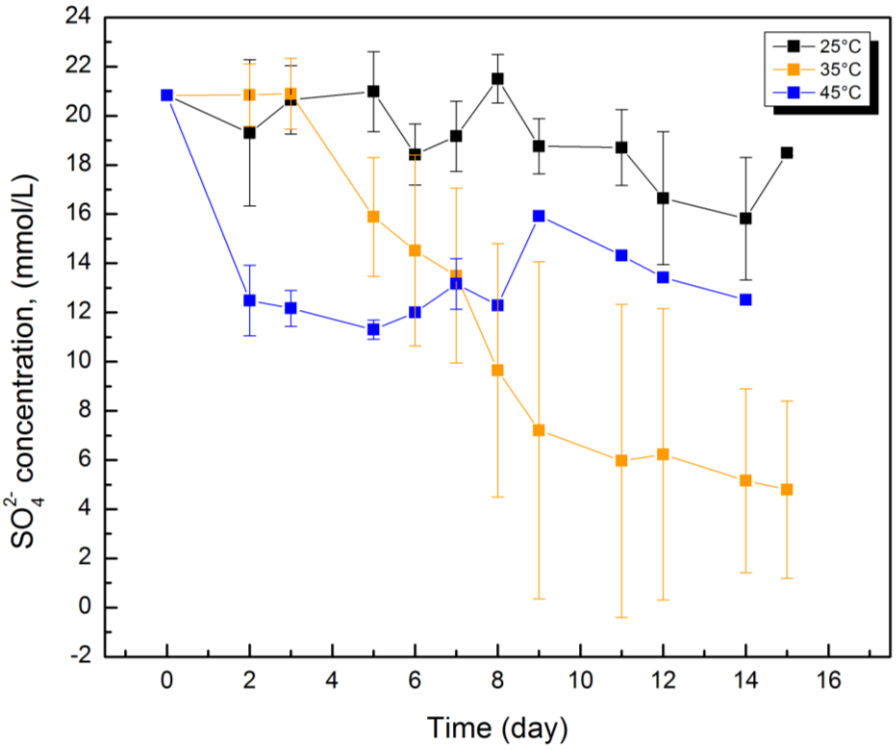

Figure 4.10- Average sulfate concentration for D. vulgaris in 1249-LFR media

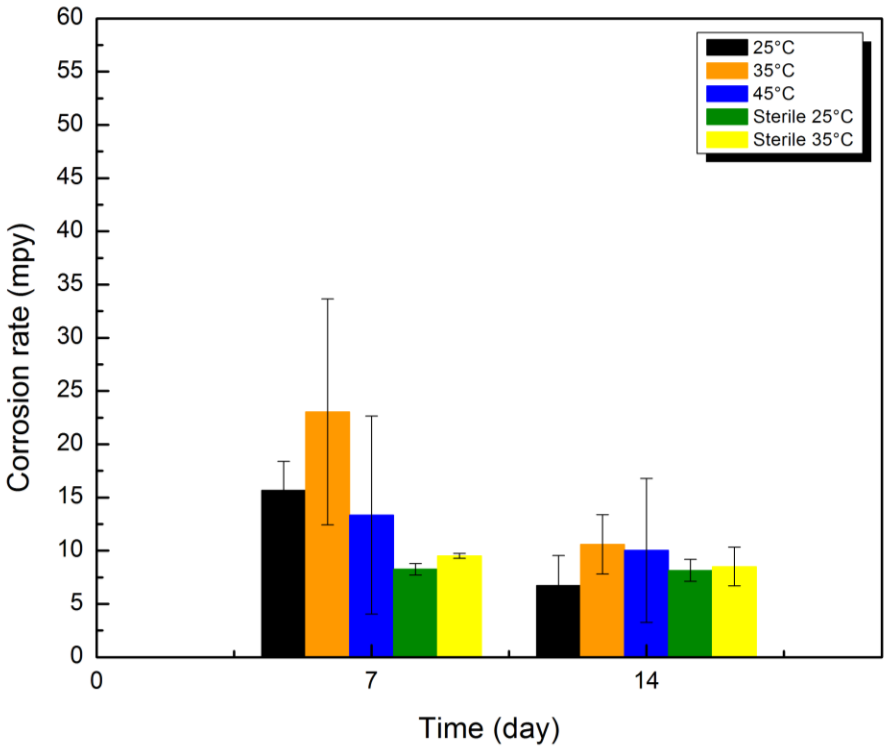

Figure 4.11- Average corrosion rate vs. time for D. vulgaris in 1249-LFR media

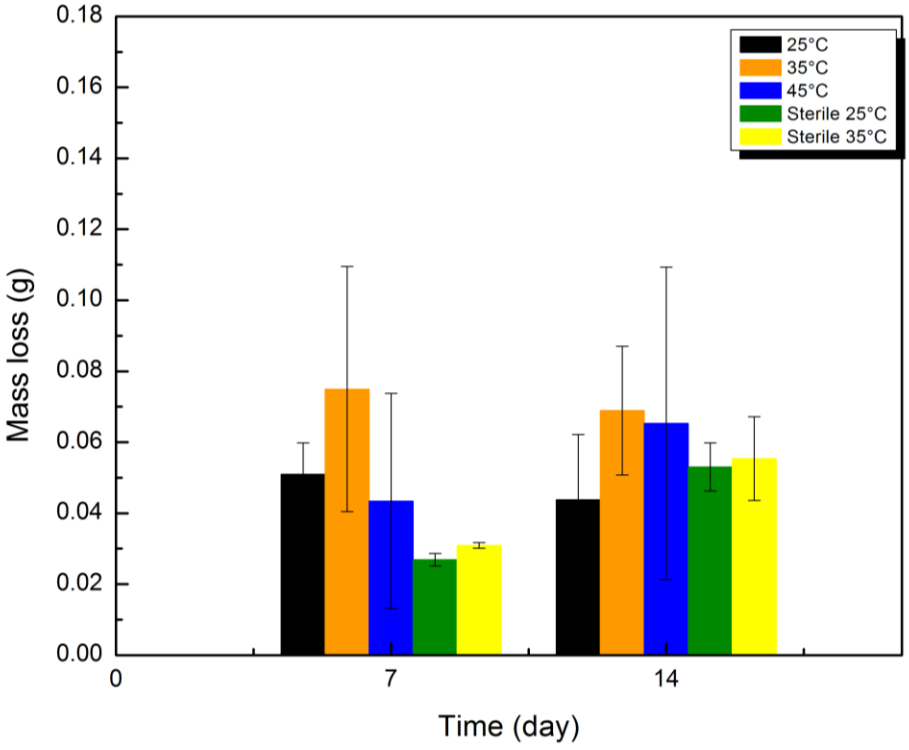

Figure 4.12- Average mass loss vs. time for D. vulgaris in 1249-LFR media

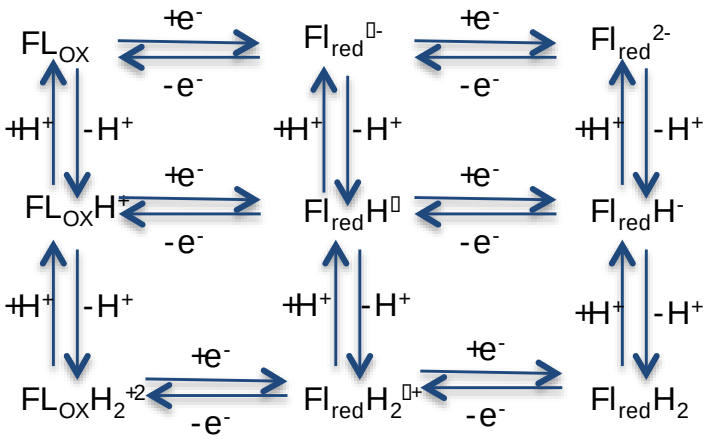

Figure 4.13- Possible pathways of flavins oxidation-reduction in aqueous solution- adapted from [108].

4.3.4 Growing of D. vulgaris in the (1249, 1249-LF, and 1249-LFR media) absence of carbon steel coupons

D. vulgaris was grown in 1249, 1249-LF, and 1249-LFR media in the absence of any carbon steel coupons. These experiments reveal whether D. vulgaris can grow in the latter two media without the presence of iron as a potential electron donor, or not. Samples were placed at 35˚C, the optimal growth temperature. Figure 4.14 shows the sulfate content curves as a function of time for D. vulgaris in these three media. Clearly there is no growth in 1249-LF and 1249-LFR media based on this figure. Also, there is no observed consumption of sulfate over 14-day period. In absence of Fe and organic electron donor SRB did not grow. It was previously demonstrated in section 4.3.2 and 4.3.3 that D. vulgaris survived in 1249-LF and 1249-LFR media in the absence of organic electron donor and presence of carbon steel coupons. This shows D. vulgaris used Fe^0, as the only potential electron donor, in order to thrive. As the iron was eliminated from samples along with organic electron donor, D. vulgaris did not survive. The growth of D. vulgaris in 1249 media, in presence and absence of iron, is the same with a consumption rate of 12.5 mmol/L/day for both conditions. This shows lactate is a competitive electron donor for metal. As long as lactate is present SRB utilize that as a source of energy and does not exploit metallic iron. As soon as lactate was eliminated, cells attack the iron for survival. These data validates the

conclusions made in the previous sections and confirms D. vulgaris direct-electron uptake capabilities.

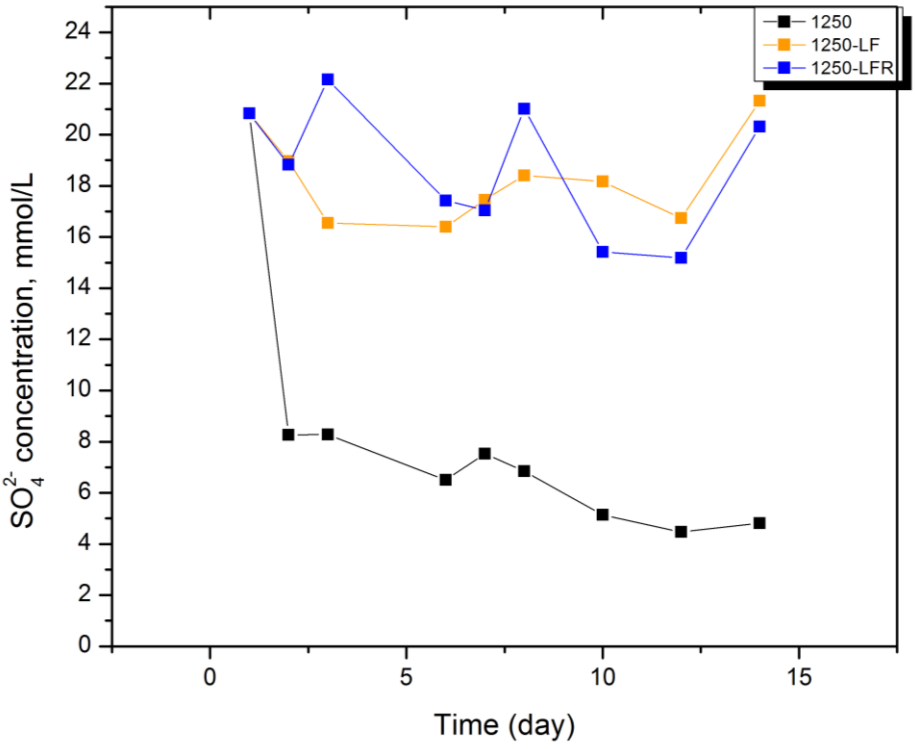

Figure 4.14- D. vulgaris in 1249, 1249-LF, and 1249-LFR media without coupon

4.3.5 Comparison of different conditions

4.3.5.1 Effect of types of growth media on mass loss

Three different media in this study were selected to evaluate possible pathways of MIC; full ATCC 1249 medium, ATCC 1249 medium minus lactate, and ATCC 1249 medium minus lactate plus riboflavin.

Figure 4.16 categorizes weight loss based on different immersion duration (7 & 14) and temperature (25, 35 & 45°C). In each category, three different media used in this study can be compared. For longer immersion periods of 14 days, there is more weigh loss in LF media in comparison to original media. It was shown in section 4.3.2 that SRB remains active during the whole period of 14 days in 1249-LF media, in spite of organic electron donor exclusion. This

agrees with the results of Xu and Gu (2014). It was shown by Xu and Gu that more weight loss was observed under carbon source scarcity conditions with D. vulgaris, although there were less sessile cell coverage on the coupons [103]. They concluded that D. vulgaris becomes more aggressive towards the metal in absence of organic electron donors, and in spite of the decrease in the cell population, weight loss increases. This phenomenon can be described by SRB cell-induced oxidation of the metallic iron. Cells can utilize Fe^0 through direct electron transfer (DET) or indirect mechanisms (Figure 4.15). Direct mechanisms include attaching to the surface of the metal or enabling transfer through bacterial nanowires. Indirect mechanisms happen through electron mediator compounds. These mediators facilitate electron transfer from the metal surface to the cells. Vitamins generally play the role of these mediator compounds. In this PhD study, we investigated riboflavin as a potential mediator compound. However mass loss data in Figure 4.16 did not indicate any rise in corrosion in presence of riboflavin. Corrosion was only enhanced at 45°C in LFR media in presence of riboflavin. The rise in mass loss at this temperature can be related to how mediator compounds interact with SRB cells. It was shown previously that mediator compounds including flavins are more effective at higher temperature [112].

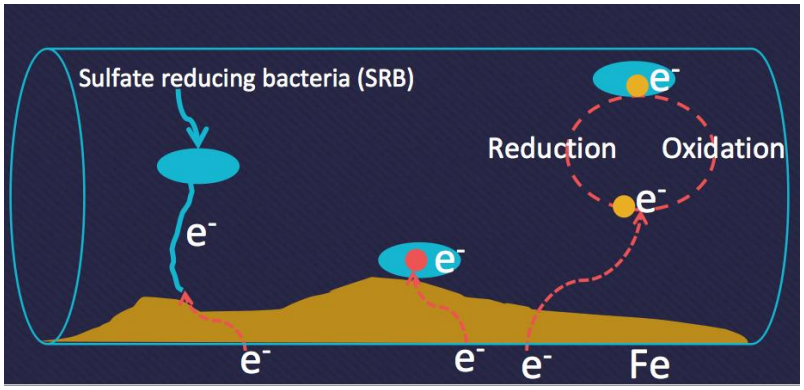

Figure 4.15-Schematic of Direct and indirect electron transfer mechanisms. Two SRB cells demonstrate direct e uptake and the one on the left demonstrate e uptake through mediator compounds.

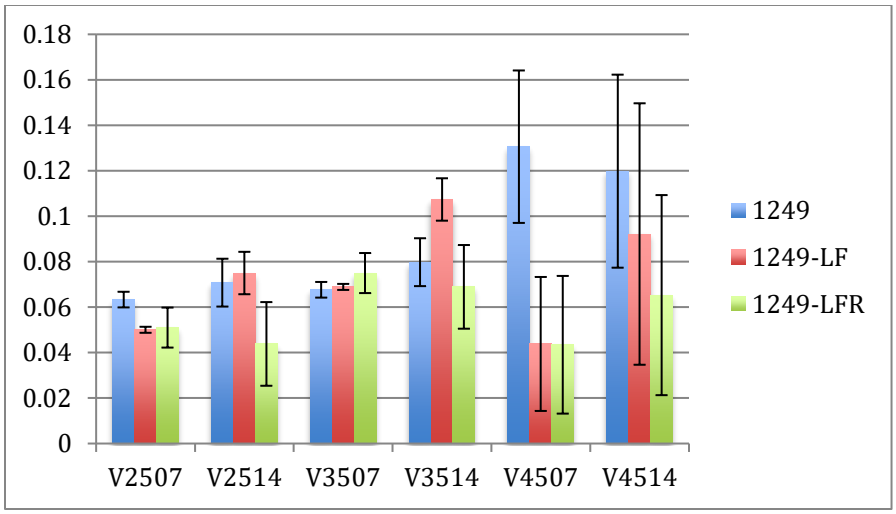

Figure 4.16- Mass loss after 7 and 14 days in different media

4.3.5.2 Determining the MIC Activation Energy

Activation energy (Ea) was calculated based on Eq. 4.6. The Arrhenius plots are presented in Figure 4.17 (Arrhenius plots in each media with error bars are included in the appendix).

$$\ln Cr\ \left(\frac{mg}{cm^2.hr}\right) = A\exp\left(\frac{-E_a}{RT}\right) \qquad \text{Eq. 4.6}$$

Activation energy values are shown in Table 4.1. No meaning full values were obtained in 1249-LF and 1249-LFR media during 7-day immersion period. As it was observed before there were not a distinctive increase in corrosion rate with temperature in these two media. However a clear increasing pattern in corrosion rate with temperature was seen in 1249 media.

During longer immersion periods, goodness of fit for 1249-LF and 1249-LFR media was significantly higher. This is mainly because there was an increasing trend in corrosion rate with rising temperatures. How the corrosion behavior changes at different conditions were already discussed in previous sections.

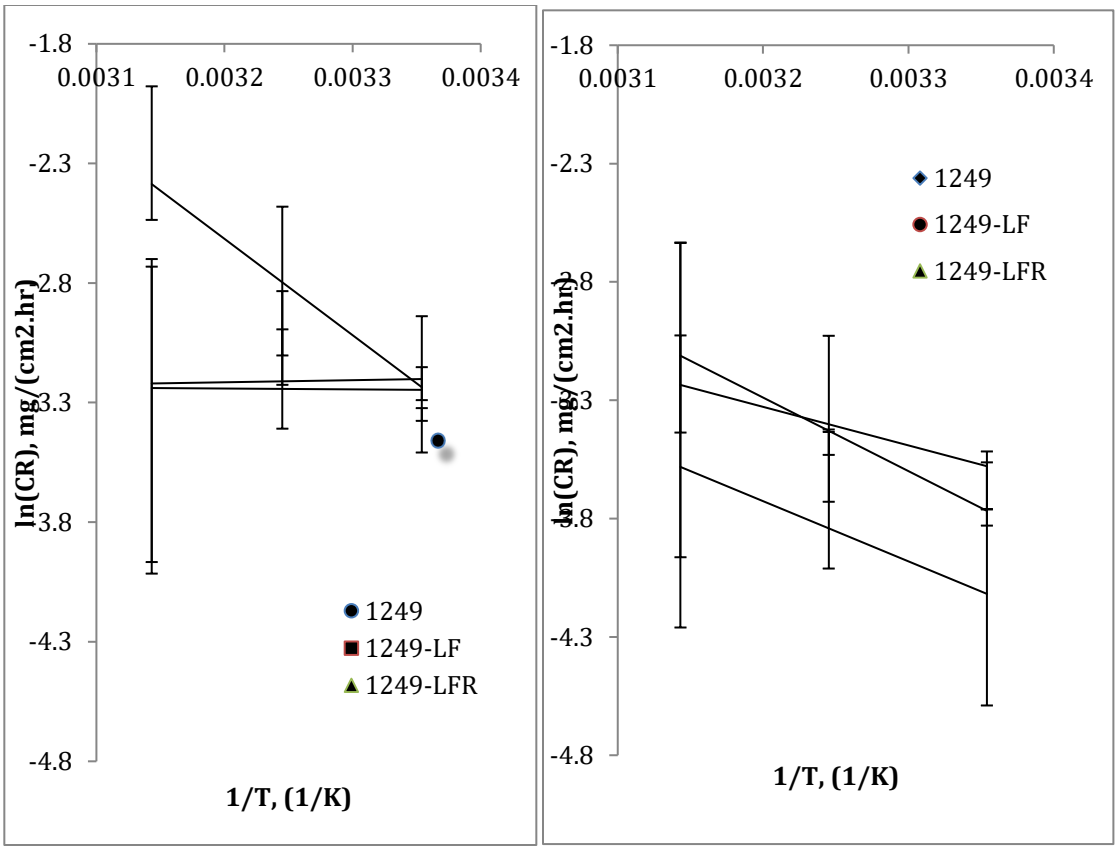

Figure 4.17- Arrhenius plot of corrosion rate; Left: 7 days, right: 14 days.

Table 4.1- Activation energy for D. vulgaris in kJ/mol

Media/ Immersion time	7 days	R^2	14 days	R^2
1249	33.487	0.792	25.838	0.868
1249-LF	0.296	0.0004	13.545	0.7248
1249-LFR	0	0.0016	21.149	0.872

4.3.5.3 The changes in pH

It was mentioned before that in SRB cultures, pH is expected to increase in spite of H_2S production. Because the sulfate reduction system in SRB produces HS^-, which consumes protons in the aqueous solution to produce H_2S ($HS^- + H^+ \rightarrow H_2S$). Thus, the pH increases during this process. pH has an increasing trend in media 1249 in Figure 4.18-a due to the reason mentioned. The decrease in pH in the second 7-day period at 45˚C in 1249 media can be related to less SRB

activity during this period. However, the total pH change over the whole 14 days is still positive (+0.5).

In media 1249-LF, however, pH decreases at 35°C, in spite of SRB's continued activity. In the LF media, there is no organic electron donor in the bulk solution. Thus SRB need to utilize electrons from the iron to survive. We have already observed in section 4.3.2 that SRB stays active in the absence of organic electron donors. In order to utilize the iron, SRB need to be close to the iron surface. They cannot find electrons in the bulk solution. When they colonize on the iron surface, most of the HS^-produced through SRB sulfate reduction system is concentrated on the surface of the metal rather than in the bulk solution. Thus this bisulfide species is adsorbed to the surface of the metal. This adsorbed bisulfide species can react with iron to produce iron sulfide and proton [114]. These species can be formed through chemical or electrochemical pathways (Eq. 4.7 and Eq. 4.8) [115]. This explains the decrease in pH in LF media at 35°C. The suggested chemical reactions are as follows:

$$Fe + HS^-_{aq} \rightarrow FeHS^-_{ads} \qquad \text{Eq. 4.7}$$

$$FeHS_{ads} \rightarrow FeHS^+_{ads} + e^- \qquad \text{Eq. 4.8}$$

$$FeHS^+_{ads} \rightarrow FeS_{ads} + H^+ \qquad \text{Eq. 4.9}$$

a. b.

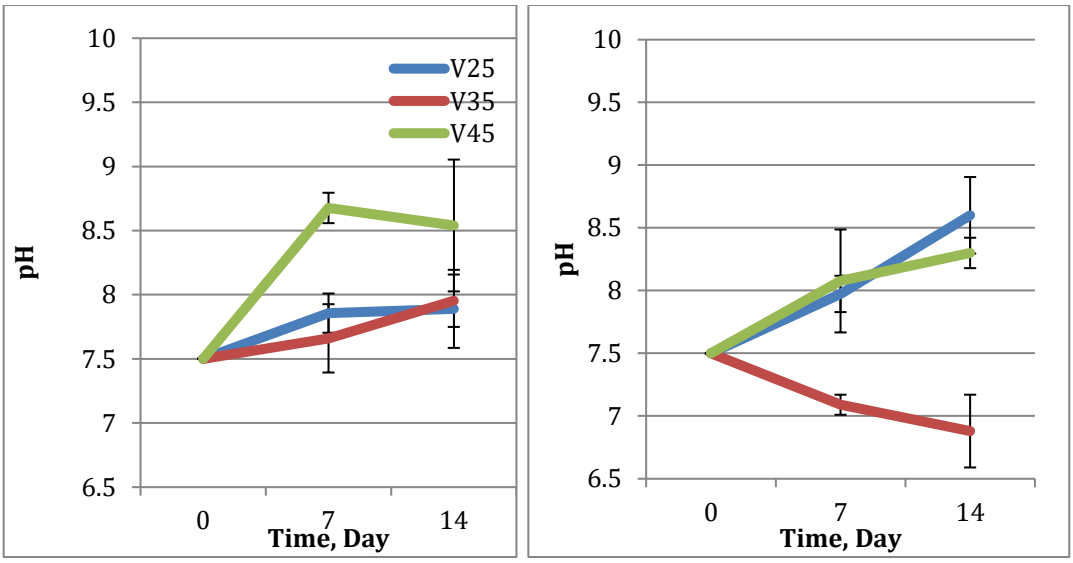

c.

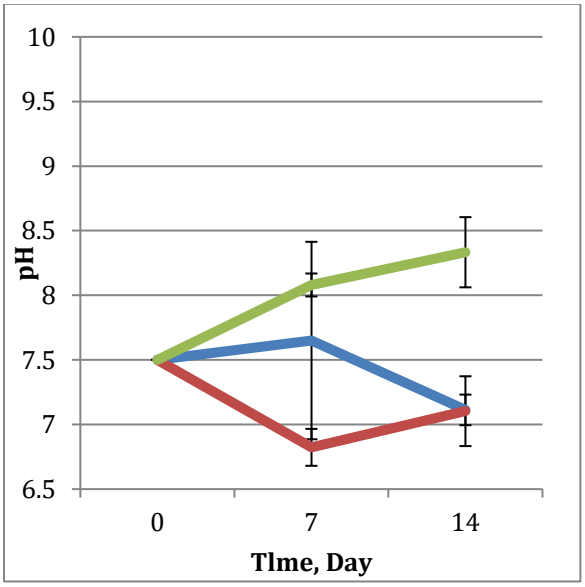

Figure 4.18- Average pH values vs. time in (a) Media 1249. (b) 1249-LF. (c)1249-LFR.

Unlike the decrease in the pH values at 35°C, at 25°C the pH increased. As shown previously in section 4.3.2, based on the sulfate content as a function of time graph at 25°C, SRB did not display that much activity, which means less HS^- production. When coupons were retrieved from the media at 25˚C, slight orange powder was seen on the coupons and the black FeS layer was very thin, unlike the 35˚C samples. This suggests that a less dense biofilm was

formed on the surface of V25-LF samples and most of $HS^-$was diffused through the solution and consumed protons. Another explanation is that $Fe(OH)_2$ was formed through the chemical reaction in Eq. 4.11 ($Fe(OH)_2$ is identified with reddish orange color) [116]. Then the $Fe(OH)_2$ reacts with HS^- and produces hydroxyl ions (OH^-) that promote pH increase. Same reasoning can be used for coupons at 45˚C in LF media. Traces of reddish orange powder can be found on 7-day and 14-day coupons from both LF and LFR media (Figure 4.19).

A B

Eq. 4.10- A. coupons retrieved from media 1249-LF after 7-days (3 coupons on the left were at 35°C and 3 coupons on the right were at 25°C) B. coupons retrieved from media 1249-LF after 14 days (3 coupons on the left were at 25°C and 3 coupons on the right were at 35°C).

Figure 4.19- Coupons tested at 45˚C from left to right: V4507. V4507-LF, V4507-LFR, V4514, V4514-LF, V4514-LFR.

$$Fe + 2H_2O \rightarrow Fe(OH)_2 + 2e^- + 2H^+ \quad \text{Eq. 4.11}$$

$$Fe(OH)_2 + HS^-_{aq} \rightarrow FeS + OH^- + H_2O \quad \text{Eq. 4.12}$$

pH decreased at 35˚C in 1249-LFR media. Similar trend was observed for this temperature in 1249-LF media. Similar explanations can be attributed to the pH decrease in this

media as well. Growth was mainly observed at 35˚C in LFR media. Thus trapped HS^- under biofilm and formation of $FeHS_{ads}$ layer can be the cause of pH decrease. pH increased at 45˚C, which can be interpreted in terms of proton scavenge by HS^- species.

4.3.6 SEM Analysis at 45˚C

Coupons at 35˚C were mostly covered with corrosion products after they were withdrawn from the solution. Samples at 45˚C demonstrated higher SRB activity than 25˚C. Thus they were selected for SEM analysis. It can be seen from Figure 4.20-a SRB colonized on carbon steel surface. Visualization of the cells was hard in this media because there were more SRB activity (sulfate consumption) in this media and coupons were covered with FeS. Figure 4.20-b shows carbon steel coupon in media 1249-LFR. SRB cells were not detected on the surface of this coupon. It was mentioned in sulfate consumption calculation in LFR media, SRB did not demonstrate much activity. Figure 4.20-c shows carbon steel coupons in 1249-LF media. SRB cells were clearly visualized on this sample. It shows that despite of organic electron donor elimination, cells survived and colonized on the surface of metal to access Fe^0.

a. b.

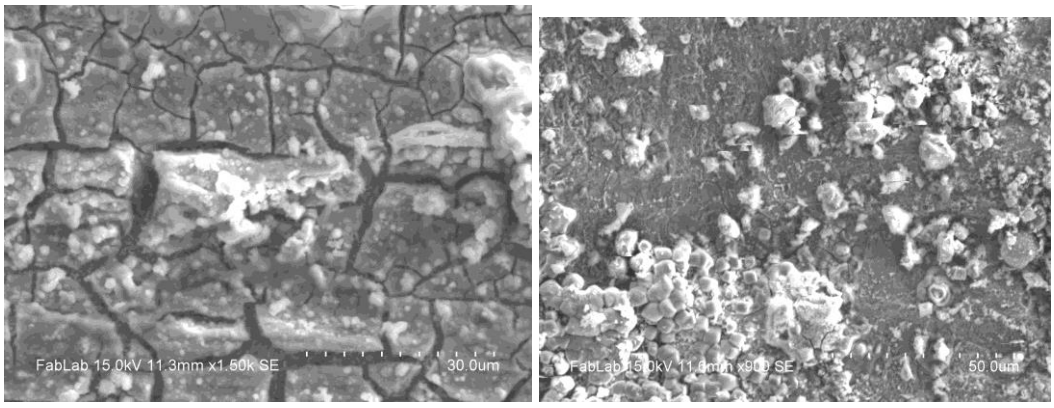

Figure 4.20-(a) SEM image of carbon steel coupon at 45˚C in 1249 media for 7 days. (b) SEM image of carbon steel coupon at 45˚C in 1249-LFR media for 7 days

c.

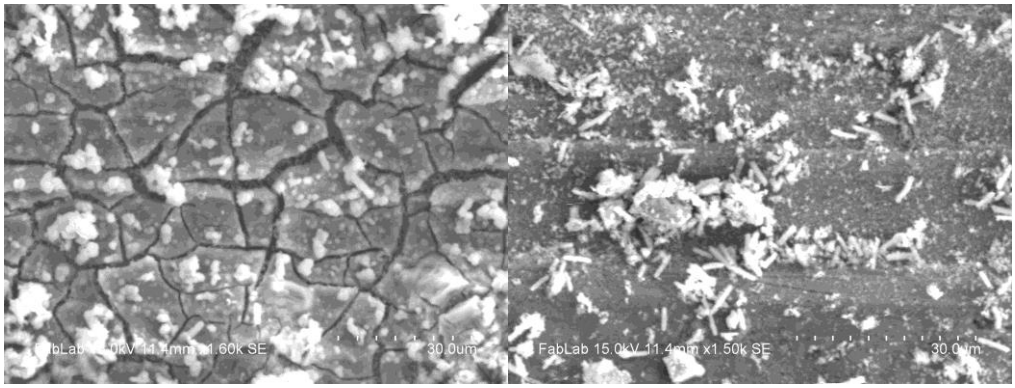

Figure 4.21- SEM image of carbon steel coupon at 45˚C in 1249-LF media for 7 days

4.3.7 Pitting Corrosion

Coupons were analyzed under SEM after cleaning for detection of pitting corrosion patterns. Coupons were cleaned and dried before SEM measurements. Pitting analysis was performed on coupons at 25˚C and 35˚C in all 3 media. At each condition 2 images are included at two different magnifications. First image is at 350X magnification to give a vision of pitting pattern at each spot. Second image is the same spot at 1.5K magnification to better visualize pits depth on the coupon surface.

Figure 4.22 and Figure 4.23 depict coupon surface at 25˚C in 1249 media. Coupons at this condition were covered with pits at different spots. Similar trend was observed for coupons at 35˚C in 1249 media (Figure 4.24 and Figure 4.25). Dense pitting patterns were observed on the surface of the coupons. However pits seemed deeper at 35˚C than 25˚C.

In 1249-LF media pitting patterns seem to alter slightly. There was less densely pitting clusters. Pits were more scattered on the surface (Figure 4.26-Figure 4.29). Another clear trend in this media was deeper pits at longer exposure times. In this media, partial population of SRB are supressed due to the elimination of lactate as it was mentioned in section 4.3.2. This explains less pitting clusters on the surface. However less pitting does not mean less corrosion. Pits are deeper in this media due to higher affinity of SRB to metal surface. This is another proof that D. vulgaris extract electrons directly from Fe. D. vulgaris needs to stay close to the iron surface to survive. It takes up electrons from the metal and induces deeper localized pits on the surface. Deep pits are

more critical than wide pits because deep pits can finally perforate the material. This leads to disastrous pipe failures in oil and gas industry. SRB initiated a more critical attack in LF media. Corrosion rate might be comparable or even less than 1249 media, however SRB triggers a more aggressive attack by penetrating deep into the metal. This type of corrosion is of crucial importance. Uniform corrosion or general loss of material does not necessarily lead to failure of material. This clearly reveals why the MIC pathways should be fully understood to design appropriate preventive measures.

Figure 4.30 and Figure 4.31 illustrate pitting in LFR media at 25˚C and 35˚C. Pitting pattern is similar to LF media. There are scattered localized pitting spots. This suggests that there was a patchy less populated biofilm on the surface of the coupon. A clear distinction of pitting pattern could not be made between LF and LFR media.

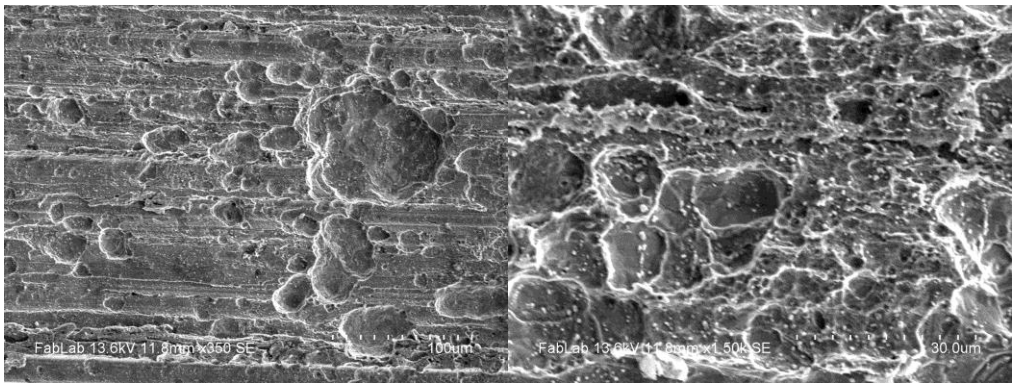

Figure 4.22-Coupon at 25˚C and 7days in 1249 media

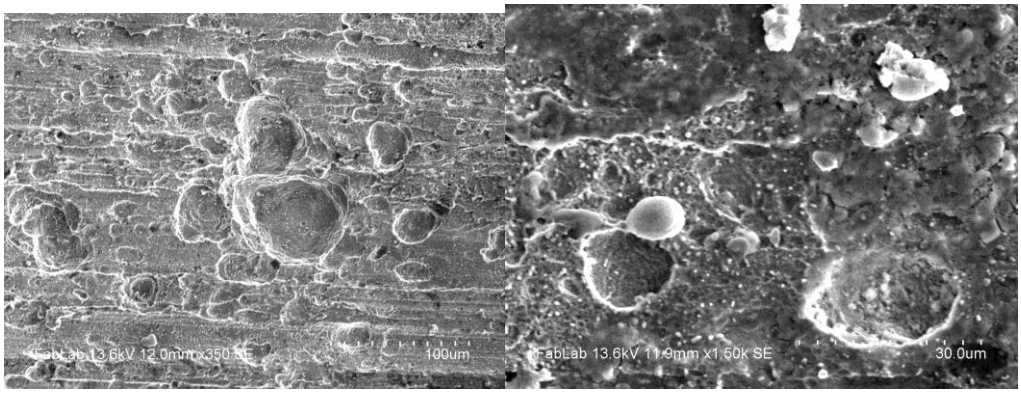

Figure 4.23-Coupon at 25˚C and 14 days in 1249 media

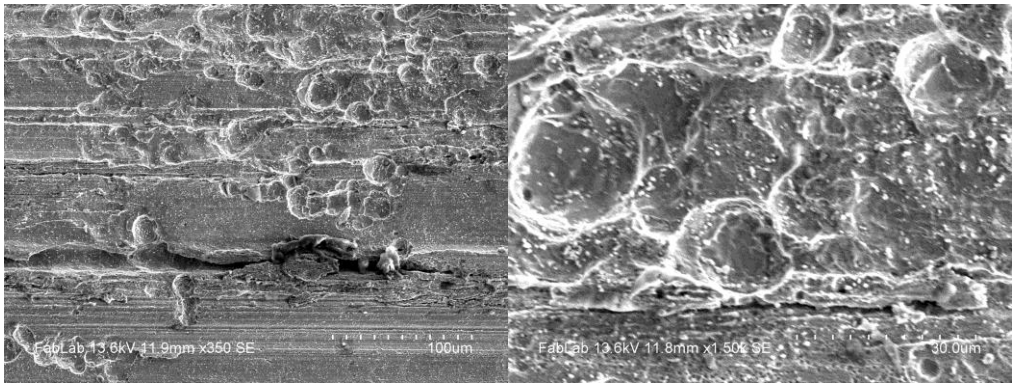

Figure 4.24-Coupon at 35˚C and 7 days in 1249 media

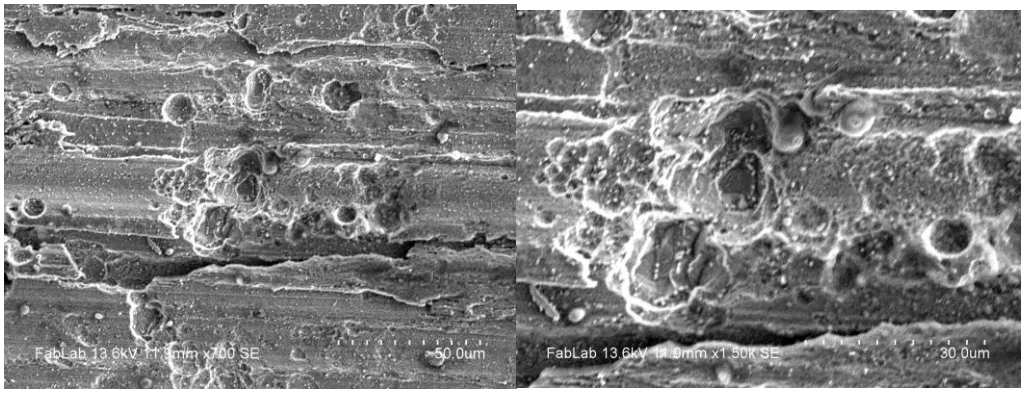

Figure 4.25-Coupon at 35˚C and 14 days in 1249 media

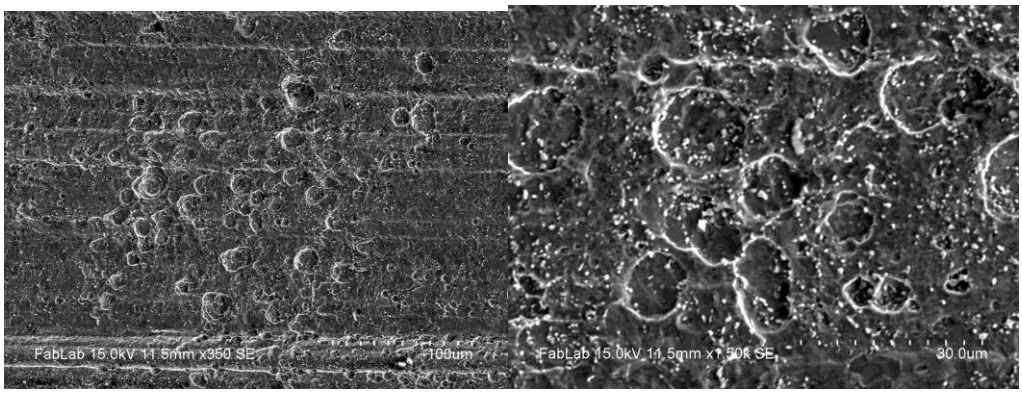

Figure 4.26-Coupon at 25˚C and 7 days in 1249-LF media

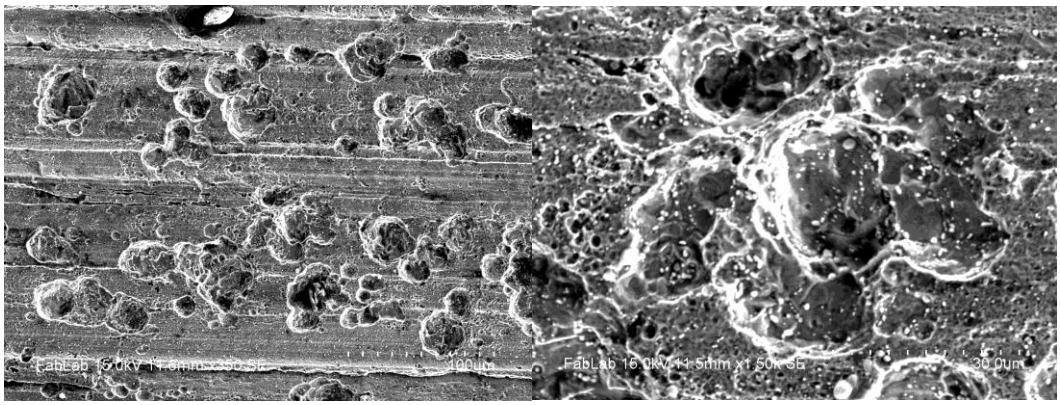

Figure 4.27-Coupon at 25˚C and 14 days in 1249-LF media

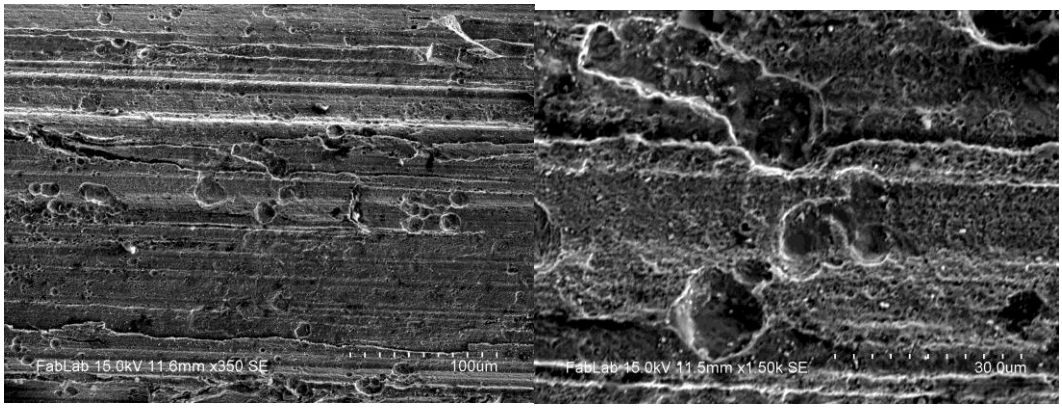

Figure 4.28-Coupon at 35˚C and 7 days in 1249-LF media

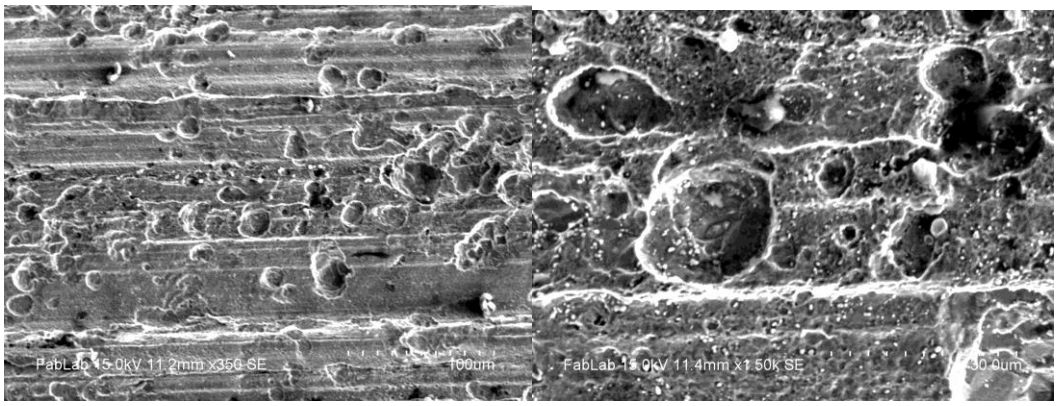

Figure 4.29-Coupon at 35˚C and 14 days in 1249-LF media

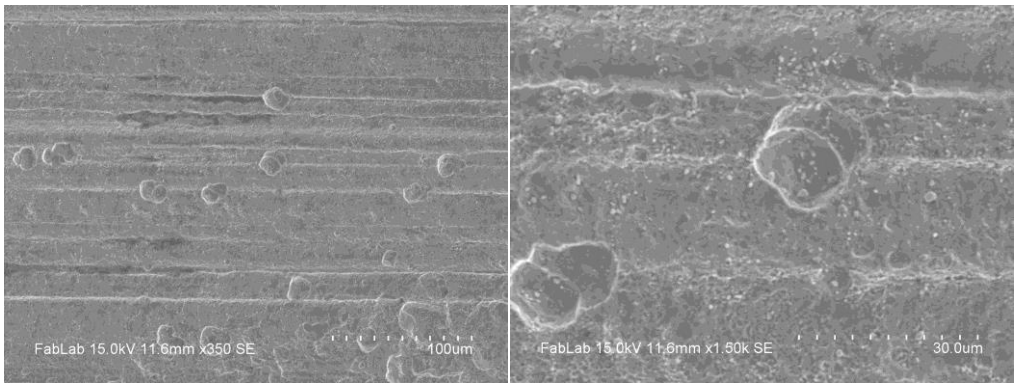

Figure 4.30-Coupon at 25°C and 7 days in 1249-LFR media

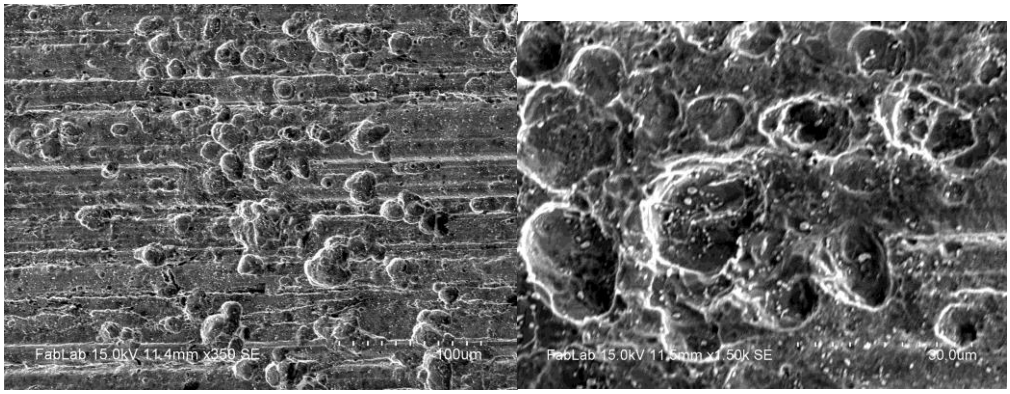

Figure 4.31-Coupon at 35°C and 7 days in 1249-LFR media

4.3.8 Identification of the corrosion products using FTIR spectroscopy

The chemical structures of the corrosion products (in form of powder) were identified with FTIR after the samples were taken out from the solutions. Samples were left to dry for one day in the desiccator to reach complete dryness. Then the powder was scraped off and grinded for FTIR analysis. The powders were partially oxidized during these processes. Thus iron (oxyhydr) oxide minerals peaks were observed in the FTIR spectra. Sulfide is a byproduct of SRB metabolic activity. Mackinawite (FeS), and pyrite (FeS_2) are expected to be the main corrosion products. Mackinawite is a metastable and can transform to greigite (Fe_3S_4) and pyrite [117]. Under reducing conditions, iron sulfides are stable. However when they are exposed to humidity and oxygen they corrode and form iron sulfates [118]. Pyrite oxidation can occur through various pathways. O_2 and Fe^{3+} are generally the oxidant agents. However under anaerobic conditions the dissolved O_2 in H_2O can be the only oxidant. Pyrite can react with water to form sulfate anions

through these half reactions Eq. 4.13-Eq. 4.14 [119]. The presence of sulfate group bands in the FTIR spectra of samples were confirmed. FTIR spectra were analyzed for all samples. At each condition, one FTIR spectra is selected from the experiments that repeated three times. The FTIR spectra of samples for 7 –day and 14-day immersion period were shown in Figure 4.32 and Figure 4.33. The spectra are shown at decreasing temperatures order (45, 35, 25˚C) from bottom to top. Each temperature range belongs to one media; the first three bottom spectra are in media 1249, the second three spectra are in media 1249-LF, and the last top spectra are in media 1249-LFR. No variation in the peaks observed based on varying temperatures in each media. The narrow temperature range can explain for these observations. The FTIR spectra for different samples were also compared based on the duration of immersion at each temperature. Immersion period did not induce much of a difference in the FTIR spectra. FTIR spectra of all samples are included in appendix. The characteristic absorption peaks of mackinawite can be detected in the spectra with the following wavenumber (1030-1070, 1412, 1560, 1640) cm^{-1} [117]. Three absorption peaks are observed in the 1012- 1070 cm^{-1} range that can be assigned to S-S and Fe-S stretch [117]. The absorption peak at 1158 cm^{-1} can be assigned to Fe=S stretch [117][120][121]. The peak at 1622 suggests the presence of Fe-SO_4 group [122]. The absorption peak at 3150 cm^{-1} can be assigned to OH stretch in the goethite which can be formed due to the oxidation of the powder of the corrosion products during the preparation process. Additionally, there are two peaks in the range of 740-877 cm^{-1} appear in the FTIR spectra of 1249-LF and 1249-LFR media. These absorption peaks can be assigned to goethite structure [123]. As mentioned in the previous section, orange powder was observed in 1249-LF and 1249-LFR samples that is the typical color of goethite. The powder from 1249 media was completely black, which explains the absence of these peaks.

$$FeS_2 + 8H_2O \rightarrow Fe^{3+} + 2SO_4^{2-} + 16H^+ + 15e^- \qquad \text{Eq. 4.13}$$

$$FeS_2 \rightarrow Fe^{3+} + 2S + 3e^-$$ Eq. 4.14

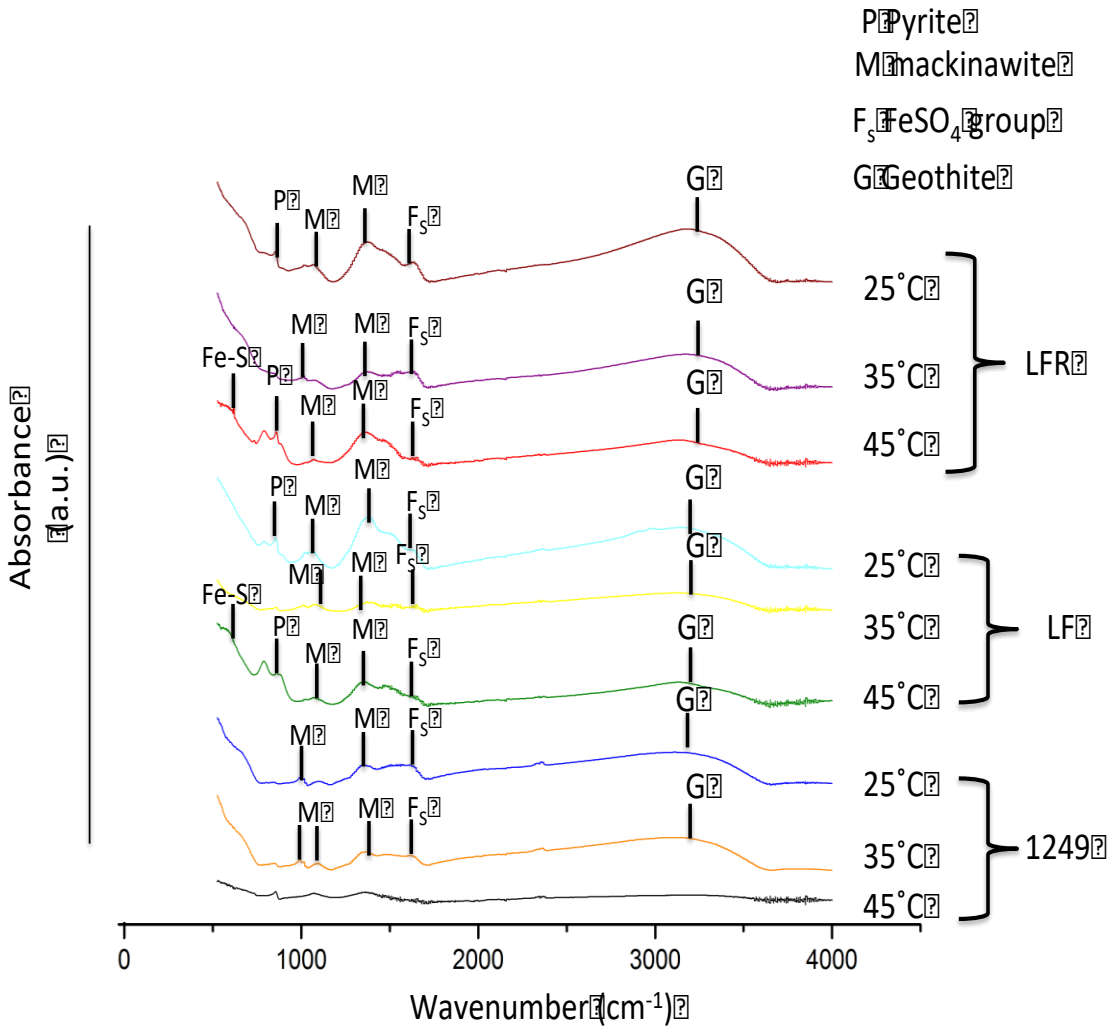

Figure 4.32- FTIR spectra of 7-day samples

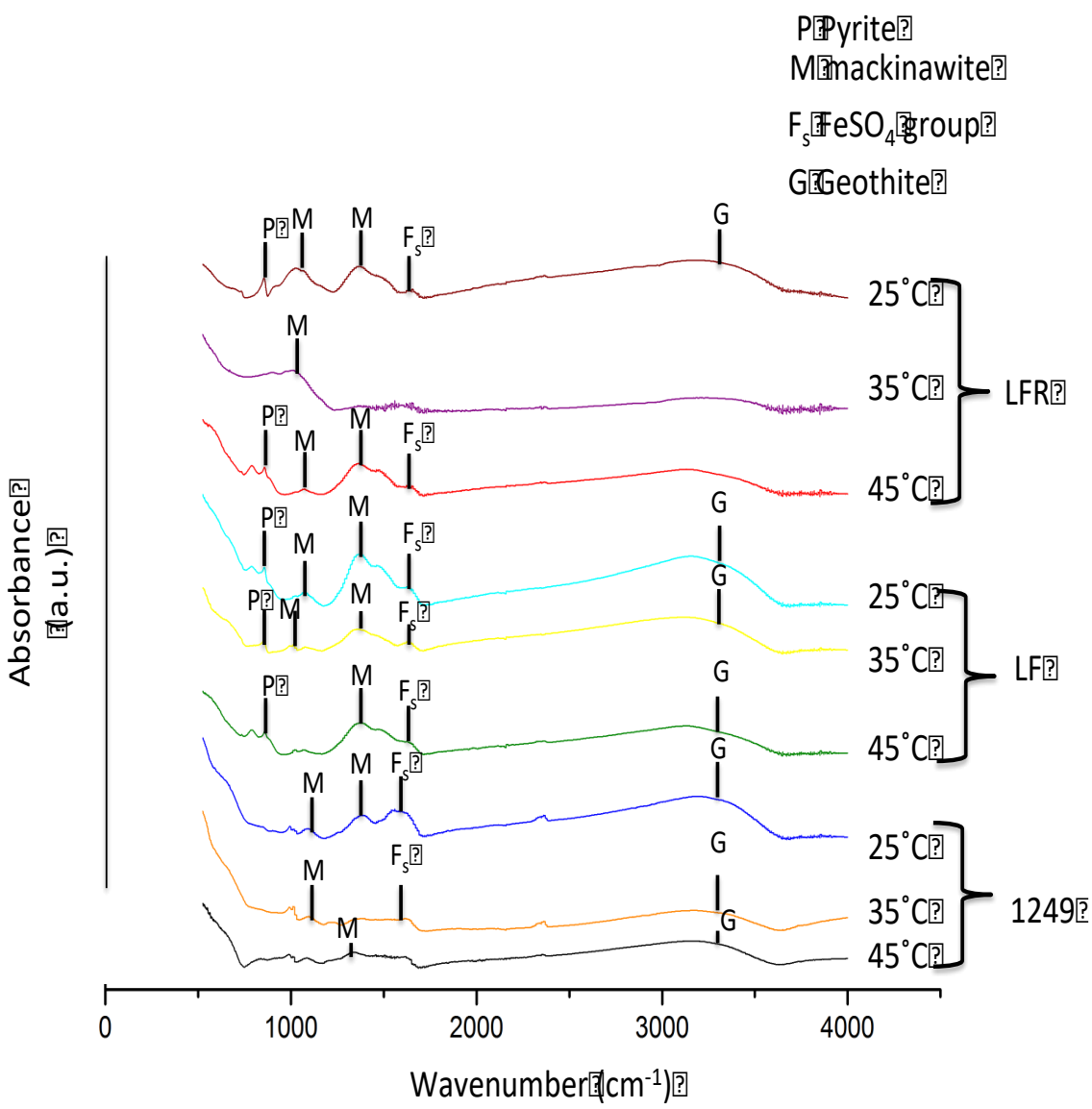

Figure 4.33- FTIR spectra of 14-day samples

4.3.9 Electrochemical measurements

In order to shed further lights on the mechanisms of MIC by SRB, a series of electrochemical measurements were performed. These tests were performed in a span of 2-3 weeks on sterile (abiotic) and incubated samples. Media 1250 was used for sterile samples. Abiotic tests were conducted anaerobically with deoxygenated media. In biotic tests, D. vulgaris was cultured and added to 1249-LF media in the electrochemical cell. Media 1249-LF was used for the electrochemical tests for the purpose of stimulating D. vulgaris electron uptake

capabilities. In this test, electrochemical cell was filled with 750 ml 1249-LF media. 2 ml of D. vulgaris culture was added to the solution in the anaerobic chamber and left in the incubator for 24 hrs. Then the electrochemical cell was connected to potentiostat for electrochemical measurements. In addition to these test conditions, after a 3-week span for solution with D. vulgaris, working electrode was taken out and immersed in 2% glutraldehyde solution to inactivate SRB cells. Then it was placed back in the electrochemical cell with fresh media for further testing.

4.3.9.1 Polarization resistance vs. time

Evolution of polarization resistance (Rp) was monitored over time. Rp in the solution with D. vulgaris increased till day 8 (Figure 4.34). Then it started dropping significantly to 300 $\Omega.cm^2$. The primary increase in Rp can be related to formation of a film on the surface of the metal by cells [124][125]. This film contains macromolecules like proteins and lowers the corrosion current due to its non-conductivity[126]. However biofilm has a patchy structure and does not provide a protection layer on the metal over time. Polarization resistance is inversely proportional to corrosion current. Drop in the Rp is an indication of high current on the surface of the metal. This high current can be related to electron transfer from the metal to SRB cells. The Rp drops after SRB colonize completely on the surface of the electrode. As the cells continue metabolizing, they require the electrons from the metal and start utilizing electron from metallic surface. The current can also be related to the formation of conductive FeS layer.

Rp was measured after glutaraldehyde treatment to evaluate only the role of the corrosion layers without the presence of SRB. Recorded values show a rise in Rp. It reaches values of 500 $\Omega.cm^2$after inactivation of SRB cells. This shows that elimination of SRB reduces the corrosion vulnerability of the electrode.

The trend in sterile solution was the opposite. At the beginning of the measurement, there was an increase in Rp (Figure 4.34). This was due to the hydrogen film formation at the initiation

of corrosion process. Literature suggests 3 major hydrogen reactions in metal-liquid systems: hydrogen ion reduction, adsorption, and diffusion of hydrogen atoms into metal lattice [127]. In aqueous solution the surface of metal is charged due to polarity of water molecules. Hydrogen ions adsorbed to the metal surface and form a double layer with capacitor properties [128]. In essence, H_3O^+ ions are discharged on metallic phase and provide protection for the metal.

Then polarization resistance in abiotic system started decreasing over first 8 days. This is due to hydrogen evolution reaction when hydrogen atoms are combined and return into the solution in form of gas. After day 9th Rp started increasing up to 16 $k\Omega.cm^2$. The increase in Rp in the sterile solution is due to the precipitation of media components on the surface of the electrode that remained unused in absence of SRB. (Note: abiotic test was conducted for 2 weeks and biotic test was continued for 3 weeks)

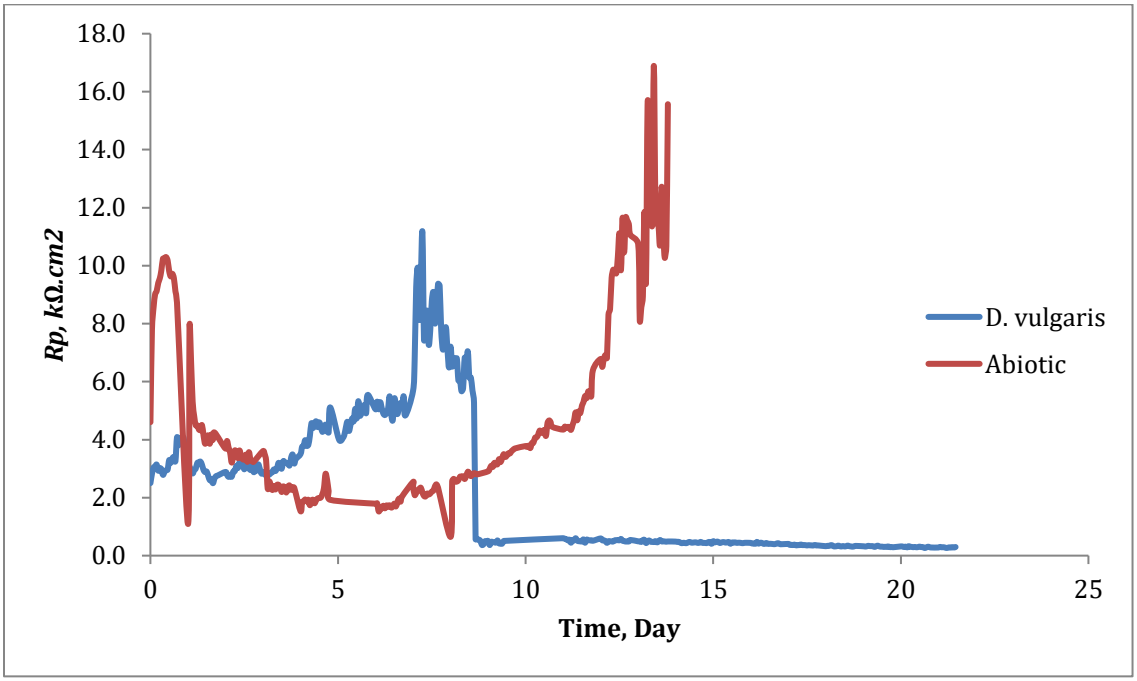

Figure 4.34-Daily measured polarization resistance values in span of 2-3 weeks for D. vulgaris and abiotic system.

4.3.9.2 Potentiodynamic current monitoring

Cathodic current was recorded during 2 weeks for two separate systems; system incubated with D. vulgaris and abiotic system. Cathodic current density is a very good measure

of quantifying electron transfer due to SRB activity. SRB activities affect the cathodic reaction. Therefore any increase in cathodic current can be interpreted in terms of enhancement in electron transfer. Working electrode was polarized in negative direction for up to 0.4 mV during these experiments. Direct electron transfer in SRB cells are usually ascribed to proteins called cytochrome [126]. These proteins go through oxidation-reduction reactions through iron ions presents in their heme structure [37]. The iron in cytochrome structure can alternate between Fe (II) and Fe(III) oxidation states to transfer electrons (Figure 4.35). It was shown that these proteins operate at low redox potentials to enable electron transfer in bacterial outer membrane [129][130]. Studies have shown that these proteins enable electron transfers in the range of -0.125 to -0.4V vs. SHE [131–134]. More specifically redox potential of cytochrome c3 in D. vulgaris was in the range of -0.120 to -320 V vs. SHE (-0.32 to -0.520 V vs. Ag/AgCl) [131]. Thus carbon steel electrode was polarized to very low potentials to attain suitable conditions for these proteins to operate.

Cathodic current density is displayed at 5 different time points in Figure 4.36. Two-time points were selected at the beginning of the experiment (day 1 and 2), two-time points where the Rp trend in both systems transform (day 9 and day 12) and one time point at the end of experiment. On day 1 and 2, cathodic current density for incubated system is higher than abiotic system (Figure 4.36a). On day 9 and 12, cathodic current density even diverges more from abiotic system and the highest current recorded is more than one order of magnitude greater than abiotic system (Figure 4.36b). This indicates the biological cathodic activity in the biotic system due to more cell activity [42]. This current density in the biotic system can also be due to semiconductive FeS layer. Similar trend is observed at day 14 (Figure 4.36c). The cathodic current density in biotic system dominates the abiotic system. It can be seen as the potential moves towards the more negative the current increases exponentially. As previously mentioned, this is in agreement with operation of cytochrome at low redox potentials [135]. In contrast, in abiotic system the variation in current has a much smaller range due to absence of bacteria.

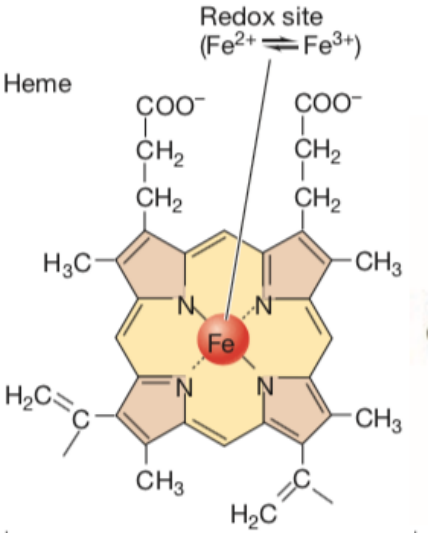

Figure 4.35- structure of iron-containing cytochrome. Cytochromes undergo redox reactions through loss or gain of electrons by the iron atom in their structure [37]**).**

a. b.

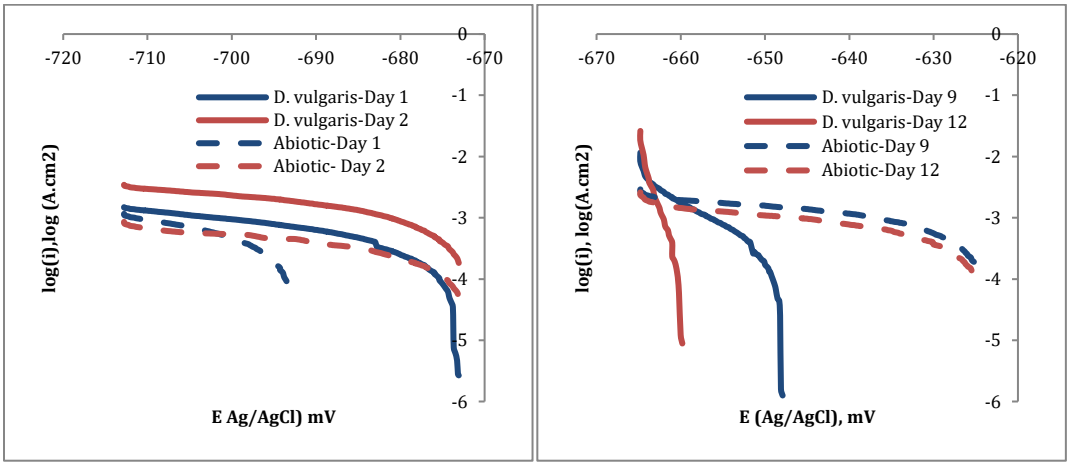

c.

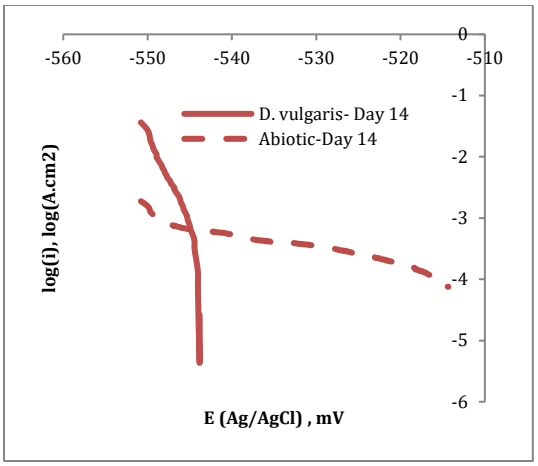

Figure 4.36-Cathodic current density vs. applied potential (displayed vs. standard Ag/AgCl reference electrode, E (Ag/AgCl)) for incubated system with D. vulgaris and abiotic system at different time points. (a) Day 1 & day 2. (b) Day 9 & day 12. (c) Day 14. Abiotic system is shown with dashed line in all figures.

4.3.9.3 Corrosion potential monitoring

Corrosion potential was measured daily every 20s for duration of 1.5 hr. There was not much of a change in corrosion potential in 1.5 hr. The E_{corr} values were averaged for that duration and depicted in Figure 4.37 (error bars are very small as you can see due to little variations of E_{corr}). It can be visualized from this figure that there is positive shift in E_{corr} after 8 days. E_{corr} in biotic system, shifts from -694 mV/Ag/AgCl to -523 mV/Ag/AgCl at this point and reaches a steady state. This shift is an indication of SRB activity that promoted redox quality of the medium [124]. This positive shift in E_{corr} is called ennoblement [136]. This is due to biofilm formation on the surface of the metal [137]. Ennoblement lead to higher probability for pitting corrosion for passive alloys [138]. The colonization of SRB on the metal surfaces affect the electrochemical process by accelerating cathodic reaction [139]. Acceleration of cathodic reaction was also exhibited in light of ennoblement by numerous researchers studying different alloys [140][141][142]. There is also a positive shift in E_{corr} in abiotic system, however this shift is very small in comparison to biotic system (25 mV).

Two red points displayed in Figure 4.37 are measured E_{corr} values after glutaraldehyde treatment. When the 3-week experiment for D.vulgaris was finished, carbon steel electrode was taken out of the aqueous solution and placed in glutaraldehyde solution to deactivate SRB cells.

After one day, it was placed in electrochemical cell with fresh 1249-LF media to measure E_{cor}. There was a significant drop in E_{cor} post-treatment. This confirms that the ennoblement was due to SRB cells and the acceleration of cathodic reaction by cells. The corrosion potential data also agrees with that of Rp measurements. The shift in both data occurred at day 8. Al Abbas et al. also observed initiation of ennoblement after 7 days during E_{cor} measurements in their biotic system [124].

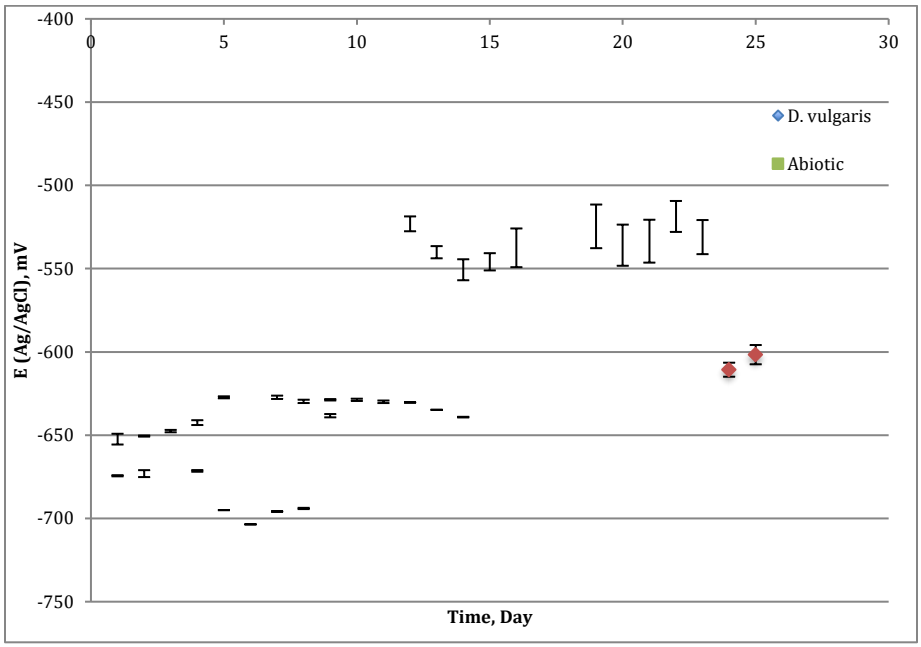

Figure 4.37- Corrosion Potential (displayed vs. Ag/AgCl reference electrode) for D. vulgaris and abiotic system. Two red dots are for post-glutaraldehyde treatment.

Chapter 5 - Microbial-induced corrosion on C1018 carbon steel by D. bastinii

5.1 - Background and motivation

Introduction of direct electron uptake theory has received a lot of attention from many researchers. In 2004, Dinh et al. enriched sulfide-rich marine sediment samples that led to finding of a novel SRB strain that could corrode iron without utilization of hydrogen. As mentioned earlier, cathodic depolarization theory, which is generally accepted as the main MIC mechanisms, explains MIC by SRB removal of the hydrogen from cathodic sites to accelerate cathodic reaction. In Dinh et al. (2004) study, iron was used as the sole electron donor. He successfully isolated two novel strains that demonstrated direct electron uptake capabilities. This opened a new path in MIC research. However, this mechanism has only been tested for a few SRB strains. This leaves the question whether this mechanism is the dominant pathway for MIC. If it is, then other SRB strains should posses the same capability of direct electron uptake from metallic iron. In order to answer this question, in this PhD work, D. bastinii, a common SRB strain, is subjected to various designed experiments including corrosion immersion tests and electrochemical analysis to investigate possibility of the direct-electron-uptake theory. This chapter summarizes and discusses the results for D. bastinii.

5.2 - Experimental Set-up

The following three different media were tested for D. bastinii:

4. The first media was the original growth media (ATCC 1250 media). Since this is the original media, whenever the name of the media is not mentioned in the graphs and texts throughout this chapter, it means ATCC 1250 media was used.
5. The second media was designed to study organic electron donor starvation conditions. In the second media lactate was eliminated from ATCC 1250 media. This media is referred

as LF throughout this section. Lactate was eliminated from the media to create organic electron donor scarcity.

6. The third media was designed to study electron transfer through mediator compounds. These compounds act as electron shuttles. They are secreted from the cell. They oxidize metallic iron by extracting electrons from it. As a result, theses compounds are reduced. Then the reduced forms of these compounds enter the cells and are oxidized by giving up electrons to the cell. Vitamins can act as these mediator compounds. In order to study this mechanism riboflavin was added to LF media. This media is referred as LFR throughout this section.

Experiments on D. bastinii are similar to that of D. vulgaris. Please refer to section 4.2 -for detailed explanation of the tests set up. The nominal process is also similar to that of D. vulgaris. Please refer to section 4.2.1.1 for detailed explanations.

5.3 - Results

5.3.1 Corrosion results in Media 1250

In this media, due to abundance of nutrients SRB grow very well. They consume more than 90% of the sulfate in the first 2 days as it can be seen from Figure 5.1. Sulfate consumption rate for all the samples ranges from 5 mmol/L/day to 7.5 mmol/L/day.

Corrosion rate results are illustrated in Figure 5.2. Corrosion rates for sterile samples at 25 and 35°C are included in this plot. Corrosion rate had the highest value at 35˚C samples in this media. The expected result of increase of corrosion rate with temperature is violated. We must not forget however that the corrosion is not merely chemically influenced here. Bacteria are inducing most of the corrosion and we know D. bastinii grows best at 35˚C. That is why most of the corrosion models fail to predict MIC. It does not follow general rules of chemical corrosion as it can be seen in this case. Corrosion rate at 35˚C was significantly higher than two other

temperatures at 7 days. Corrosion rate dropped during the second 7-day period, which is expected based on sulfate consumption curves. Sulfate reduction slowed down after the first 2 days. This halt in metabolic activity shows that cells start to die, and with MIC being the main pathway, corrosion rate slows down. Similar information can be attained from mass loss curves (Figure 5.3). The amount of weight lost during second 7-day period was smaller than the first 7 days. This can be explained by the fact the most of the sulfate had consumed in the initial days and consequently the metabolic activity did not increase afterwards.

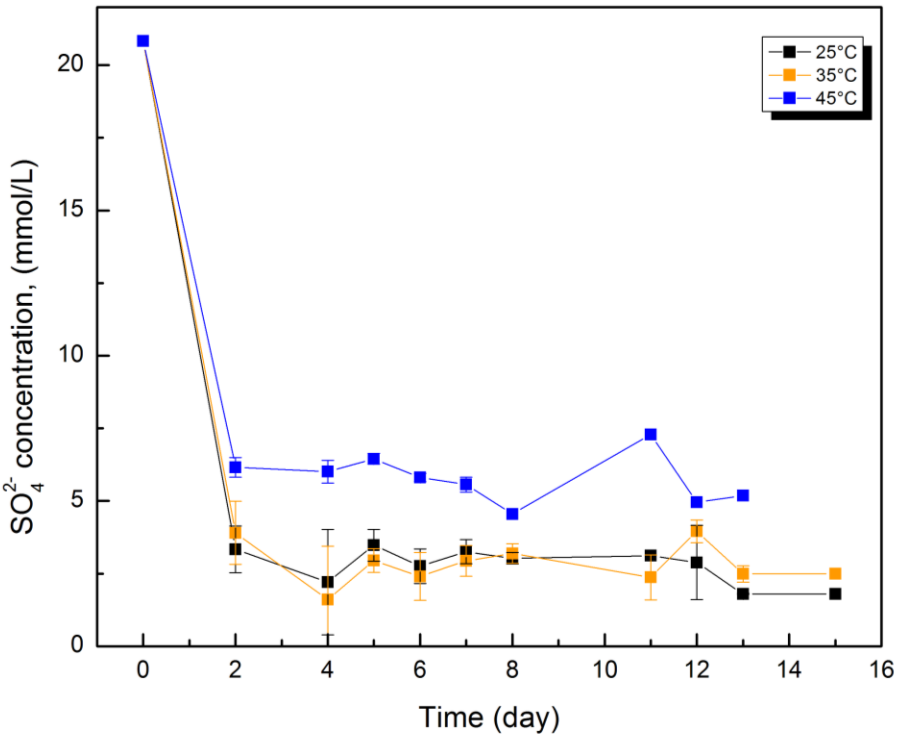

Figure 5.1- Sulfate concentration vs. time for D. bastinii in 1250 media

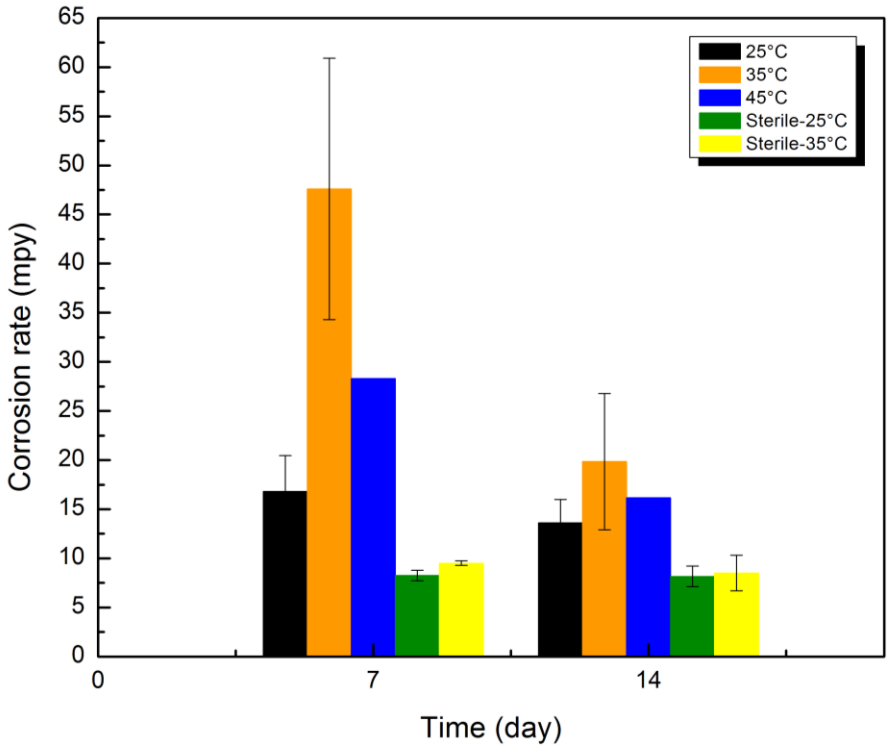

Figure 5.2- Corrosion rate vs. time for D. bastinii in 1250 media

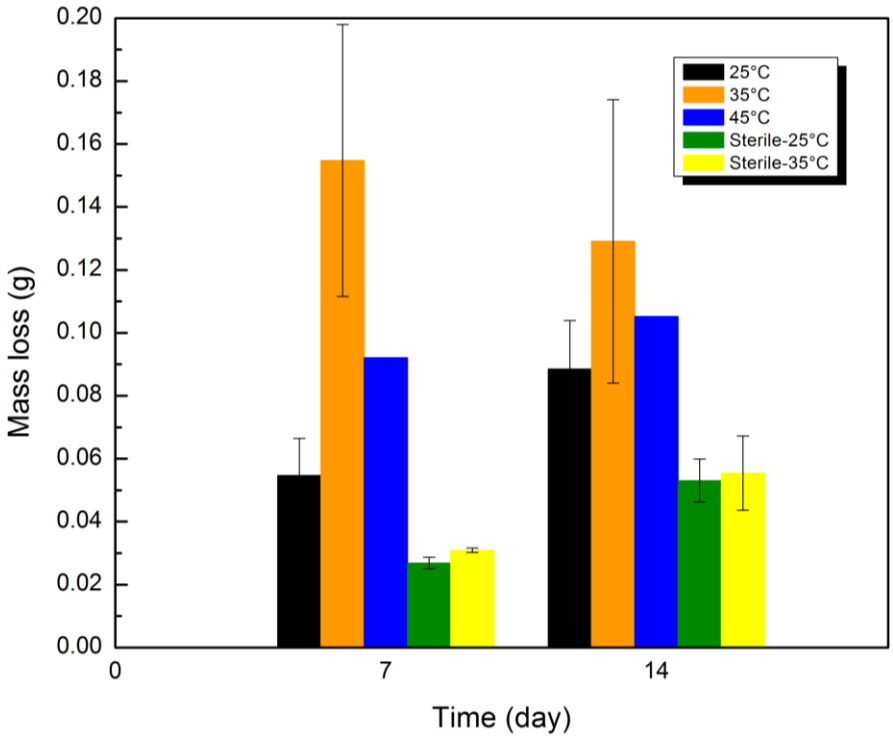

Figure 5.3- Mass loss vs. time for D. bastinii in 1250 media

5.3.2 Corrosion results in Media 1250-LF

In this media a different SRB activity pattern is depicted in Figure 5.4. There is no sharp decrease in sulfate content within the first couple of days. Instead there is a steady slow reduction in amount of sulfate. Any specific distinction cannot be made based on temperature of the samples.

Interestingly in this media like 1249 media (original growth media for D. vulgaris), corrosion rate did not necessarily increase with temperature. This is because that the MIC is the main corrosion pathway in these experiments, and the absence of the chemical corrosion. Again 35˚C samples had the largest corrosion rate amongst three temperatures (Figure 5.5). This is the optimal temperature for D. bastinii.

Figure 5.6 shows the mass loss in this media. Mass loss in this media, unlike 1249 media, did not drop during day 7-14. Mass loss doubled for most of individual samples during the second week. These results very well agreed with sulfate content curves. There was a steady decrease in amount of sulfate in the cultures. The sulfate consumption did not stop after the first week, neither did the mass loss curve. Since the sulfate was continuously being consumed during the whole 14-day period, the mass loss in the first and second week was almost the same for each period. This trend is similar to what was observed in 1249-LF media for D. vulgaris. The rate of sulfate consumption in most of the samples was around to be 1-2 mmol/L/day. The rate of mass loss had a narrow range of 0.07-0.01 g/day. The sterile samples mass loss rate was significantly smaller than the cultured samples with sterile sample at 25˚C and 35˚C, having mass loss rate of 0.0037 and 0.0039 g/day, respectively.

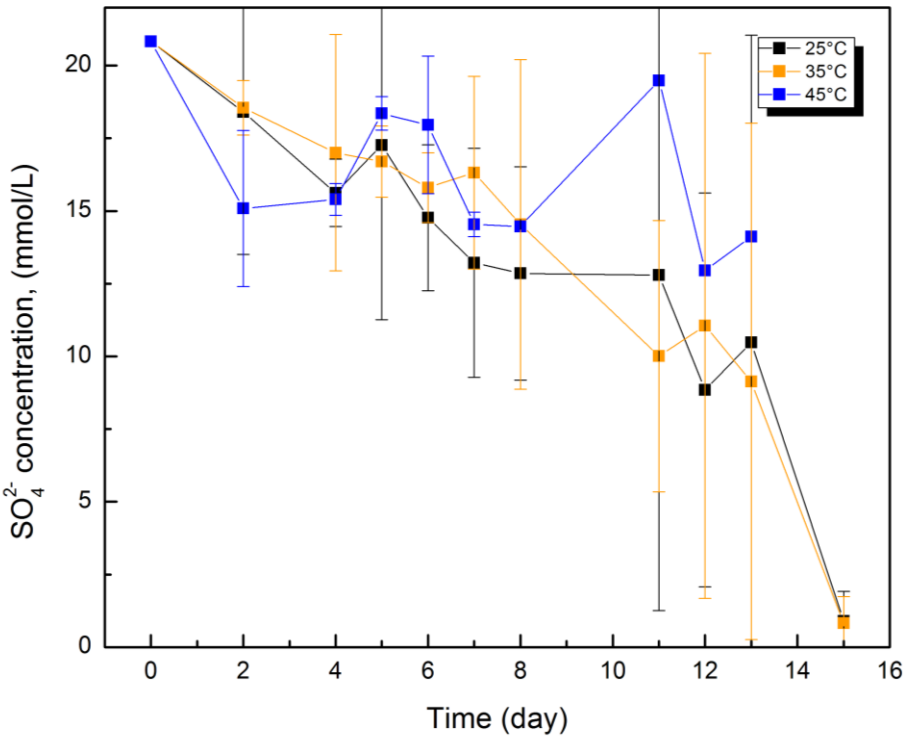

Figure 5.4- Sulfate concentration for D. bastinii in 1250-LF media

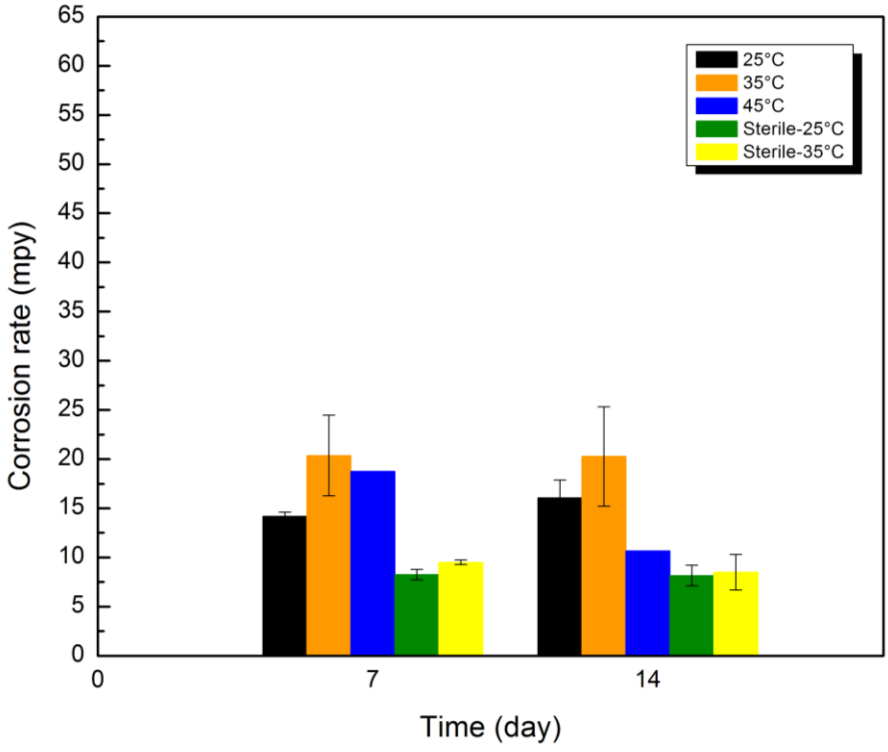

Figure 5.5- Corrosion rate vs. time for D. bastinii in 1250-LF media

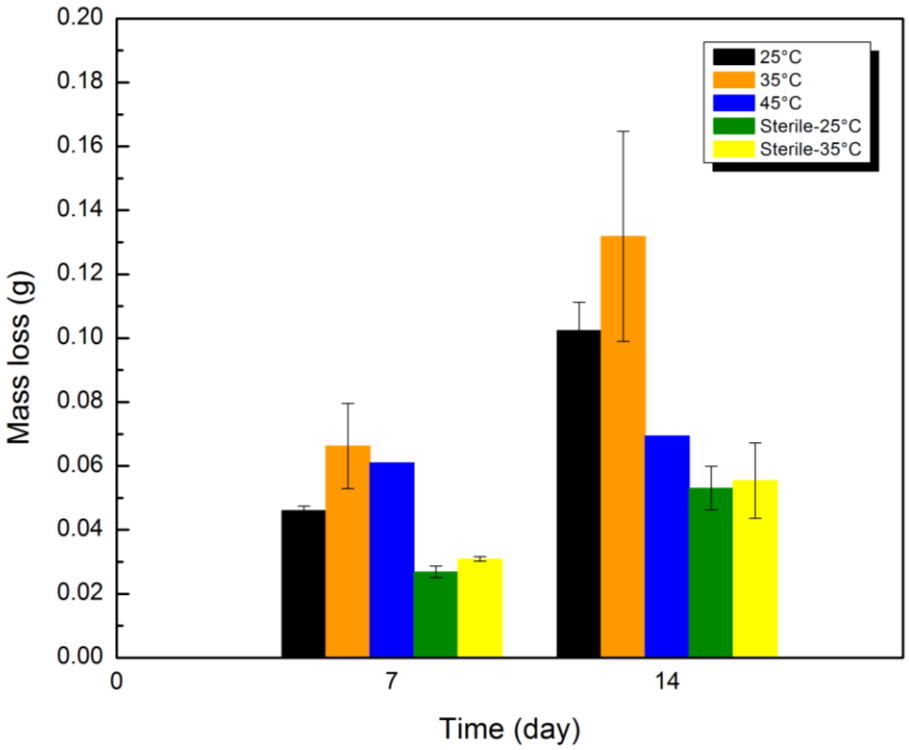

Figure 5.6- Mass loss vs. time for D. bastinii in 1250-LF media

5.3.3 Corrosion results in Media 1250-LFR

In this media not much SRB activity was observed according to Figure 5.7. There was negligible activity in 25˚C samples. In the 35˚C samples more SRB metabolizing activity were observed. Sulfate consumption rate for the samples within first two days ranged from 1.9-6.25 mmol/L/day amongst samples. Then sulfate consumption stopped and went through second consumption phase from day 6 to day 8. Consumption rate in this second period ranged from 1.46-4.6 mmol/L/day. At the end of 7-day and 14-day experiments more than half of the sulfate remained unused in cultures. This indicates that very small population of SRB thrived in this media. We can deduce from these results that riboflavin did not enhance SRB growth and did not promote MIC for D. bastinii. As noted before, riboflavin is a complex vitamin that can go through multiple redox pathways depending on environmental conditions. In a similar study, riboflavin was added to methanogen cultures to determine whether this enhances MIC through these mediator compounds [143]. Measured weight loss comparison of bacterial cultures with controls

showed no significance increase in corrosion in presence of riboflavin. Riboflavin's inefficacy can also be attributed to the fact that most microbial cells are relatively impermeable to external flavins [113]. This could be the reason these vitamins did not enhance corrosion. If riboflavin cannot enter D. bastinii cell wall, then it cannot transfer the electron. Iron can also pose an inhibitory role in biosynthesis of riboflavin inside bacterial cell walls [113].

Corrosion rates in this media are also less than the other two media. There was less sample variability in the corrosion rate in Figure 5.8.

Mass loss increased linearly in this media i.e. with doubling of time mass loss doubled. This is because similar amount of sulfate was consumed in the first and second 7-day periods. Which shows almost similar SRB population were metabolizing in each period. The SRB did not contribute much to the corrosion of the carbon steel in this media because they were not thriving in this media.

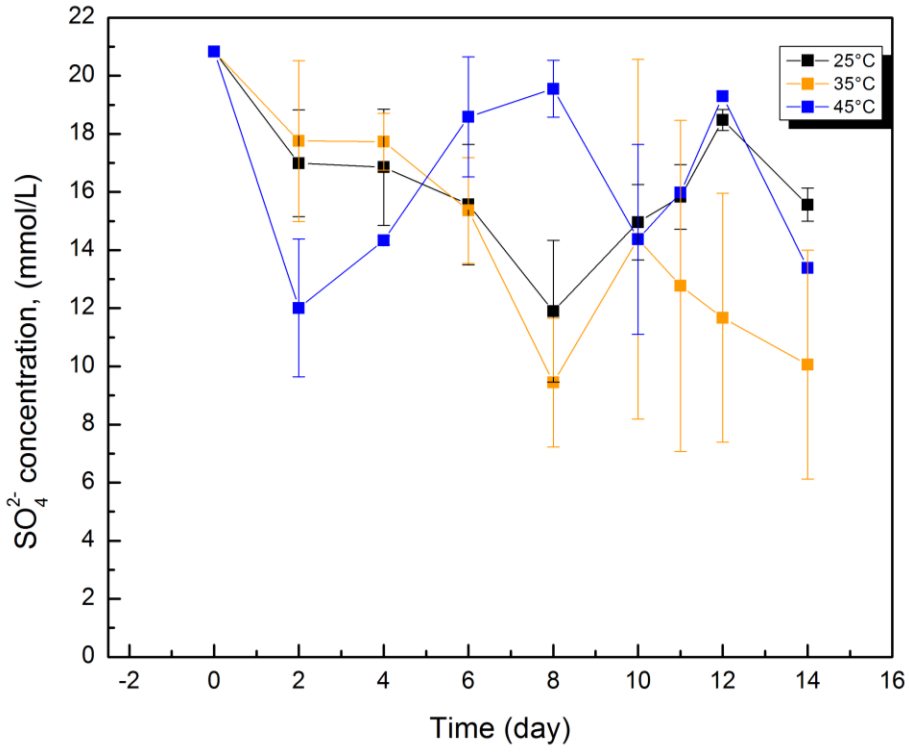

Figure 5.7- Sulfate concentration for D. bastinii in 1250-LFR media

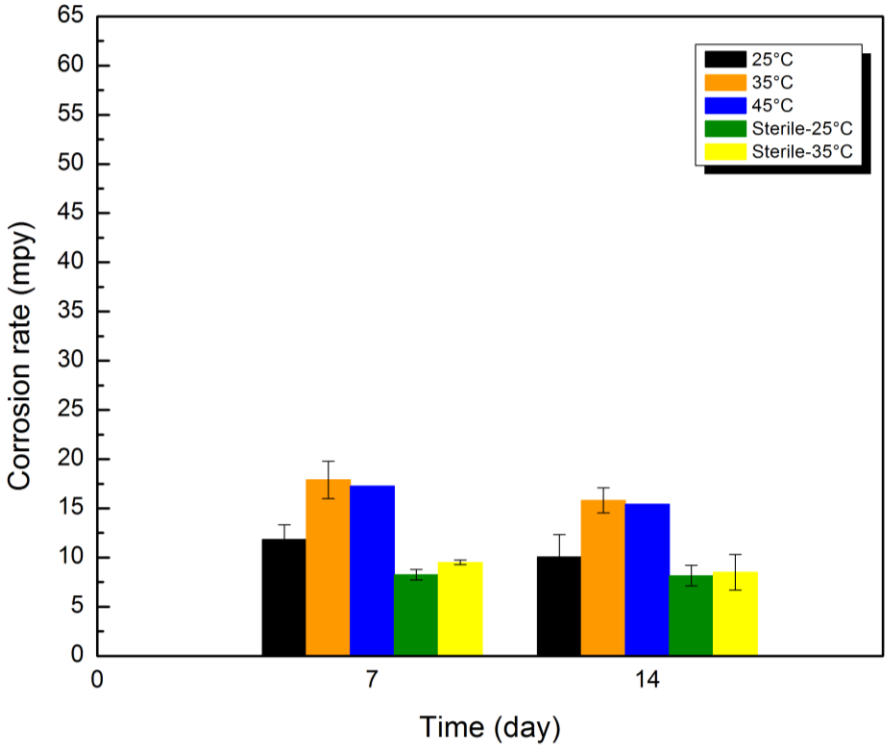

Figure 5.8- Corrosion rate vs. time for D. bastinii in 1250-LFR media

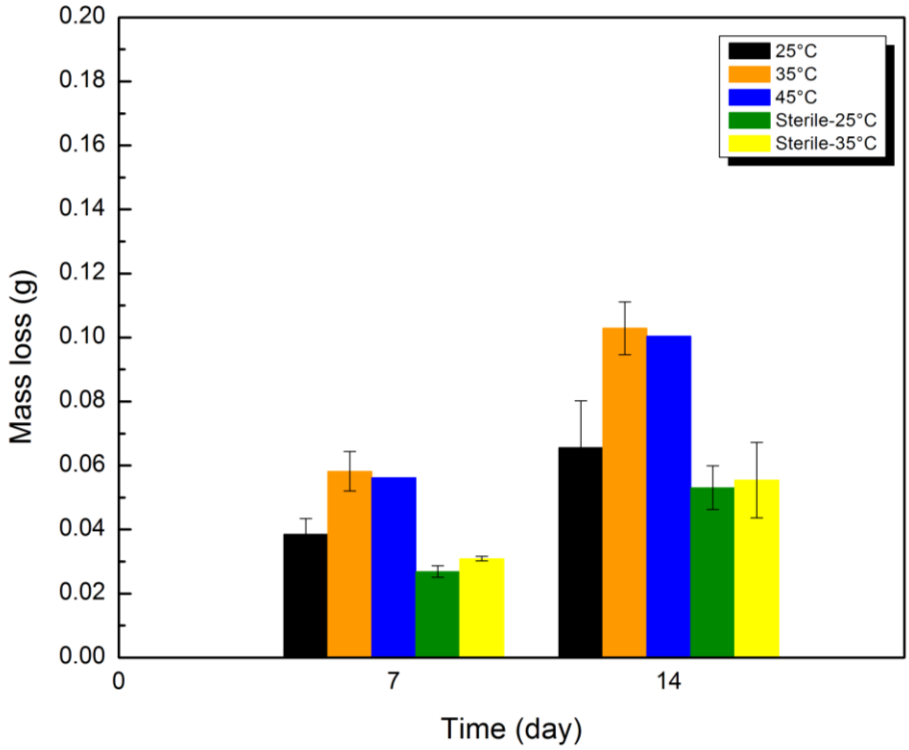

Figure 5.9- Mass loss vs. time for D. bastinii in 1250-LFR media

5.3.4 Growing of D. bastinii in the absence of carbon steel coupons (1250, 1250-LF, and 1250-LFR media)

As control samples, D. bastinii was grown in 1250, 1250-LF, and 1250-LFR media without any carbon steel coupons. These experiments reveal whether D. bastinii can grow in the latter two media without the presence of iron as a potential electron donor. Samples were placed at 35˚C, the optimal growth temperature. Figure 5.10 shows the sulfate consumption as a function of time for D. bastinii in these three media. Clearly there was no growth in 1250-LF and 1250-LFR media based on this figure, since there was no observed consumption of sulfate over 14-day period. Sulfate concentration fluctuates near initial 20 mmol/L concentration, which indicates not much sulfate was consumed. In the absence of Fe and organic electron donor, SRB did not grow. It was previously demonstrated in section 5.3.2 that D. bastinii survived in 1250-LF media in the absence of organic electron donor and presence of carbon steel coupons. It shows that iron plays a key role in D. bastinii survival. This confirms the electron utilization from iron by D. bastinii. Once the iron was eliminated from these samples along with organic electron donor, D. bastiinii did not survive. The growth of D. bastinii in 1250 media, in the presence and absence of iron, is the same with a consumption rate of 7.3 mmol/L/day for both conditions. These data corroborates conclusions made in previous sections and confirms D. bastinii direct electron uptake capabilities.

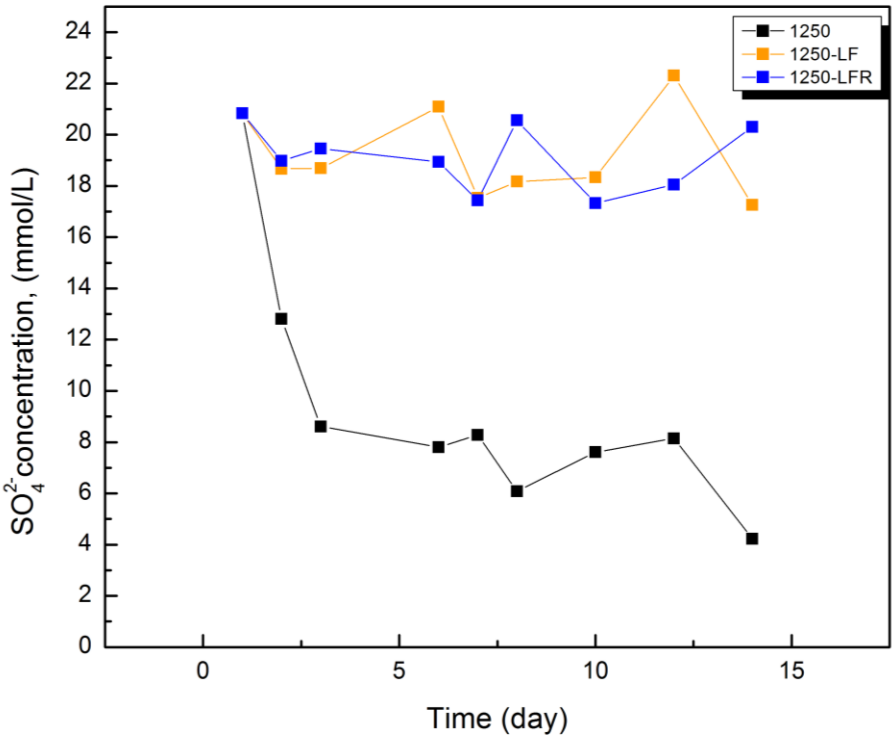

Figure 5.10- D. bastinii in 1249, 1249-LF, and 1250-LFR media without coupon

5.3.5 Comparison of different conditions

5.3.5.1 Effect of types of growth media on mass loss

Figure 5.11 grouped weight loss data based on temperature and duration of immersion. In each group three different media can be compared. In the 1250 media at 35˚C and 7 days highest weight loss is observed. This can be explained by the abundance of nutrients and the ideal temperature at these conditions. The weight loss dissipates as we deviate from these conditions.

In the absence of lactate, D. bastinii switches to electron uptake from the metal after a delay. There is more weight loss in 14-day samples in LF media at 35˚C and 25˚C than in 1250 media as it can be seen from Figure 5.10. It shows elimination of lactate did not decelerate MIC in cultures in LF media. It actually forced the cells to switch to exploitation of metallic iron as electron source. Xu and Gu conducted a series of experiments with exclusion of 90-100% of carbon source in SRB media, and observed more weight loss in solutions containing 10% and 1%

of the carbon source in the original media [103]. These two media contained less sessile cell counts than the original media, however more microbial corrosion was induced [103]. This higher corrosion rate with less cell counts, thus, has to be related to other than H_2S - induced corrosion. Because of the reduced cell numbers, metabolic activity decreases and less H_2S is produced. This has to be due to SRB attack on metallic iron. Observation similar to that of Xu and Gu were observed in this PhD work i.e. elimination of lactate during long-term immersions induced more mass loss. Thus we can say D. bastinii switches to electron uptake from metallic iron during organic electron donor starvation period.

Weight loss data in 1250-LFR media did not show any enhancement in the corrosion rate. Riboflavin was added to this media to test the indirect electron transfer pathways as a possible mediator compound. These types of compounds transfer electrons from outside the cell into cell membrane structure. However the adsorption of flavins on the metal surface for electron uptake depends on various parameters like: temperature, pH, metal surface, redox potential of the solution, etc. [144, 145]. Riboflavin inefficacy can be due to impermeability of D. bastinii to these compounds.

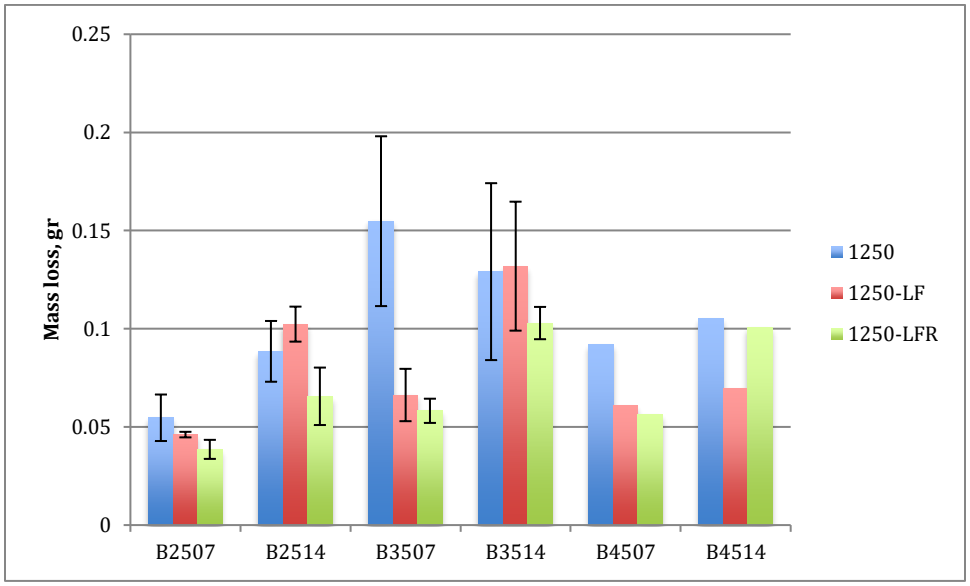

Figure 5.11- Mass loss after 7 and 14 days in different media

5.3.5.2 *Determining the MIC Activation Energy*

Activation energy in each media for 7 days and 14 days is calculated based on the slope of Arrhenius plot (Figure 5.12). These values are presented in Table 4.1. Activation energy was calculated for mean values at each condition. The activation energy in media 1250-LF at 14 days is not presented here due to very low goodness of fit statistics (less than 0.2). The activation energy in 1250-LF media is lower than 1250 media at 7 days. Other experimental data were in accordance with this result. D. bastinii electron uptake capabilities facilitates corrosion. Elimination of electron donors acted as a catalyst and reduces the energy barrier for MIC.

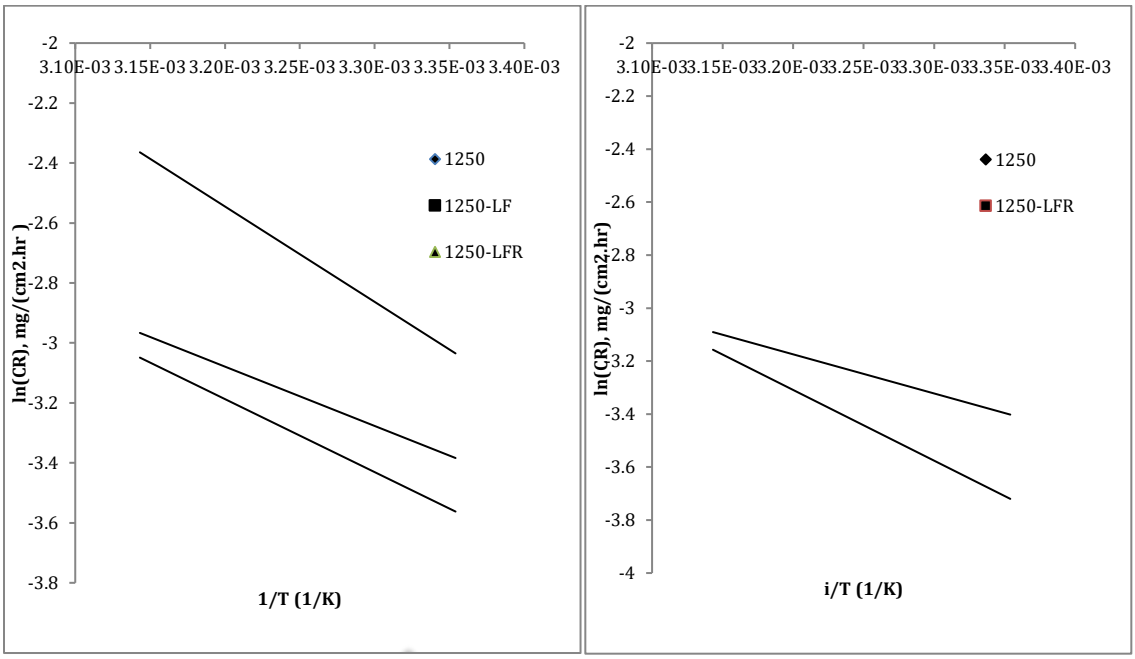

Figure 5.12- Arrhenius plot of corrosion rate; Left: 7 days, Right: 14 days.

Table 5.1- Activation energy for D. bastinii in kJ/mol

Media/Immersion time	7 days	R^2	14 days	R^2
1250	26.448	0.41	12.28	0.6
1250-LF	16.4543	0.8543	-	-
1250-LFR	20.251	0.901	22.196	0.9011

5.3.5.3 *The changes in pH*

Metabolic activity of SRB induces pH increase in the culture. SRB sulfate reduction system produces HS^-, that later combines with protons in the solution and produces H_2S. If this

H_2S is trapped in the biofilm, it incurs pH reduction due to its acidity. However if is in the bulk solution, it eventually goes into headspace and cause pH increase due to consumption of protons.

Figure 5.13 shows pH trend in 1250, 1250-LF and 1250-LFR media. In media 1250, the pH trend is increasing for all temperatures. In media 1250-LF, at 25˚C there is a sharp decrease in pH after 7 days. This is due to entrapment of sulfides in the biofilm. In the next section, SEM image of the coupons at 25˚C in the LF media shows extensive biofilm coverage on the surface of the coupon at 25 ˚C in LF media (Figure 5.15). This extensive biofilm coverage on the surface led to entrapment of HS^-species on the surface. Therefore HS^- species did not scavenge protons in the bulk solution. Therefore the pH did not increase. More biofilm coverage was observed in LF media, which is due to the absence of organic electron donors that forces SRB to seek it from the metal. In the 1250-LFR media, the pH trend is increasing due to the consumption of the protons by HS^- species. There is again a decrease in pH at 35˚C. In this media growth was mainly observed at 35˚C and biofilm was formed only at this temperature. Due to the inactivity of SRB in this media, and at low H_2S pressure, more Oxygen diffused into the media. Oxygen diffusion leds to the formation of goethite, which can be identified by the color and FTIR spectroscopy. Geothite reacts with $HS^-$to produce more OH^- according to Eq. 5.1-Eq. 5.4 [146] , leading to the pH increase.

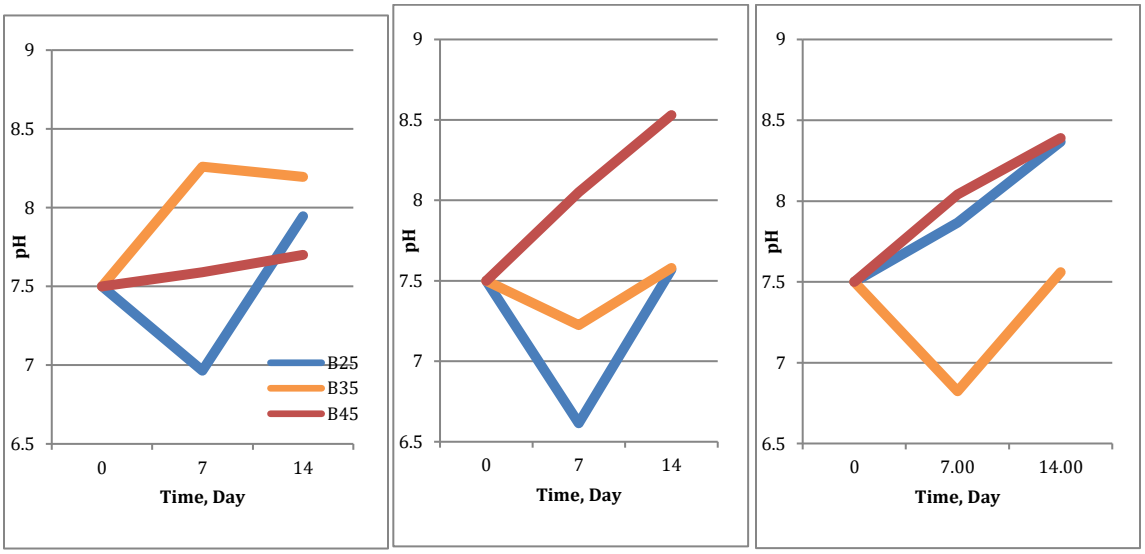

Figure 5.13- Average pH values vs. time. From left to right: Media 1250, 1250-LF, 1250-LFR.

$$H_2O + 2FeOOH + HS^- \rightarrow S^0 + 2FeOH^+ + 3OH^- \quad \text{Eq. 5.1}$$

$$2H_2O + 6FeOOH + 4HS^- \rightarrow S_4^{2-} + 6FeOH^+ + 8OH^- \quad \text{Eq. 5.2}$$

$$3H_2O + 8FeOOH + 5HS^- \rightarrow S_5^{2-} + 8FeOH^+ + 11OH^- \quad \text{Eq. 5.3}$$

$$3H_2O + 8FeOOH + 2HS^- \rightarrow S_2O_3^{2-} + 8FeOH^+ + 8OH^- \quad \text{Eq. 5.4}$$

5.3.6 SEM Analysis

Samples at 25˚C and 35˚C in 1250 and 1250-LF for one week and two weeks were visualized under SEM. Samples were prepared according to guidelines explained in chapter 3 for biofilm visualization. Samples in 1250-LFR media were not visualized due to little/no growth of cells on the surface of the coupons. Figure 5.14 depicts sample at 35˚C in 1250-LF media for 14 days (B3514-LF). The surface of the coupon is covered with SRB cells. It was shown in Figure 5.11 that the weight loss in LF media at 35˚C compares with that of 1250 media and it even slightly surpasses it, in spite of organic electron donor elimination. The well-established colonization of SRB on the surface of the coupon corroborates this and explains high corrosion rate in LF media. Figure 5.15 shows the sample at 25˚C in 1250 media for 7 days (B2507). SRB cells can be visualized amongst the corrosion products not as dense as in B3514-LF (Figure 5.14). It is a bit hard to visualize the cells in this figure. The transparent rod shapes are the SRB cells (This is due to nonconductive nature of SRB cells. They are better visualized by gold coating, however this process is costly and time-consuming. Therefore, glutaraldehyde fixation method was chosen for imaging). By referring to the weight loss comparison in Figure 5.11, it can be seen that B2507 category had the lowest amount of mass loss, which can be explained via poor colonization of SRB on carbon steel surface.

Figure 5.16 shows sample at 25˚C in LF media for 14 days (B2514-LF). It was previously mentioned that for longer durations there were more weight loss in LF media than in 1250 media in spite of nutrient limitation. Figure 5.16 shows massive colonization of D. bastinii

on the surface of the coupon. SRB completely covered the surface. SRB colonized better on the surface of the metal during lactate limitation for longer periods because metal is vital for their survival. They bound to the metal to consume electrons from it. Thus they trigger a more aggressive corrosion attack to the metal.

Figure 5.17 shows sample at 25˚C in LF media for 7 days. In shorter periods SRB did not show much of an aggressive attack on carbon steel samples. This can be seen from mass loss comparison graph (Figure 4.16). SRB cells can steel be visualized on the surface of the metal, but they are rather scarce. 7-day period did not prompt metal-utilization capabilities of SRB.

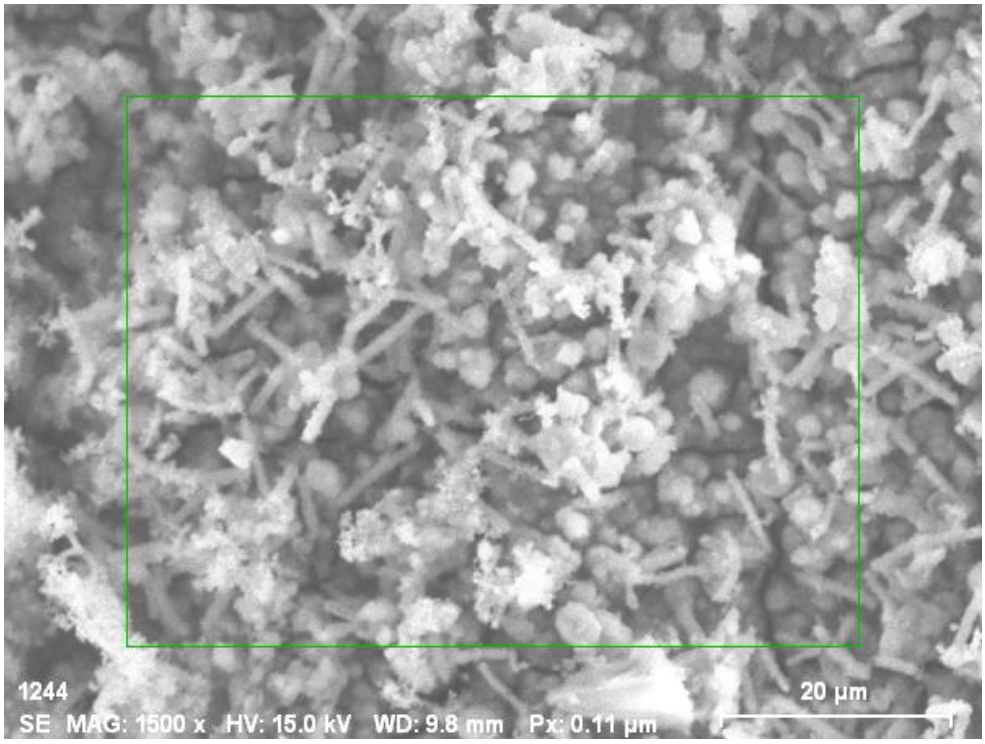

Figure 5.14- SEM image of sample at 35˚C in 1250-LF media for 14 days

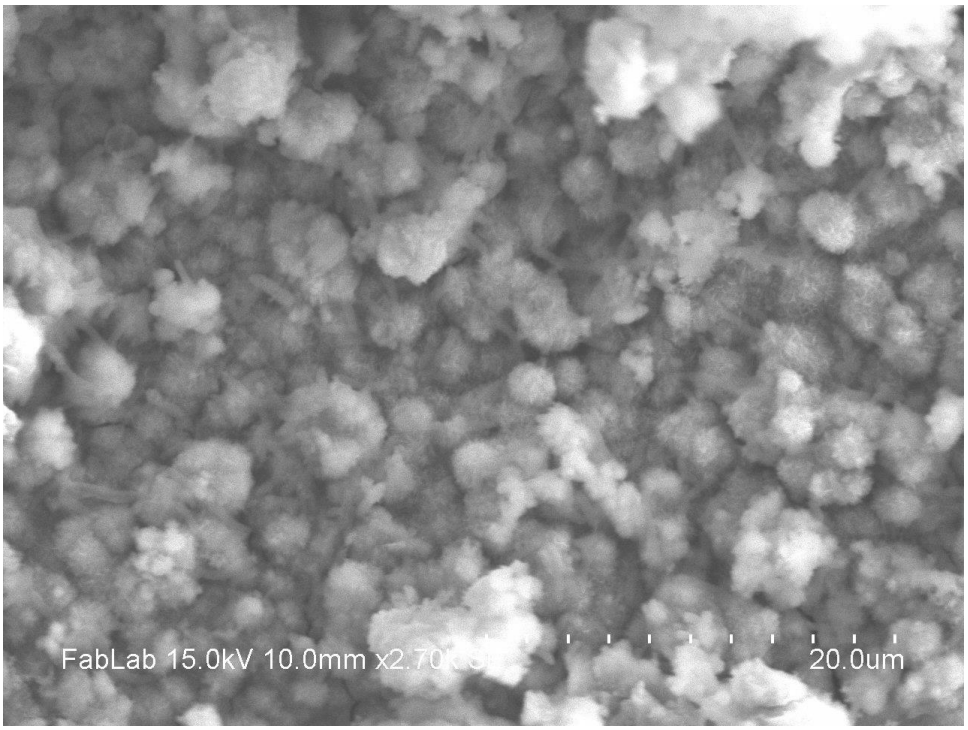

Figure 5.15- SEM image of sample at 25˚C in 1250 media for 7 days

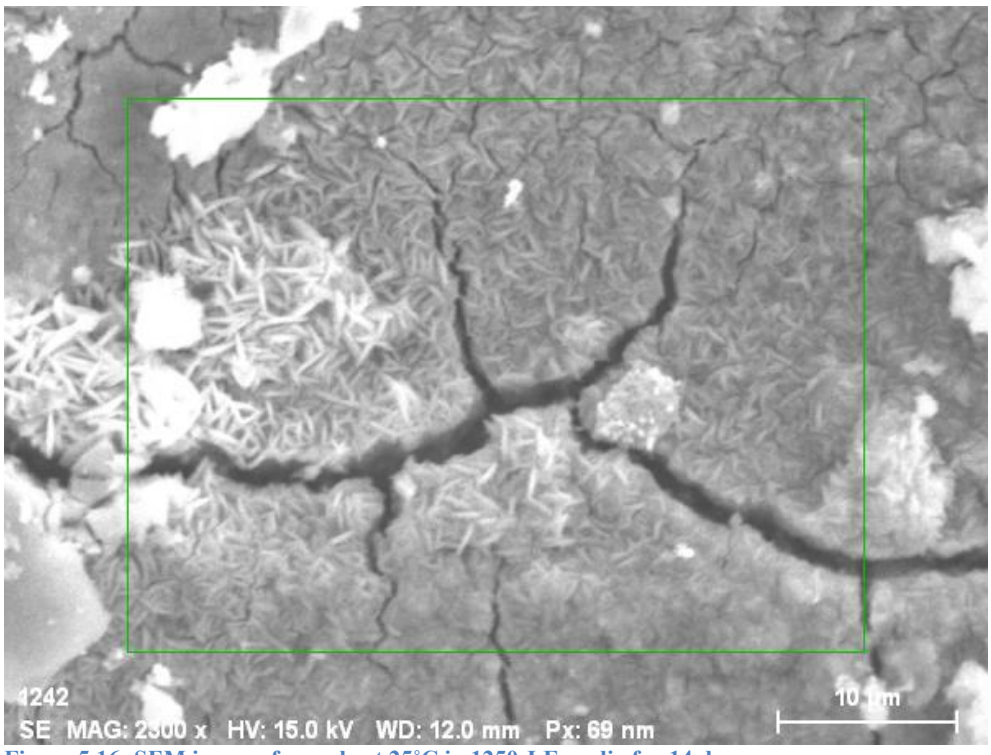

Figure 5.16- SEM image of sample at 25˚C in 1250-LF media for 14 days

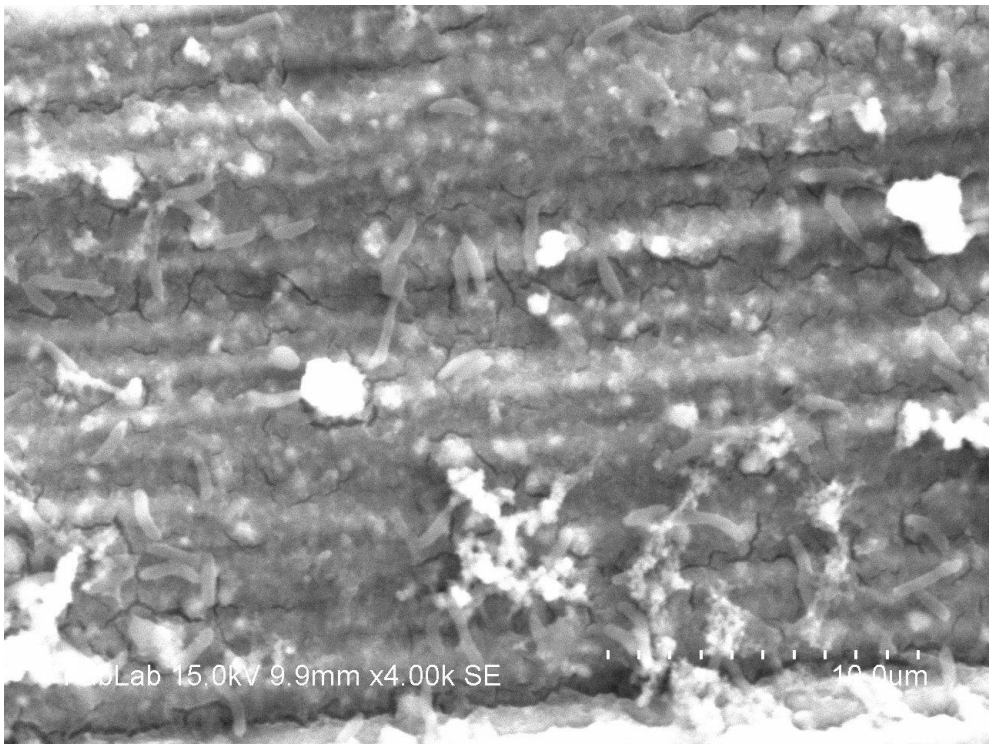

Figure 5.17-SEM image of Sample at 25˚C in 1250-LF media for 7 days.

5.3.7 Identification of corrosion products using FTIR spectroscopy

Samples powder were tested with FTIR after samples were taken out of the solutions. Samples left to dry for one day in the desiccator to reach complete dryness. Then the powder was scraped off and grinded for FTIR analysis. The powders were partially oxidized during these processes thus iron (oxyhydr)oxide minerals peaks were observed in FTIR spectra. Sulfide is a byproduct of SRB metabolic activity. Mackinawite (FeS), pyrite (FeS_2), and greigite (Fe_3S_4) are expected to be the main corrosion products. Mackinawite is metastable and can transform to greigite (Fe_3S_4) and pyrite [117]. Under reducing conditions, iron sulfides are stable. However when they are exposed to humidity and oxygen they corrode and form iron sulfates [118]. Pyrite oxidation can occur through various pathways. O_2 and Fe^{3+} are generally the oxidant agents. However under anaerobic conditions the dissolved O_2 in H_2O can be the only oxidant. Pyrite can react with water to form sulfate anions [119]. The presence of sulfate group bands in the FTIR spectra of samples were confirmed. FTIR spectra were analyzed for all samples. One FTIR

spectra is selected from the experiments that repeated three times is depicted. Similar peaks to that of D. vulgaris were observed for D. bastinii. Please refer to section 4.3.8 for more detailed analysis.

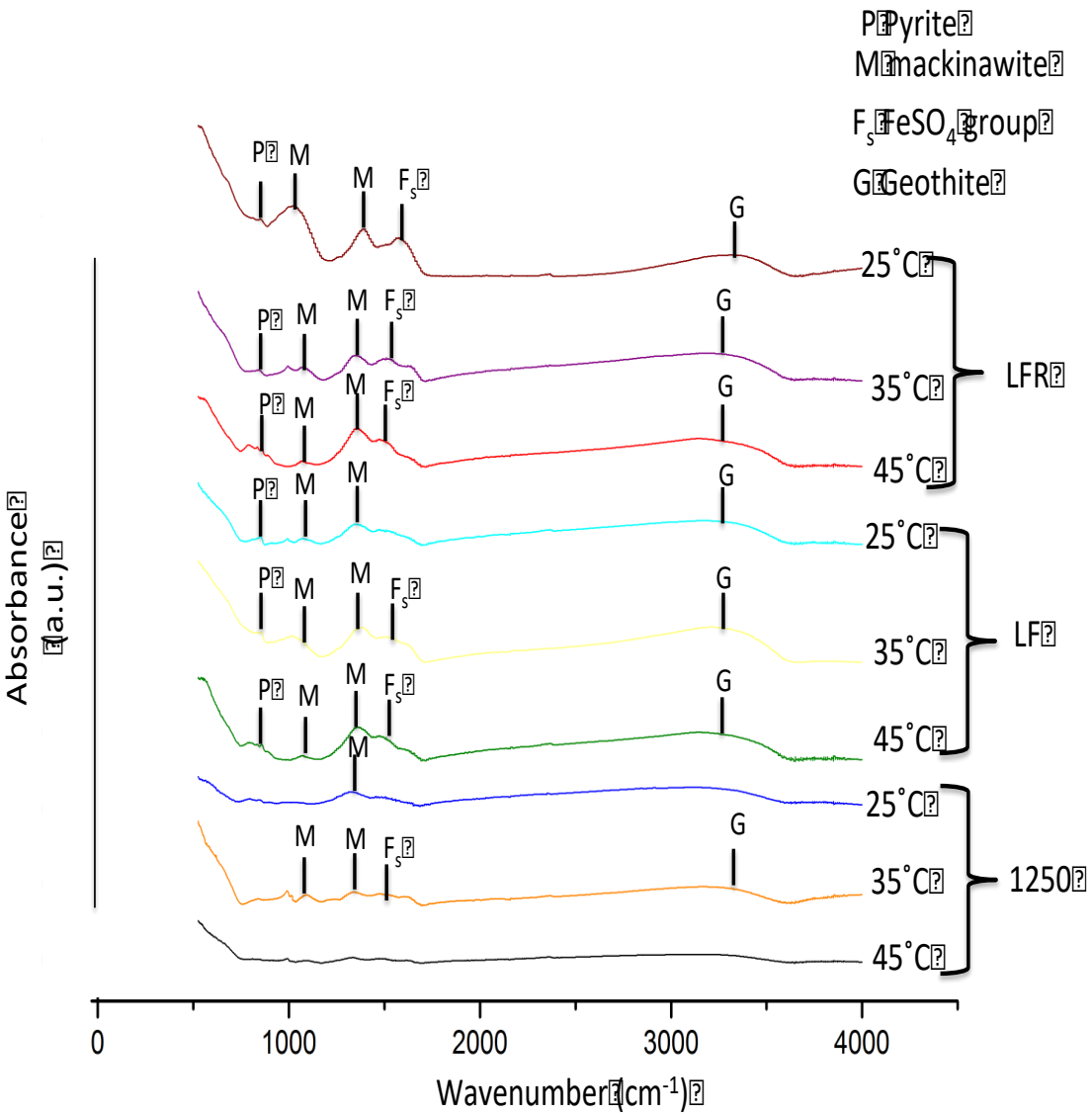

Figure 5.18- FTIR Spectra for 14-days

5.3.8 Electrochemical measurements

A series of electrochemical measurements were performed to delve deeper into MIC mechanisms by D. bastinii. These tests were performed in a span of 2-3 weeks on sterile (abiotic)

and incubated samples. Media 1250 was used for sterile samples as mentioned before. Abiotic tests were conducted anaerobically with deoxygenated media. In biotic tests, D. bastinii was cultured and added to 1250-LF media in the electrochemical cell. Media 1250-LF was used for the electrochemical tests for the purpose of stimulating D. bastinii electron uptake capabilities. In this test, electrochemical cell was filled with 750 ml 1250-LF media. 2 ml of D. bastinii culture was added to the solution in the anaerobic chamber and left in the incubator for 24 hrs. Then the electrochemical cell was connected to potentiostat for the electrochemical measurements.

5.3.8.1 Polarization resistance vs. time

Polarization resistance was measured overtime in both biotic and abiotic systems. At the beginning of the incubation period the biotic system starts developing a higher resistance than the abiotic system, It was mentioned in D. vulgaris analysis in section 4.3.9 that this resistance is due to biofilm formation on the surface of the electrode. Previous studies have shown that biofilm (both aerobic and anaerobic) can have a protective role against corrosion [147–152]. Jayaraman et al. (1999) showed that inhibited anaerobic biofilm of SRB can reduce corrosion of stainless steel [152]. According to Figure 5.19, in the first 4 days there is a resistance development due to formation of biofilm. It slowly starts to decay after day 5. The decay is mainly due to aggressive sulfide anions and D. bastinii switching to electron uptake from metal surface. Rp reaches 0.2 $k\Omega.cm^2$ at the end of 2 weeks. In the D. vulgaris culture there was a more pronounced drop after day 9, however in bastinii cultures the change happened gradually.

In the abiotic system, unlike the biotic one, Rp starts rising at the end of the test period. This is an indication of protective corrosion layers formation on the surface of the electrode. Iron sulfide is the main mineral formed during anerobic corrosion by SRB. Iron sulfide film protective ability depends on the type of iron sulfide formed [153]. However in absence of sulfide in the abiotic media, the increase in Rp can be due to precipitation of media components on electrode

surface. Since in the abiotic system nutrients are not consumed and during electrochemical cycles and longer exposure time they are likely to precipitate.

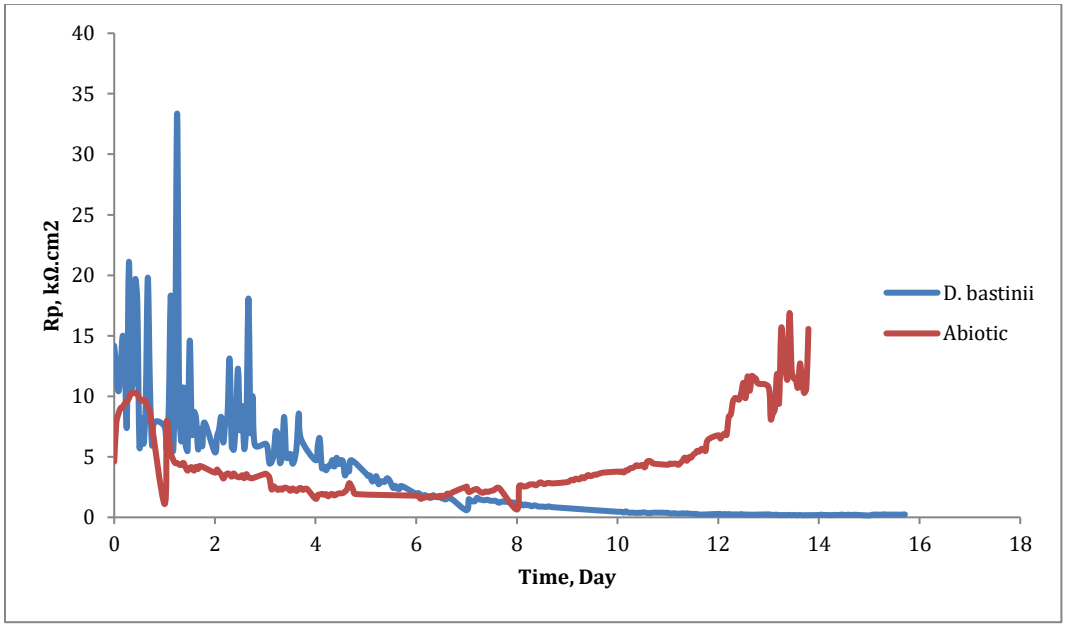

Figure 5.19-Evolution of Rp over time for D. bastinii and abiotic system

5.3.8.2 Potentiodynamic current monitoring

Cathodic current was measured for D. bastinii during a 2-week period. Figure 5.20 shows cathodic current density at three time points. Figure 5.20a shows cathodic current density at the beginning of incubation on day 1 and 2. This is when Rp is high for the biotic system. The cathodic current density in biotic system is larger than abiotic system but they are close in value especially on day 1. At the midpoints (day 8 and 9) difference in cathodic density of biotic and abiotic systems diverges more. Biotic system has more than 1 order of magnitude higher current than the abiotic system. SRB is inducing massive changes on the surface of the electrode. This can be due to FeS formation and electron uptake by D. bastinii. It was previously shown that other potential MIC pathways (e.g cathodic depolarization) does not lead to cathodic current surge [42]. This surge can be related to electron uptake from the electrode if it is not due to H_2 utilization based on cathodic depolarization theory. In Figure 5.20c cathodic current density in biotic system even deviated more from abiotic sample. It was previously shown D. bastinii

remained active in 1250-LF media during 14 days and mass loss did not decrease after the first 7 days. The electrochemical results confirm this by continuous increase in amount of cathodic current density. It can be inferred D. bastinii colonizes on the surface of electrode and keep consuming electrons from the metal surface inducing high currents on the surface of the electrode.

a. b.

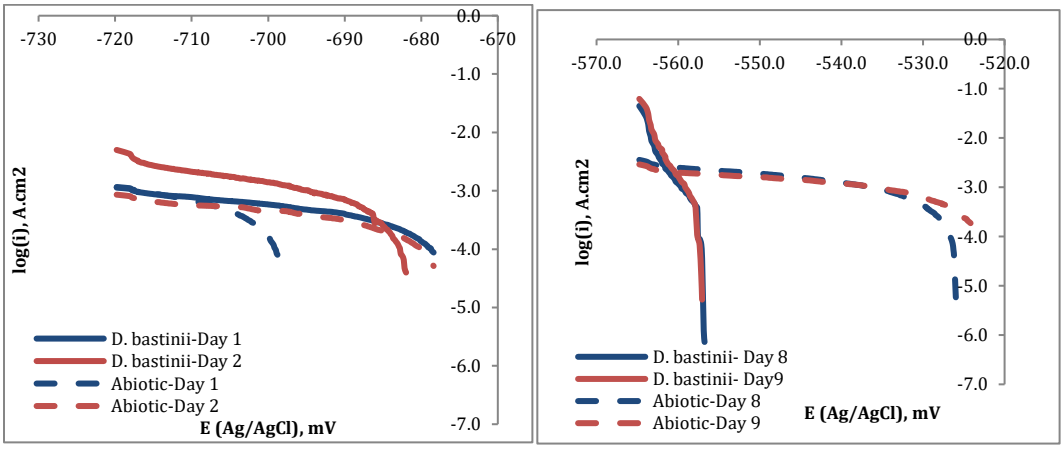

c.

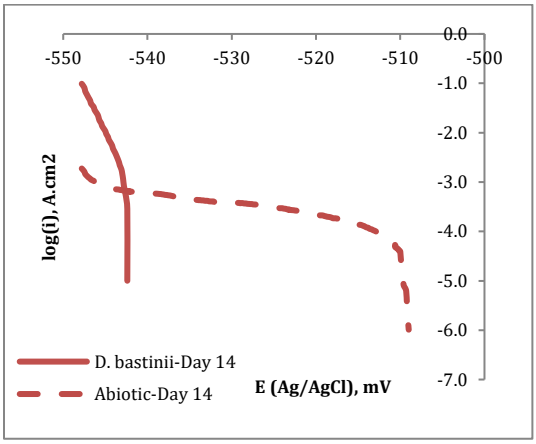

Figure 5.20-Cathodic current density vs. applied potential (displayed vs. standard Ag/AgCl reference electrode, E (Ag/AgCl)) for incubated system with D. bastinii and abiotic system at different time points. (a)Day 1 & day 2. (b) Day 8 & day 9. (c) Day 14. Abiotic system is shown with dashed line in all figures.

5.3.8.3 Corrosion potential monitoring

Corrosion potential was measured daily every 20s for duration of 1.5 hr. There was not much of a change in corrosion potential in 1.5 hr. The E_{corr} values were averaged for that duration

and presented in Figure 5.21. Corrosion potential in the biotic system increased with time based on Figure 5.21. The corrosion potential started at -693 mV (vs. Ag/AgCl). It quickly moved towards more positive potentials within two days. It jumped more than 100 mV in two days and reached -524, which is greater than abiotic system potential (-642). Ennoblement happened in the biotic system. As explained before, the shift of corrosion potential towards positive values is called enobblement. This is an indication of accelerated cathodic reaction [139].

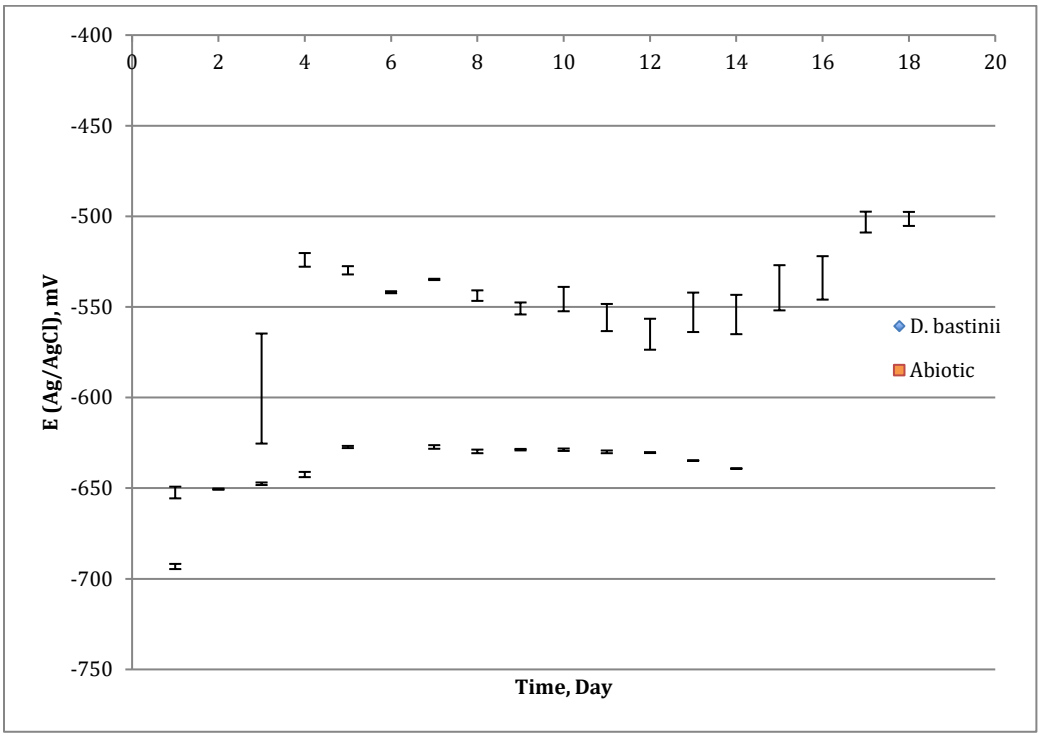

Figure 5.21- Corrosion Potential (displayed vs. Ag/AgCl reference electrode) for D. bastinii and abiotic system.

Chapter 6 - MIC Modeling

This chapter is divided into two main sections. In the first section, initially a sensitivity analysis is performed to evaluate the correlation of measured environmental parameters with corrosion rate. Intercorrelation of environmental parameters is also investigated. Then experimental data were compared with field data to confirm the validity of data for developing a predicting model. In the second section the modeling procedure is explained and final produced models are discussed.

6.1 - Sensitivity Analysis

6.2 - Background and motivation

Melchers and Wells (2005) suggested a phenomenological model for general corrosion in marine environment [154]. This model consists of two main sections: aerobic and anaerobic corrosion as shown in Figure 6.1. There are four phases depicted in this figure. Phase 1 and 2 describe aerobic corrosion. Anaerobic corrosion happens at phase 3 and 4. Based on this model anaerobic corrosion starts with a high rate and as it shifts to phase 4, it gradually dissipates. This slow down in corrosion rate can have multiple reasons. As time passes, more corrosion layers are formed on the surface of metal that limit access to non-corroded metal. The inhabitant cells in these layers also have limited access to nutrients due to slower diffusion of nutrients into the layers. These eventually slow down corrosion over time. In this PhD work, similar trend was observed from the experimental data. The corrosion rate slowed down during the second period. Phase 3 and 4 were calibrated based on the data obtained from the experiments in this study. The anaerobic corrosion was parameterized with three coefficients: r_a, r_s, c'_s. This parameterization helps condensing all the data gathered in the study in a simple mathematical form that can be used for comparison with field studies.

Phase 3, is the initiation of anaerobic corrosion governed by SRB. In the marine environment as oxygen is depleted on metal surface, SRB activities start. r_a represents the slope of mass loss curve at phase 3. Phase 4 represents the semi-steady state phase reached after phase 3. Phase 4 plays the key role in MIC prediction, since phase 3 is a temporary phase that will transition into phase 4 eventually. r_a represents slope of mass loss curve at phase 4. c'_s represents intercept of the curve at phase 4. The corrosion loss curves obtained in this study had similar structure to this model. There was a sharp increase in the mass loss during SRB active period (first 7 days), then the rate slowed down due to nutrition depletion (In a few cases r_s had a negative value. This was because 7-day and 14-day tests were conducted on different samples. Because once the coupon is withdrawn from the solution and mass loss is measured, it cannot be placed back into the solution to measure corrosion rate for another 7 days). Nutrient diffusion at field conditions has a more complex form, however it can be assumed by proceeding of corrosion process and formation of corrosion layers, diffusion of nutrients is hampered and cells suffer from nutrition depletion.

$r_a, r_s, and\ c'_s$ were calculated for all of the samples in the study. Then the dependency of these values on other parameters affecting corrosion like temperature, duration of immersion, etc. was investigated. All these three values calculated in the study were compared with values obtained from other field studies.

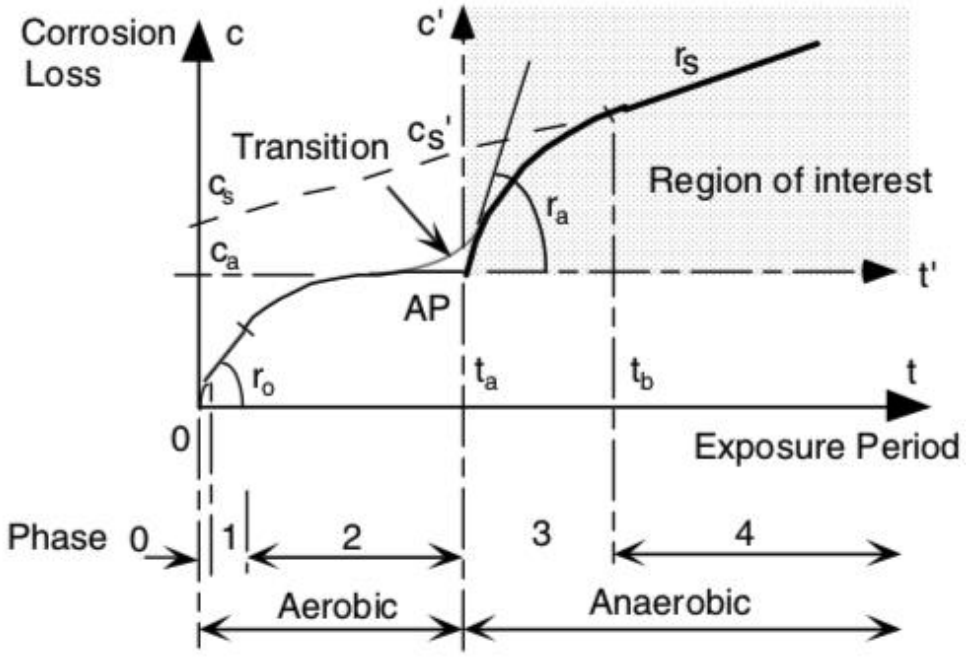

Figure 6.1-Phenomenological model for general marine corrosion of steel suggested by Melchers and Wells (2005)

6.2.1 Correlation analysis

In this study, a relatively large dataset was produced in microbial corrosion. Corrosion rates were calculated under 18 different environmental conditions (3 temperature, 2 immersion duration, 3 media) for two different SRB strains. The correlations amongst environmental parameters and corrosion rate are calculated. The intercorrelations of environmental parameters were calculated as well. This quantification helps understanding MIC better. The media used in this study curated different nutrients to SRB. Nutrient was shown to play a significant role in MIC [154, 155]. It was also shown throughout this study, that SRB behave differently in each media. Therefore, correlation analysis was performed in each media separately. The environmental parameters include: Immersion duration, pH of the solution, temperature, duration of immersion, initial sulfate consumption rate (1-sulfcons), secondary sulfate consumption rate (2-sulfcons), mass loss rate in 1st week (r_a), slope of mass loss curve in 2nd week (r_s), and intercept of the mass loss curve in 2nd week (c'_s). (Note that sulfate consumption rate has a negative value. For 1-sulfcons and 2-sulfcons, absolute values were plugged in for correlation

analysis). Correlation analysis was performed for each two parameters. Parameters with correlation coefficient more than 0.5 were considered significant. This information helps identifying important parameters in MIC. As a reminder D. vulgaris was cultivated in 1249, 1249-LF, and 1249-LFR media. D. bastinii was cultivated in 1250, 1250-LF, and 1250-LFR media.

6.2.1.1 Correlation analysis in 1249 media

The corrosion rate in this media was correlated with the immersion time. The correlation coefficient is negative which means two parameters have indirect relationship. In this media, D. vulgaris, consumed most of the sulfate within the first couple of days. This means that the cells started dying after 5 days, and the corrosion rate reduced during the 2nd week. So there were more mass loss recorded in the first week than the 2nd week.

The pH of the media was correlated with 1-sulfcons, c'_s and r_a. All the coefficients were positive. Higher 1-sulfcons and higher r_a indicate more corrosion (higher 1-sulfcons means higher metabolic activity, higher r_a means more mass loss within 7 days), which agrees with higher pH. Because in this media, SRB took advantage of lactate presence to produce more HS^-. These species scavenged protons in the solution and as result the pH increased.

Temperatures in this media was correlated with c'_s and r_a. High r_a and c'_s indicate higher corrosion and having a positive correlation with temperature is expected.

Immersion duration only had correlation with corrosion rate as mentioned before.

Sulfate consumption at the beginning of immersion period was correlated with r_a, r_s, c'_s. This shows how SRB metabolic activity directly impact all the parameters defining anaerobic corrosion model.

Table 6.1-Correlation coefficients in 1249 media

	pH	Temperature	Duration	Initial Sulfate-consumption rate	Intercept (c'_s)	Slope (r_s)	Slope (r_a)

Corrosion rate	0.362	0.260	-0.876	0.195	0.271	-0.175	0.342
pH		0.313	0.048	0.517	0.536	-0.430	0.582
Temperature			0.000	0.364	0.644	-0.490	0.731
Duration				-0.037	0.000	0.000	0.000
Initial Sulfate-consumption rate					0.626	-0.561	0.612
Intercept						-0.943	0.925
Slope (r_s)							-0.746

6.2.1.2 Correlation analysis in 1249-LF media

Lactate was eliminated from 1249-LF media, thus the sulfate consumption pattern had changed in this media. Sulfate consumption happened at two steps. Slope of the sulfate consumption at both steps were included in the correlation analysis as "Initial sulfate consumption rate (1-sulfcons)" and secondary sulfate consumption rate (2-sulfcons)".

In this media, corrosion rate was correlated with temperature, 1-sulfcons, r_s, and r_a. All correlation coefficients were positive. Corrosion increased with increasing temperature in this media. The higher sulfate consumption denoted higher corrosion rate. This is intuitive because higher SRB activity induces more corrosion.

The pH was correlated with 2-sulfcons. Apparently SRB activity during the 2nd phase of sulfate consumption triggered more pH decrease. This was previously shown in chapter 4 that higher SRB activity at 35˚C induced more corrosion and a pH decline (Note that as mentioned before, absolute values for 2-sulfcons were used. This is because the larger absolute values denote higher SRB activity, and thus higher corrosion rate and it is easier to grasp in terms of numbers).

Temperature was correlated with corrosion rate and 1-sulfcons. First correlation was discussed earlier. The positive correlation of temperature and 1-sulfcons shows the higher the temperature, the higher SRB activity, however care should be taken in extrapolation of temperatures significantly higher than 45˚C.

No significant correlation was observed for this particular duration of immersion.

1-sulfcons was correlated directly with r_a. This says the mass loss rate in the first 7 days was directly correlated with SRB sulfate consumption in the first 7 days.

Intercept (c'_s) and slope (r_s) of mass loss curve in the second week were inversely correlated (c'_s was correlated with corrosion rate and temperature, as mentioned before). This is expected because higher positive slopes lead to smaller intercepts. Most of r_s values obtained in this study were positive.

Table 6.2- Correlation coefficients in 1249-LF media

	pH	Temperature	Duration	Initial Sulfate-consumption rate	Intercept (c'_s)	Slope (r_s)	Slope (r_a)	Secondary sulfate consumption rate
Corrosion rate	-0.333	0.772	-0.388	0.654	-0.199	0.662	0.809	0.395
pH		-0.288	0.089	-0.038	-0.284	0.001	-0.418	-0.922
Temperature			0.000	0.609	-0.273	0.726	0.806	0.413
Duration				-0.494	0.000	0.000	0.000	0.028
Initial Sulfate-consumption rate					-0.191	0.475	0.509	0.128
Intercept (c'_s)						-0.804	0.135	0.233
Slope (r_s)							0.481	0.106
Slope (r_a)								0.521

6.2.1.3 Correlation analysis in media 1249-LFR

Corrosion rate in media 1249-LFR was correlated with duration of immersion and r_a. Dependency of corrosion rate on r_a states that the mass loss during first week was governing the total mass loss.

pH was correlated with r_s. This states that higher corrosion loss in the second week occurred at higher pHs.

1-sulfcons was correlated with r_s. This means that initial sulfate consumption had a direct relationship with mass loss in the first 7 days.

c'_s, r_a, and r_s, were all intercorrelated. c'_s was also correlated with 2-sulfcons.

r_s was correlated with pH and 1-sulfconc as mentioned before.

r_a was correlated with 2-sulfconc corrosion rate and c'_s.

Table 6.3- Correlation coefficients in 1249-LFR media

	pH	Temperature	Duration	Initial Sulfate-consumption rate	Intercept (c'_s)	Slope (r_s)	Slope (r_a)	Secondary sulfate consumption rate
Corrosion rate	0.162	0.462	-0.657	-0.007	0.385	0.075	0.641	0.430
pH		0.190	-0.111	0.436	-0.414	0.645	-0.022	-0.424
Temperature			0.000	0.448	-0.022	0.577	0.499	0.330
Duration				0.063	0.000	0.000	0.000	-0.081
Initial Sulfate-consumption rate					-0.398	0.552	-0.083	-0.340
Intercept (c'_s)						-0.753	0.795	0.647
Slope (r_s)							-0.198	-0.380
Slope (r_a)								0.613

6.2.1.4 Correlation analysis in media 1250

Corrosion rate in media 1250 was correlated with pH, c'_s, and time of immersion. Higher pH indicated higher corrosion rate, which make sense in this media because SRB grew very well in this media and sulfide production was not hampered due to presence of lactate. Therefore there was more HS^-species to combine with protons.

The correlation with c'_s is harder to interpret. If the mass loss rate in the second week is very high, this high slope can lead to small c'_svalues. On the other hand high c'_s can be an indication of high mass loss in the first week and not necessarily high mass loss in second week.

Correlation with immersion duration is also hard to rely on since there were only two immersion periods tested.

pH was correlated with corrosion rate and r_a. Higher r_a values had higher pH. Higher $r_a$means higher corrosion loss in first week, which agrees with increasing pH due to consumption of protons in the solution by HS^-species.

Higher consumption rate in the first 3 days was correlated with lower corrosion loss in 2nd week. This can be due to cells shrinkage in 2nd week because of less available sulfate in the solution and inhibition of cells by H_2S. In the samples that consumed more sulfate at the beginning of incubation, there were less corrosion loss at the 2nd week since they cell population started to diminish earlier.

All coefficients for parametric corrosion model (c'_s, r_a, and r_s) were intercorrelated. Higher c'_s was correlated with lower r_s, which is expected. The lower the slope, the smaller would be the point the line crosses vertical axis.

Table 6.4- Correlation coefficients in 1250 media

	pH	Temperature	Duration	Initial Sulfate-consumption rate	Intercept (c'_s)	Slope (r_s)	Slope (r_a)
Corrosion rate	0.541	0.317	-0.553	0.030	0.543	-0.429	0.613
pH		0.239	0.323	-0.147	0.390	-0.247	0.502
Temperature			0.000	0.163	0.378	-0.264	0.461
Duration				0.040	0.000	0.000	0.000
Initial Sulfate-consumption rate					0.484	-0.660	0.268
Intercept						-0.959	0.959
Slope (r_s)							-0.571

6.2.1.5 Correlation analysis in media 1250-LF

In media 1249-LF, the corrosion rate was correlated with r_a, and r_s. This is a good indication that these two parameters describe corrosion very well.

pH was correlated with temperature. Higher temperatures led to higher pH in cultures. This means that corrosion process through sulfide species was enhanced by temperature. pH was also correlated with c'_s and r_s. However data points at 45˚C, skewed the data significantly, with elimination of those data no correlation was observed.

Temperature was correlated with c'_s, r_s and r_a. The first correlation was positive. However the 2nd was negative because at 45˚C, mass loss drops in 2nd week. This data point again skewed the results. Temperature and r_a had a positive correlation that was not impacted significantly with the data point at 45˚C.

Table 6.5- Correlation coefficients in 1250-LF media

	pH	Temperature	Duration	Initial Sulfate-consumption rate	Intercept (c'_s)	Slope (r_s)	Slope (r_a)	Secondary sulfate consumption rate
Corrosion rate	-0.217	0.110	-0.116	-0.200	-0.253	0.601	0.730	0.259
pH		0.617	0.458	0.492	0.688	-0.607	0.195	-0.025
Temperature			0.000	0.331	0.896	-0.614	0.631	-0.333
Duration				-0.365	0.000	0.000	0.000	0.325
Initial Sulfate-consumption rate					0.488	-0.496	0.000	0.085
Intercept (c'_s)						-0.891	0.267	-0.296
Slope (r_s)							0.424	-0.265
Slope (r_a								-0.364

6.2.1.6 MIC in Media 1250-LFR

In media 1250-LFR, corrosion rate was correlated with pH, temperature, c'_s, and r_a. The correlation with pH was negative. In this media, less SRB growth was observed and therefore less HS^- species were formed. Higher corrosion rates at lower pH can be due to aggressive attack of SRB under lactate starvation. They corroded carbon steel by taking up electrons from the metal rather than producing sulfide species. Corrosion rate also increased with higher temperatures. Corrosion rate was correlated with mass loss within the first week. Correlation with c'_s can be both due to higher r_a or lower r_s values.

pH had a weak correlation with sulfate consumption rate in the second week. The correlation is weak because pH had a very narrow range in comparison to 2-sulfcons.

Temperature had a good correlation with r_s and r_a (and corrosion rate as mentioned before). Higher temperature led to higher r_s and r_a values. Temperature can be considered as one of variables impacting coefficient of parametric corrosion model. Empirical relationship of coefficients and temperature can be developed to enable predicting these coefficients based on temperature. The relationship of these coefficients and temperature is evaluated in the further sections.

1-sulfcons had an inverse relationship with 2-sulfcons. At higher sulfate consumption rates during first week, less sulfate was remained for second period. Therefore 2-sulfcons was smaller.

c'_s *and* r_s were correlated which is expected because they are two coefficients describing one line.

Table 6.6- Correlation coefficients in 1250-LFR media

	pH	Temperature	Duration	Initial Sulfate-consumption rate	Intercept (c'_s)	Slope (r_s)	Slope (r_a)	Secondary sulfate consumption rate

Corrosion rate	0.634	0.742	-0.290	0.071	0.033	0.583	0.841	0.205
pH		-0.232	0.496	0.104	0.060	-0.414	-0.483	-0.562
Temperature			0.000	0.415	0.033	0.537	0.777	-0.216
Duration				-0.175	0.000	0.000	0.000	0.067
Initial Sulfate-consumption rate					-0.048	0.032	-0.023	-0.509
Intercept (c'_s)						-0.735	0.379	0.086
Slope (r_s)							0.349	0.057
Slope (r_a)								0.197

6.2.2 Corrosion coefficients of the field vs. lab

According to the phenomenological corrosion model suggested by Melchers and Wells (2005), 3 coefficients can be used to describe anaerobic corrosion (c'_s, r_s and r_a). These coefficients were calculated for the results obtained at field are summarized in Table 6.7. Similar process was carried on the data from this study. These three coefficients were calculated in this study. The units were changed from US to SI system to be comparable to field results. c'_s was calculated in mm. r_s and r_a were calculated in mm/yr. In the next sections lab coefficients are compared with field coefficients. It is hard to control all the conditions at the field. Even some of the reported field studies demonstrated wide scatter among corrosion rates from samples at one site location [156]. Conditions including salinity, pH, water velocity, carbonate balance does not stay constant down the stream in the pipe. Controlled lab experiments help relating those environmental conditions to corrosion rate values and make a more conclusive assessment.

Table 6.7- Estimates of Parametric coefficients for anaerobic corrosion in the literature

Source	Reference	Average water temperature	ta	ra	cs	rs	c's	Steel type
Koshelev and Rozenfeld	[157]	4	4.5-4.6	0.075	0.26		0.06	Grit-blasted mild steel

Blekkenhorst et al.	[158]	10	3-3.5	0.12-0.14	0.6	0.05	0.3	Mild steel I4
Tamada et al.	[159]	17	1.4	0.21	0.1	0.09	0.08	Mild steel A
Southwell and Alexander	[160]	27.6		0.18-0.25	0.07-0.1	0.7-0.75	0.05	Mild carbon steel
Southwell et al.	[161]	27.6	0.8				0.05	
Friend		7.8	3.5					
		12.6			0.3	0.05		
	[162]	17.9			0.12	0.072		
		28.7			0.13	0.1		
Larrabee	[163]	18.5	1.5		0.12	0.062		
Larrabee	[164]	18.5	1-1.5		0.19	0.058		Structural carbon steel
Forgeson et al.	[165]	15.5	1.7	0.4				
Hudson and Stanners	[166]	12			0.45	0.056		Steel no.1
Jeffrey and Melchers	[167]	21	0.9	0.22			0.06	Mild steel
		22	0.7	0.24			0.03-0.05	Mild steel

6.2.2.1 r_a

r_a represents slope of corrosion loss curve vs. time in the initial incubation phase (first 7 days). This is temporary phase and transition to phase 4. Experimental data showed that at field conditions, this phase can range from 2 weeks to couple of months. Duration of this phase is

dependent on initial colonization rate, cells attachment to the surface of metal, and availability of nutrients [168]. Under experimental conditions in this PhD work, this phase expected to be shorter due to suitable conditions provided for incubation including: optimal temperature during incubation period, stagnant conditions in comparison to mild to high flow rates at field, higher nutrient availability, and complete exclusion of oxygen. Phase 3 was assumed to be 7 days in the experiments designed for this study. During the 7-day periods, SRB cultures had highest metabolic activity, after this period the metabolic activity slows down so does the corrosion rate and the corrosion rate pattern changes. Based on Table 6.7 data, r_a values range from 0.075 to 0.4 mm/yr at field conditions. $r_a$values obtained in this study range from 0.19 to 5.8 mm/yr. The noticeable point is that r_a values in 1249 media are significantly higher than other two media. They range from 3.4 to 5.8 mm/yr in 1249 media. This clearly shows the effect of nutrient availability on corrosion. In this media all vital nutrients for SRB growth was provided. This is not the case under field conditions. Sulfate content is lower and organic electron donors have limited availability unless the seawater is polluted [169]. Elimination of lactate from the media suppressed r_a values significantly. The range in LF and LFR media drops to 0.27- 0.88 mm/yr. 1250 media also has relatively higher r_a values than LF and LFR media, it varies in 0.36-1.45 mm/yr range. Based on Figure 6.2, D. vulgaris (cultured in 1249) demonstrated more corrosive capability towards iron than D. bastinii (cultured in 1250). Comparison of similar media (i.e 1249-LF vs. 1250-LF, 1249-LFR vs. 1250-LFR) incubated with D.vulgaris vs. D. bastinii shows that D. vulgaris had higher upper range of r_a e.g. highest r_a value in V-LFR was 0.88 mm/yr while corresponding value in B-LFR was 0.51 mm/yr. Last box in Figure 6.2 shows r_a values in sterile 1250 media. It can be seen that they are smaller in comparison to media containing SRB.

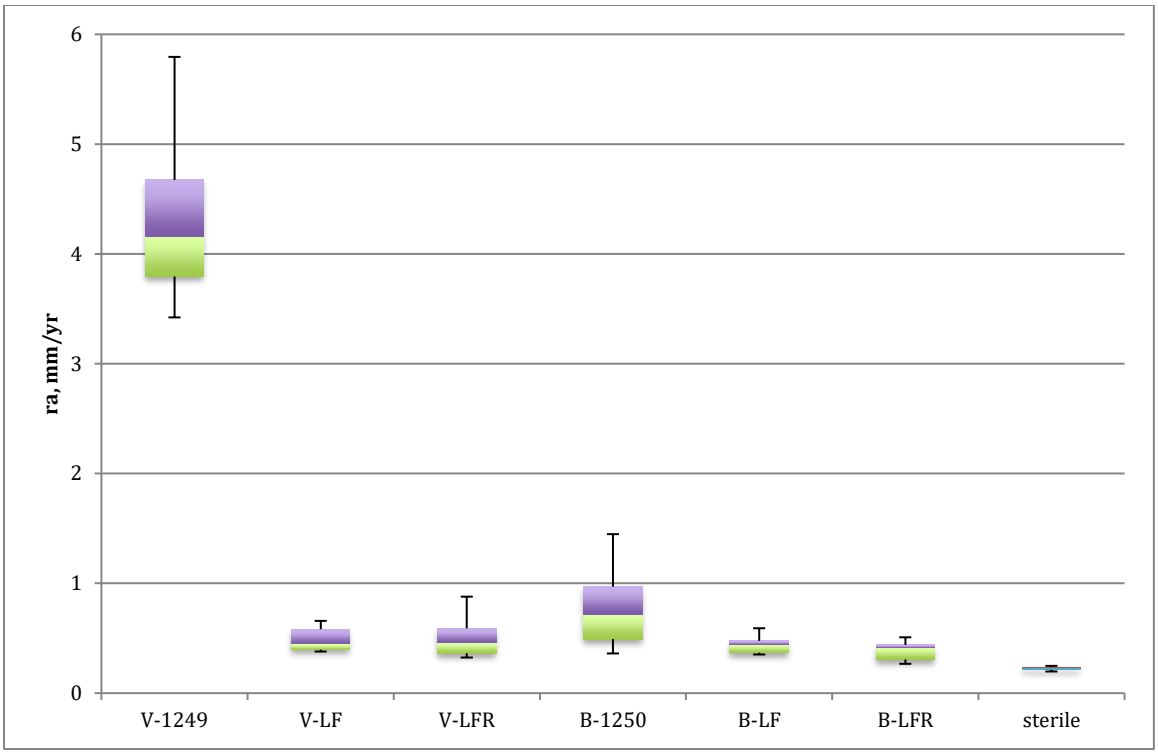

Figure 6.2-ra values obtained in the lab in 6 test media

Former studies showed that r_a values can be highly affected by temperature [170]. Temperature can be considered as a calibrating parameter for r_a. Figure 6.3 and Figure 6.4 demonstrate r_a values as a function of temperature for D. vulgaris and D. bastinii, respectively. Similar scale was used for D. bastinii. However for D.vulgaris the scale of media 1249 is different due to higher r_a values in this media. For both strains an increasing trend with temperature is observed. The trend is more pronounced in 1249 and 1250 media due to higher overall values of r_a. Rise in corrosion loss happens with increasing temperatures in all media for both SRB strains at incubation period.

Figure 6.5 shows r_a values as a function of temperature for field data. The exponential change due to temperature rise is slightly higher for field data, but they are still comparable with lab results. This slight difference can be due to wider range of temperatures at field. Field data included temperatures as low as 4˚C. Bacterial activity at these temperatures are minimal.

Therefore there is more variability in r_a values measured at 4˚C in comparison to higher temperatures like 35˚C.

a.

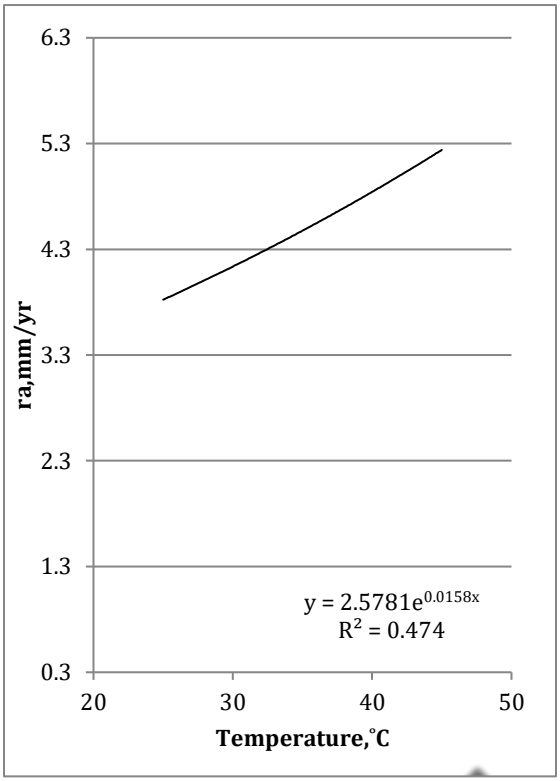

b.

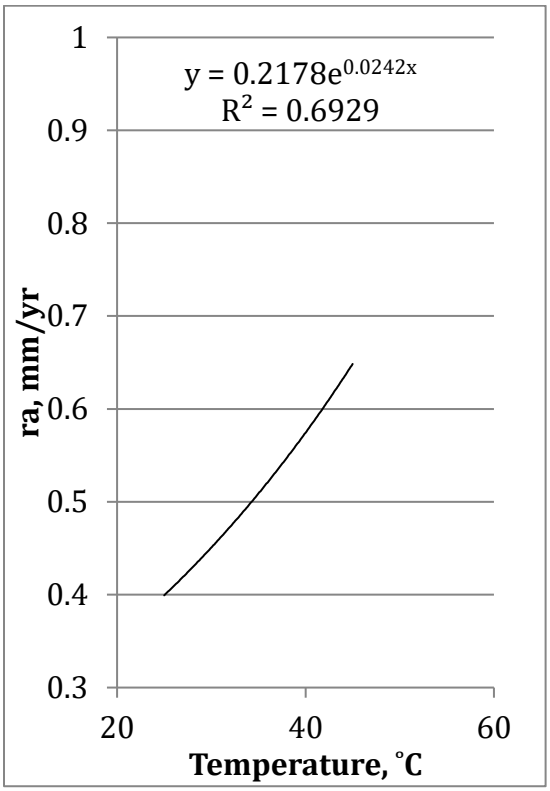

c.

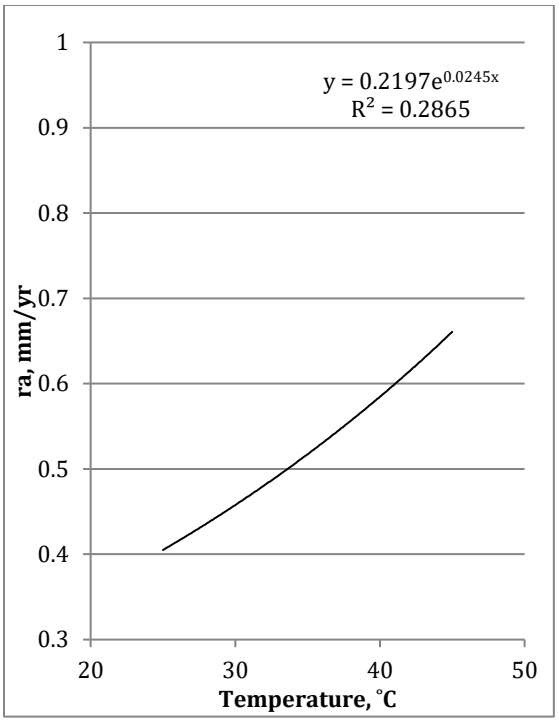

Figure 6.3- ra as a function of temperature for D. vulgaris in (a) 1249, (b) 1249-LF, (c) 1249-LFR media.

a.

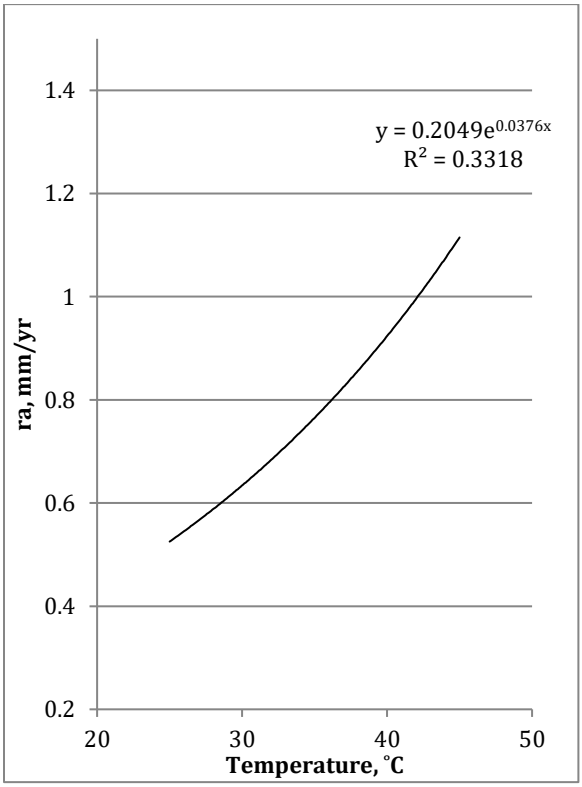

b.

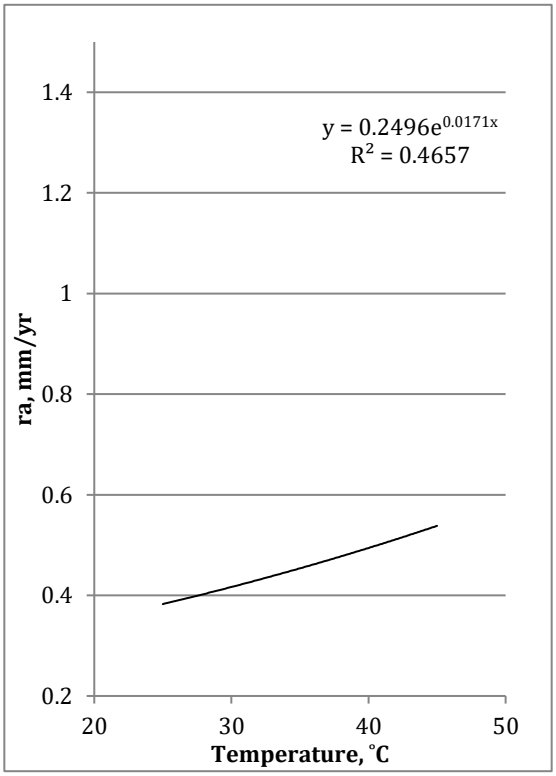

c.

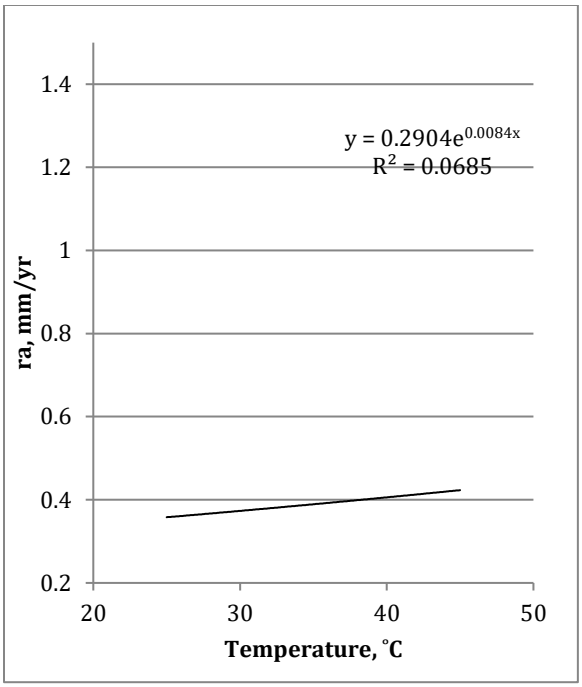

Figure 6.4- ra as a function of temperature for D. bastinii in (a) 1250, (b) 1250-LF, (c) 1250-LFR media.

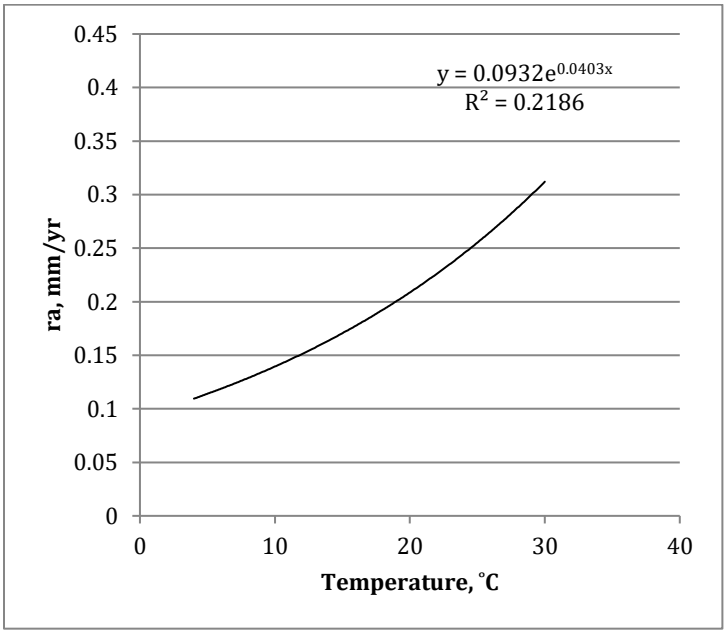

Figure 6.5- ra as function of temperature for data obtained from field

6.2.2.2 r_s

r_s represents corrosion loss in the second week of immersion. Unlike first week, all corrosion loss was not increasing for all samples. There were slight drop in corrosion loss in some samples. Note that 14-day samples and 7-day samples are different coupons i.e. separate coupons

were placed for 7 days and 14 days in solution. So some r_s values were negative. Figure 6.6 shows r_s range in different test media. SRB activity significantly drops in original growth media (1249 & 1250) after first week because most of the sulfate is consumed in the first week. This sulfate depletion along with H_2S production impedes further multiplication of SRB therefore corrosion rate drops. That is why in both of these media negative r_s values are obtained.

In the LF media, no negative r_s value is recorded. This is because cell multiplication happens during the whole period with a slower rate, instead of all the cell multiplication happening at the first week with higher rate. Less H_2S is produced as well due to smaller cell population. This pattern change in this media is due to limitation of nutrients. The sulfate consumption during the first and second week was almost equal in this media. As a result, there is no drop in corrosion loss during second period. Interestingly, LF media for both SRB strains (V-LF and B-LF in Figure 6.6) had highest r_s values.

r_s values are generally smaller than r_a values, however they have the key role in determining overall corrosion rate [170]. Figure 6.6 shows how the elimination of organic electron donor changes the long-term corrosion pattern. Intuitively, it is expected that the elimination of nutrients suppress corrosion, however, it is the other way around. Elimination of lactate increases corrosion rate overtime (higher r_s values indicating higher corrosion loss).

r_s values under field conditions ranged from 0.05 to 0.75. Similar range was observed for $r_s$values in this study (-0.7-0.62) (excluding negative values). In the long-term r_s value determines the corrosion rate. Therefore this good agreement with field and lab conditions enables us to have an appropriate prediction of long-term corrosion.

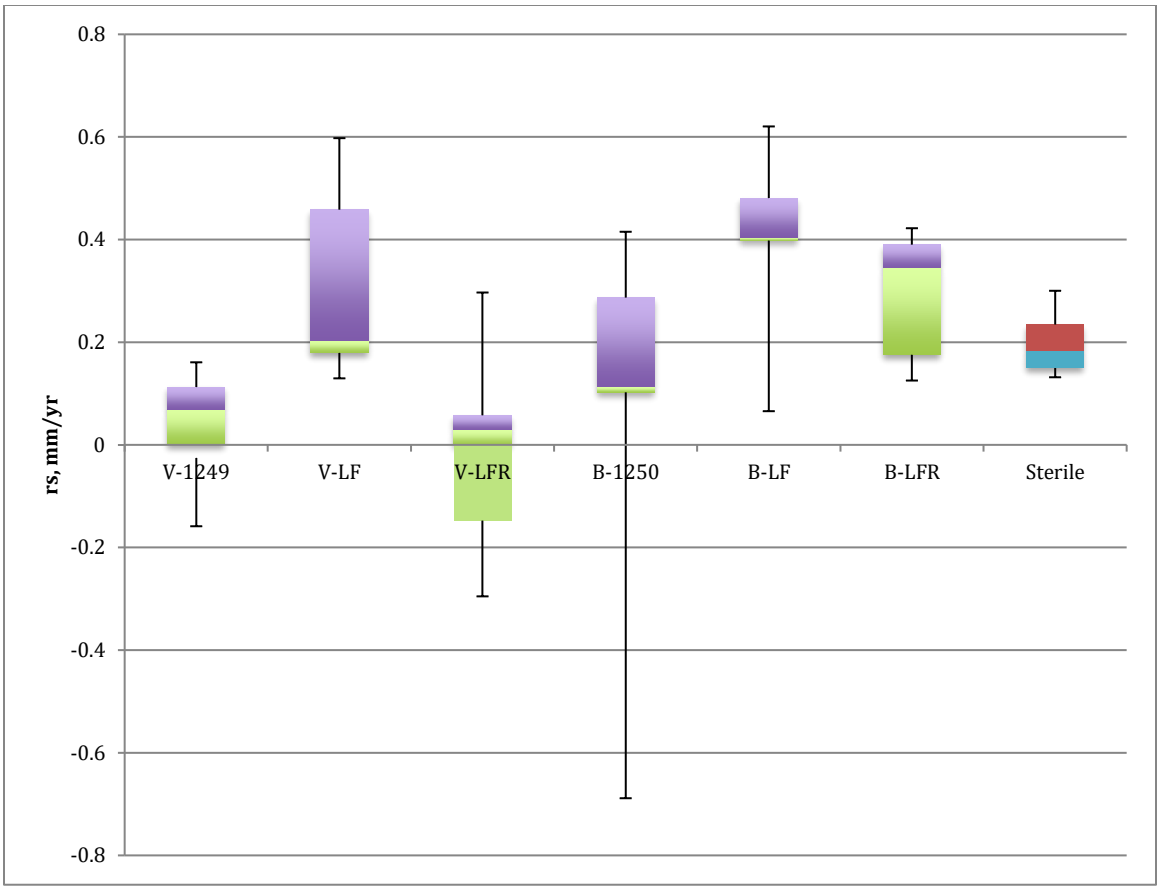

Figure 6.6- r_s values obtained in the lab in 6 test media.

r_s as a function of temperature for D. vulgaris in different media are depicted in Figure 6.7. Due to presence of negative values in 1249 and LFR media a trend cannot be visualized. However, in LF media an increasing trend with temperature is observed. This figure also shows how r_s values are suppressed in 1249 media. LF media clearly had higher r_s values.

Figure 6.8 shows the dependence of r_s on temperature for D. bastinii. Figure 6.8-a resembles its counterpart for D.vulgaris (Figure 6.7-a). In these two figures, corrosion loss dropped during second period with increasing temperatures. In media 1249 and 1250, due to availability of nutrients SRB were highly active within first week and consumed most of the sulfate, so the SRB activity diminished during second week. However, this negative values do not occur in real life.

a. b.

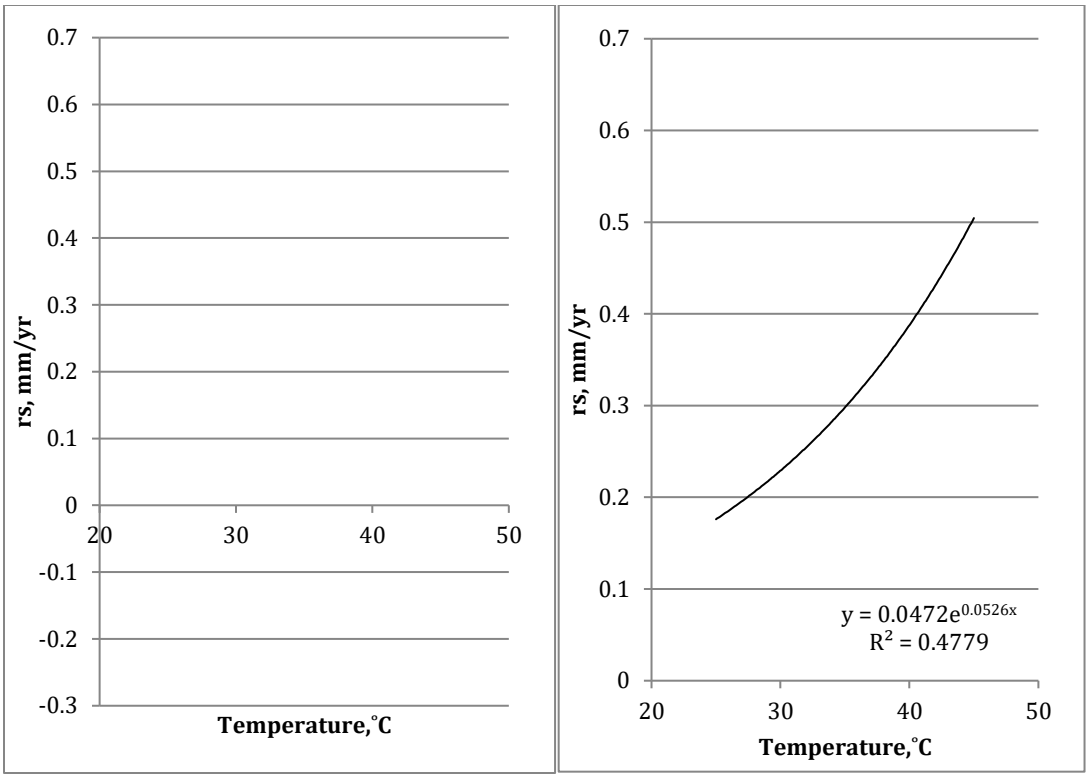

c.

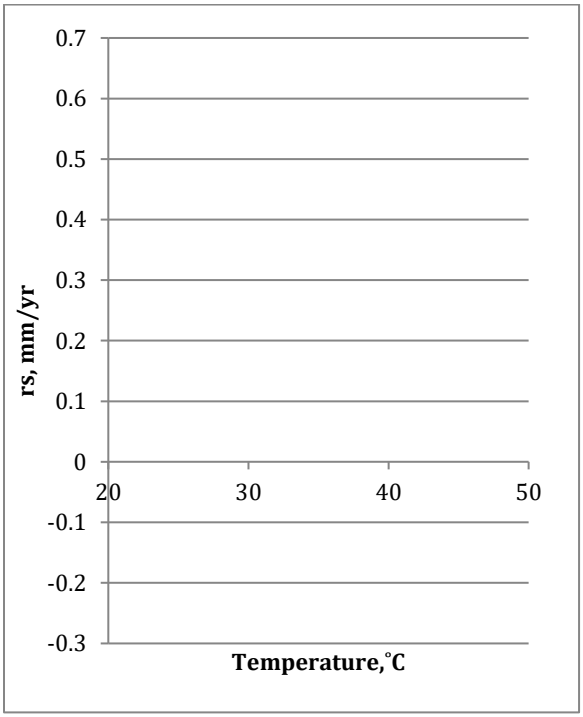

Figure 6.7-r_s as a function of temperature for D.vulgaris in (a)1249, (b)1249-LF, (c)1249-LFR media.

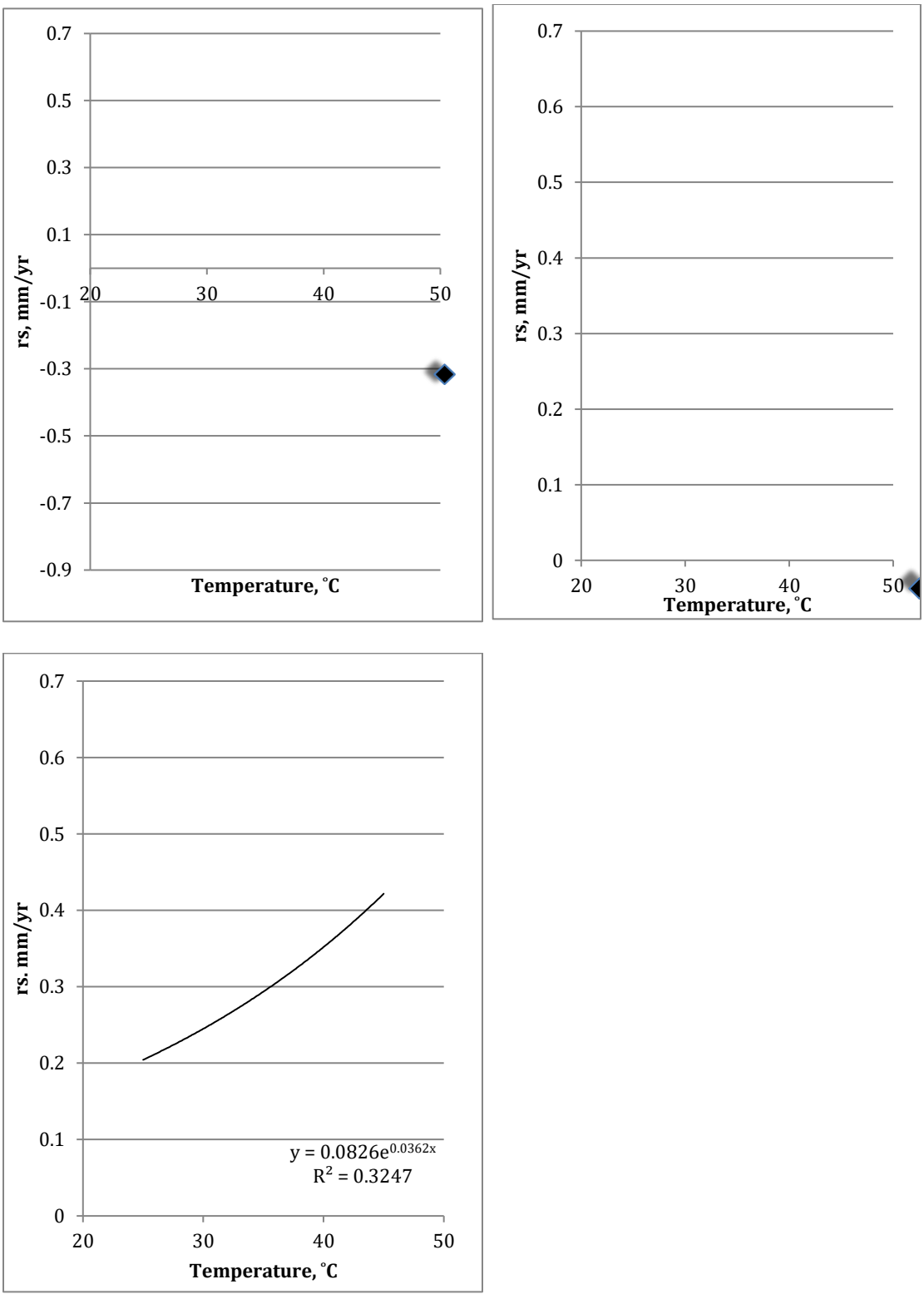

Figure 6.8-r_s as a function of temperature for D.bastinii in (a)1250, (b)1250-LF, (c)1250-LFR media.

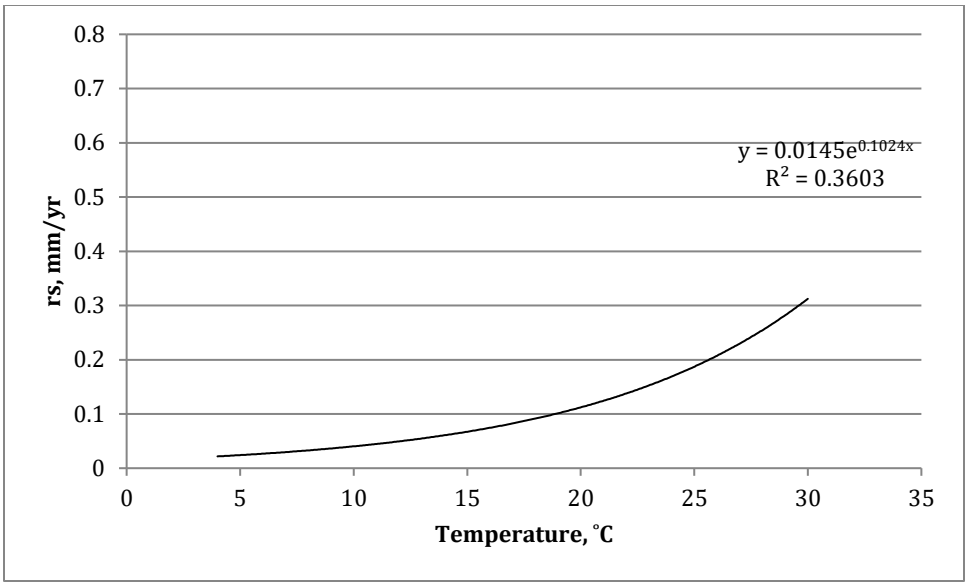

Figure 6.9- r_s as a function of temperature for data obtained from field

6.2.2.3 c'_s

c'_s reperesents the intercept of this line $corrosion\ loss = r_s t + c'_s$. Highest recorded value for c'_s is 0.041. At field conditions, c'_s ranges from 0.05 to 0.3. Ranges of lab and data are close overall. However very little data were gathered for c'_s. Most of field studies measured c_s, which is the intercept with phase 1 y axis (Figure 6.1). Therefore, a comprehensive conclusion cannot be made. Drawing conclusion based on c'_s can be misleading, since this value is dependent on r_s parameter. r_s values were analyzed in previous section. Figure 6.10 is only included to provide the range of this parameter.

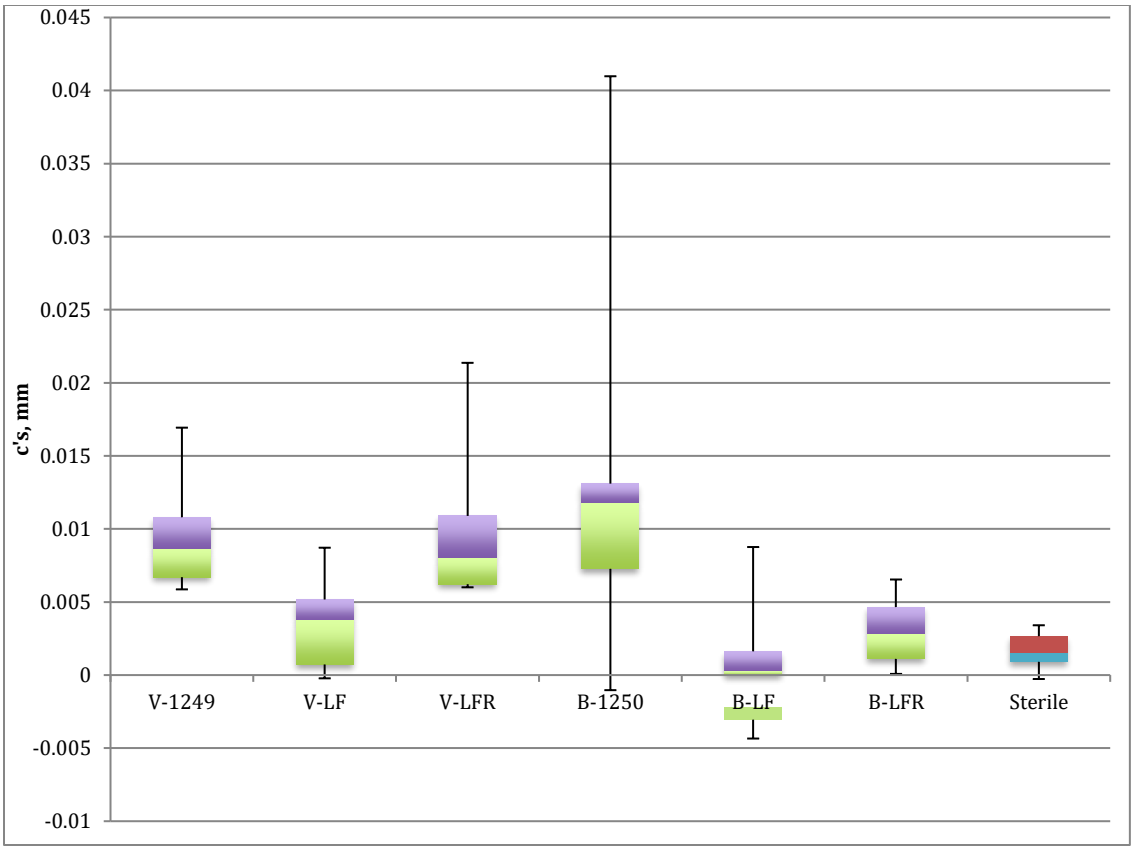

Figure 6.10-c'_s values obtained in the lab in 6 test media.

6.3 - Modeling

In this section, two distinct models developed for MIC prediction are discussed: multiple linear regression and artificial neural network based models.

6.3.1 Regression modeling

Regression analysis is the most commonly used statistical methodology applied to real-world phenomena [171]. Many other modeling tools have foundations in regression analysis. Regression analysis helps looking at real-world phenomena quantitatively and improves our decision-making strategies. In this section, regression models developed for anaerobic MIC, are discussed. Two main regression models are developed; multivariate regression model, and logarithmic multivariate regression. These models are statistically analyzed and compared. Regression models were developed using R libraries.

6.3.1.1 Multivariate linear regression model

Initially a multivariate linear regression (MLR) model is built based on experimental data. A set of predictor variables is considered as discussed in the correlation analysis section to predict mass loss. These variables are: bacteria type, media type, pH, temperature, exposure time (duration), and sulfate consumption rate (X1_sulfcons). Among the aforementioned predictors, two of them are qualitative values: media type and bacteria type. In order to include these two variables in the model, they are turned into binary values. For representing categorical variables (i.e. bacteria type and media type), number of binary-valued columns should be one less than the number of different types in the dataset. Therefore, to represent two bacteria types with binary variables, one column with 0 and 1s suffice, with 0 indicating one bacteria type and 1 the other. Also, to represent 3 different media types in the dataset, two binary columns, representing two of the media types are generated and included in the model. At most one of these two columns can take a value of one, and two zeros indicates the third media type.

As a first step, a linear model is fitted using all the available predictors. Summary of this model is presented in Table 6.8. Regression standard error shows how far the fitted data are from observed values. It has same unit as the response function, which is in grams. Coefficient of determination and adjusted R^2 are also presented. Adding more variables to the linear regression model always improves R^2. Therefore, adjusted R^2 is a better criterion for comparing models with different sets of predictors as it does not necessarily increase with addition of predictors to the model, as there exist a penalty term for number of predictor variables included in the model.

Generally, to determine whether any of the regression parameters are statistically non-zero, global usefulness test is performed. Null hypothesis for this test assumes that all regression parameters are zero. Alternative hypothesis states that at least one of these coefficients is not zero. If the null hypothesis is rejected then we can proceed to calculate regression parameter. P-value for this test was $7.05*10^{-7}$, which is very small and the null hypothesis is very unlikely to be true.

Once the regression parameters were calculated, student t test is performed on each of the coefficients for statistical evaluation. Null hypothesis for this test assumes a specific coefficient is zero while alternative hypothesis assumes it is non-zero. All of the parameters turned out to be significant for this analysis. Results of the student t test and coefficients for each variable are shown in Table 6.9; First column shows coefficients and intercept of the model. Last column shows probabilities calculated for each t value. All of the probabilities are very small, indicating the rejection of the null hypothesis with high probability (the coefficient being zero, i.e. not significant) except for pH. Therefore, all predictor variables should be included in the model. Since a simpler model is more favorable, as the next step, a new regression model is built by removing pH. Summary of this model is also presented in Table 6.8. R squared dropped less than 4% and pH seems to be a non-influential parameter.

Table 6.8-Multiple linear regression model summary

Name	Sample size	Multiple R squared	Adjusted R squared	Regression Std.Error
MLR	76	0.444	0.3869	0.02408
MLR exc. pH	76	0.4271	0.3773	0.02427

Table 6.9- Coefficients attained for multivariate regression model

	Estimated coefficient	Std. Error	t value	Pr(>|t|)
(Intercept)	-0.0473435	0.0380577	-1.244	0.21777
pH	0.0070611	0.0048973	1.442	0.15394
Temperature	0.0019557	0.0004167	4.693	1.35E-05
duration	0.002637	0.0008272	3.188	0.00217
bacteria_type_vulgaris	-0.0107318	0.0055809	-1.923	0.05867
media_type_1249LFR	-0.0163771	0.0067598	-2.423	0.01807
media_type_1249	0.0223291	0.0113525	1.967	0.05328

X1_sulfcons	-0.0241868	0.0111126	-2.177	0.03299

Assesing the residuals of the model are an important step in regression modeling, as they can show whether the underlaying assumptions of the regression model are actually met, and they can indicate outlier data points. Standardized residuals for each fitted data point in MLR model are demonstrated in Figure 6.11. Residuals appear to be spread randomly around their mean. Residuals have a small deviation, except for a few points that are marked with numbers (points 29, 47 and 62).

Residuals should also follow a normal distribution, which is checked by looking at the Quantile-Quantile plot (Q-Q plot). Q-Q plot is an excellent tool to check whether a dataset follows a distribution or not. The data set is divided into quantiles as well as the probability distribution. If plotted points of observation quantiles vs. distribution quantiles, fall on the diagonal line, population is following the specified probability function distribution. Figure 6.11-b shows the normal distribution Q-Q plot of the residuals. They seem to follow the normal distribution fairly well, except at very low probabilities and very high values, that could be partly due to outliers that are identified with numbers on the plot. Residuals is a good way of detecting outliers.

a. b.

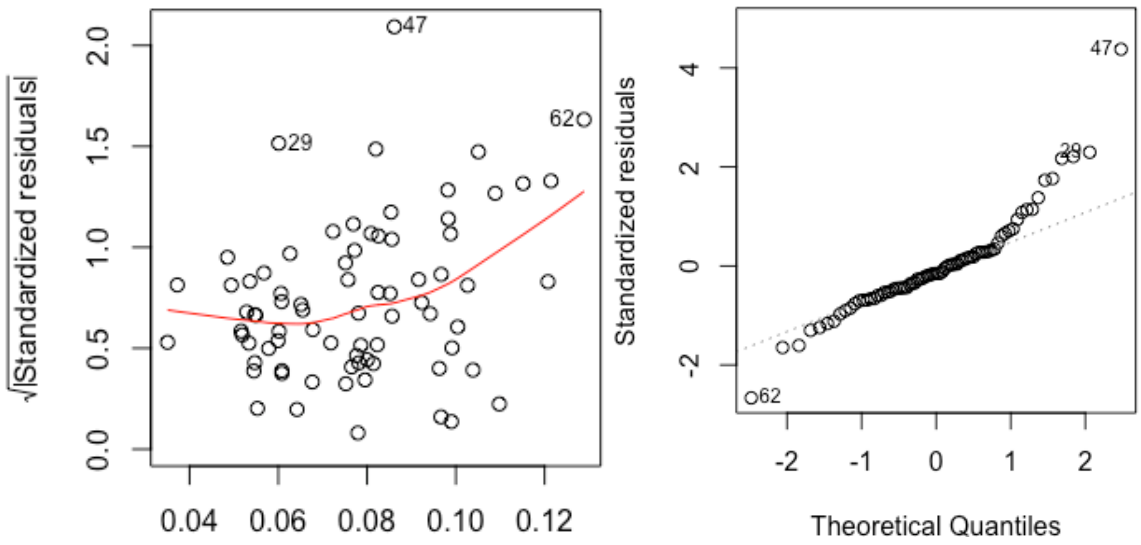

Figure 6.11- a. Standardized residuals vs. fitted values for the multiple regression model, b. quantile-quantile plot of residuals for the multiple regression model

Another method to identify outliers is through calculating Cook's distance. Cook's distance not only takes into account data points with unusual responses (y values), but also identifies sample responses with unusual predictor values (values with high leverage). Leverage represents values with unusual predictors. Figure 6.12 shows Cook's distance for the residuals of the model. If residuals are beyond Cook's distance, they have a significant effect on skewing the data and biasing the model. One of the data points (point 47) in Figure 6.12 is very close to Cook's distance.

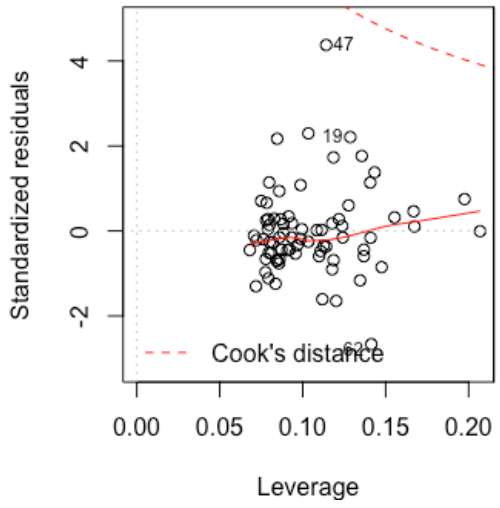

Figure 6.12-Cook's distance for the multiple regression model

Now that the outliers are detected, all previous analysis are repeated for MLR model, with exclusion of the three potential outliers from the data set. Summary of the newly fitted model is presented in Table 6.10. Both R^2 and adjusted R^2 has improved more than 40%. New regression coefficients are presented in Table 6.11. The coefficients did not change significantly.

Table 6.10-Multiple linear regression model summary without 3 outliers

Name	Sample size	Multiple R squared	Adjusted R squared	Regression Std.Error
MLR wo outliers	73	0.6213	0.5805	0.01835

Table 6.11- Coefficients attained for multivariate regression model without 3 outliers

	Estimated coefficient	Std. Error	t value	Pr(>|t|)
(Intercept)	-0.0520821	0.0300051	-1.736	0.087342
pH	0.0063967	0.0038602	1.657	0.10232
Temperature	0.0021003	0.0003276	6.41	1.88E-08
duration	0.0034933	0.0006422	5.44	8.66E-07
bacteria_type_vulgaris	-0.0109045	0.0043654	-2.498	0.015032
media_type_1249LFR	-0.0213496	0.0052575	-4.061	0.000134
media_type_1249	0.0173274	0.0087385	1.983	0.051608
X1_sulfcons	-0.0267189	0.0086559	-3.087	0.002973

Residuals plots better visualize the improvement in the model. The standardized errors range clearly shrunk (Figure 6.13-a). Residuals are spread better around their mean value, and residuals follow the diagonal line in the q-q plot (Figure 6.13-b) more accurately. Covariance of predictors are also calculated for both linear models (w/ & w/o outliers). This information is included in the appendix.

a. b.

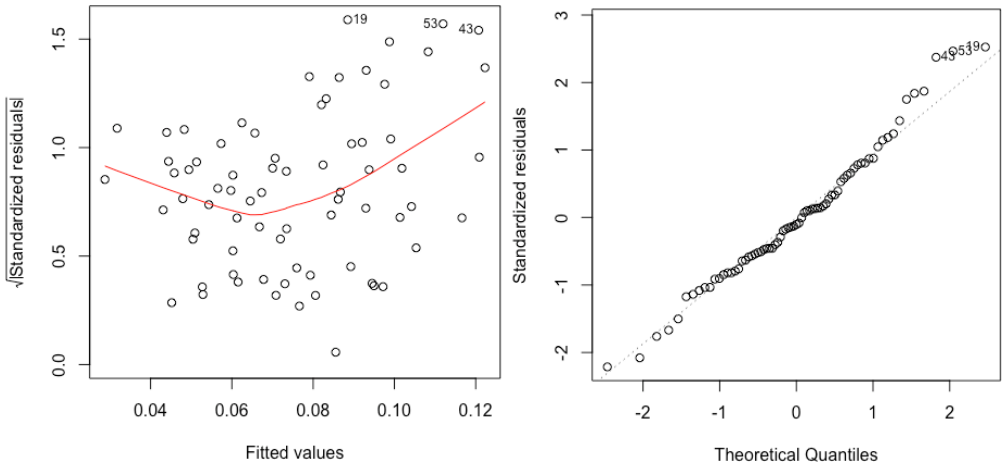

Figure 6.13- a. Standardized residuals vs. fitted values for the multiple regression model without outliers, b. quantile-quantile plot of residuals for the multiple regression model without outliers.

6.3.1.2 Logarithmic Multivariate regression model

In logarithmic multivariate regression model, a MLR is built to predict logarithm of the response variable (i.e. mass loss) based on logarithm of numerical predictors and categorical variables. A log-log model represents a non-linear relationship between the predictors and the response. Moreover, it helps to reduce the adverse effect of outliers and points with high leverages. Since removing an observation to attain better fit of the data can be considered as manipulating analysis towards our purposes arbitrary elimination of points is not appropriate. Logarithmic transformation can reduce the adverse effect of extreme observations without their complete removal from the data set.

When a logarithm transforms the non-linear relation of the predictors and response into a linear relation, suited for a MLR. Assume the following relationship between response variable A and numerical predictor C and categorical predictor B:

$$A = \alpha\beta^{B}C^{\gamma} \qquad \text{Eq. 6.1}$$

α, β and γ are the parameters that need to be calibrated. By taking the logarithm of the two sides:

$$\log(A) = \log(\alpha) + \log(\beta)\,B + \gamma \times \log(C) \qquad \text{Eq. 6.2}$$

Now, α, log(β) and γ can be estimated through MLR model.

Logarithm of mass loss, temperature, duration, X1_sulfcons and pH were calculated to fit a log multiple linear regression (LMLR). Initially global usefulness test was performed. Attained p-value was very small ($9.73*10^{-10}$). Therefore we can start the regression analysis by including all predictors. Summary of the logarithmic model with and without pH is shown in Table 6.12. R^2 has slightly improved for logarithmic model than the previous model. This can be rooted in the fact that adverse effect of outliers was slightly dampened by logarithm approach.

Coefficients of regression are shown in Table 6.13 along with t-student stats. t-student results indicate that none of the coefficients can be considered zero.

Residuals plots in Figure 6.14 help to better assess the model. Standardized residuals have a smaller range in the logarithmic model in comparison to the linear one. Residuals are better spread around their mean. The data points in the Q-Q plot are also closer to the diagonal line. Last but not least, Figure 6.15 shows how far the residuals are from Cook's distance. Residual plots overall showed that regression was improved in logarithmic scale. The final non-linear model is as follows:

$$A = -7.6767 \times bacteria\_type\_vulgaris^{-0.136} \times media\_type\_LFR^{-0.28} \times media\_type\_M^{0.1857} \times pH^{0.683} \times Temperature^{0.821} \times duration^{0.366} \times X\_1sulfcons^{-0.13} \quad \text{Eq. 6.3}$$

Table 6.12- Logarithmic multiple linear regression model summary

Name	Sample size	Multiple R squared	Adjusted R squared	Regression Std.Error
LMLR	76	0.5478	0.5022	0.2651
LMLR exc. pH	76	0.4797	0.4425	0.28

Table 6.13- Coefficients attained for logarithmic multivariate regression model

	Estimated Coefficient	Std. Error	t value	Pr(>|t|)
(Intercept)	-7.67671	0.94196	-8.15	1.17E-11
log(pH)	0.68267	0.40478	1.687	0.096276
log(Temperature)	0.82067	0.14157	5.797	1.92E-07
log(duration)	0.36614	0.09047	4.047	0.000135
Log(X1_sulfcons)	-0.1296	0.0432	-3	0.00377
bacteria_typevulgaris	-0.13558	0.06221	-2.179	0.032765
media_typeLFR	-0.28034	0.07823	-3.584	0.000632
media_typeM	0.18573	0.0909	2.043	0.044909

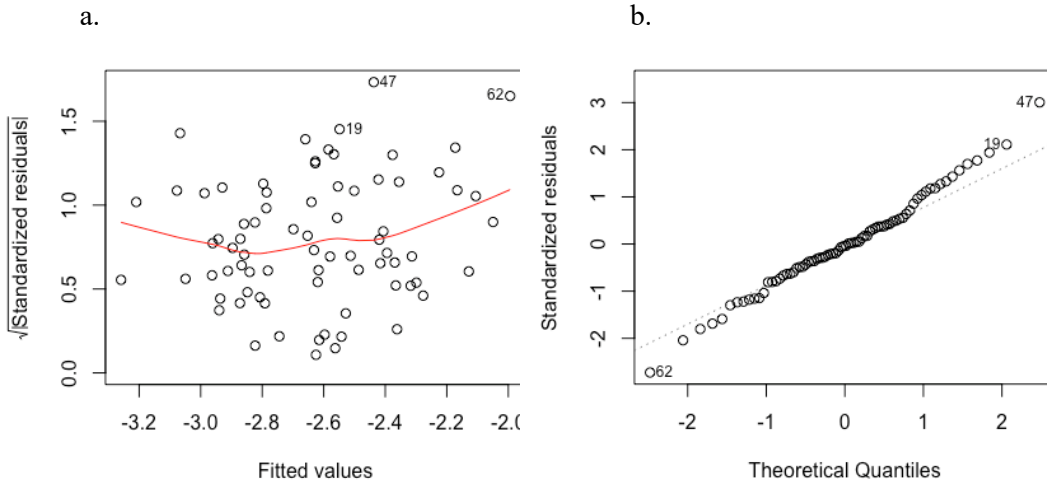

Figure 6.14- a. Standardized residuals vs. fitted values for the logarithmic multiple regression model, b. quantile-quantile plot of residuals for the logarithmic multiple regression model

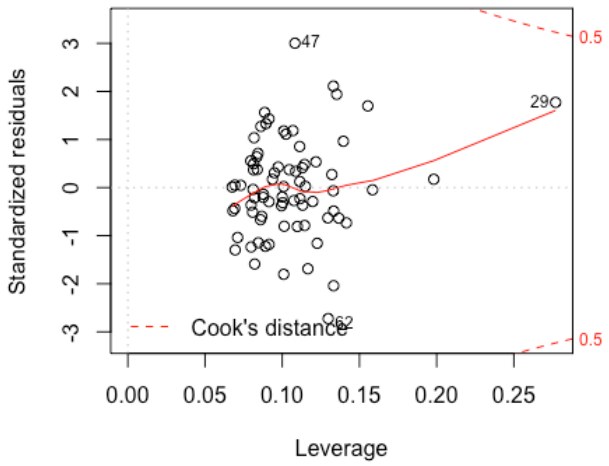

Figure 6.15-Cook's distance for the logarithmic multiple regression model

Statistical analyses were repeated excluding the outliers. Summary of new logarithmic model is presented in Table 6.14. Regression coefficients are presented in Table 6.15.

Standardized residuals after exclusion of 3 outliers are depicted in Figure 6.16-a. The Q-Q plot is also shown in Figure 6.16-b.

Table 6.14-Logarithmic Multiple linear regression model summary without 3 outliers

Name	Sample size	Multiple R squared	Adjusted R squared	Regression Std.Error
MLR wo outliers	73	0.6352	0.5959	0.2306

Table 6.15- Coefficients attained for logarithmic multivariate regression model without 3 outliers

	Estimated Coefficient	Std. Error	t value	Pr(>|t|)
(Intercept)	-7.82714	0.85417	-9.163	2.56E-13
log(pH)	0.66497	0.36399	1.827	0.0723
log(Temperature)	0.83624	0.127	6.585	9.34E-09
log(duration)	0.45328	0.08099	5.597	4.72E-07
Log(X1_sulfcons)	-0.09425	0.04247	-2.219	0.03
bacteria_type_vulgaris	-0.13952	0.05531	-2.523	0.0141
media_type_LFR	-0.31045	0.06905	-4.496	2.92E-05
media_type_M	0.08148	0.08333	0.978	0.3318

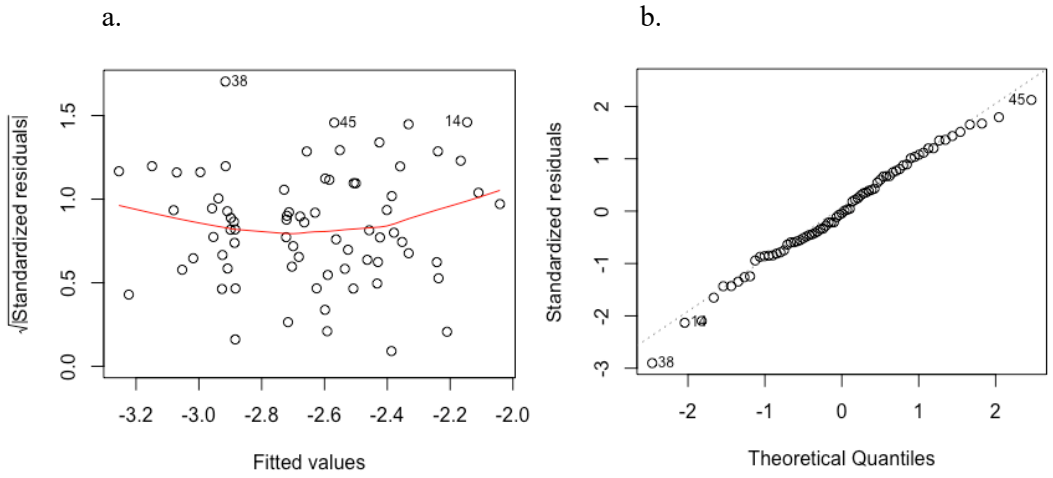

Figure 6.16- a. Standardized residuals vs. fitted values for the logarithmic multiple regression model without outliers, b. quantile-quantile plot of residuals for the logarithmic multiple regression model without outliers.

6.3.2 Regression diagnostics

Two further diagnostics were implemented on the regressions. First diagnostic is stepwise regression. This method builds the regression model in a step-wise manner, adding or removing variables as predictors, based on model statistics. Second diagnostic is K-fold cross validation. The error obtained from a regression model does not account for future (out of sample) predictions. K-fold cross validation calculates a more reliable R^2 based on K sets of out-of-sample performance. In each iteration one fold (approximately 1/K of data points) are set aside as test samples and regression model is built without those records. Then the prediction of the model is assessed solely on the set-aside data. This is repeated for all K subsets and the R^2 is calculated based on all out-of-sample predictions. These two techniques were performed on the data and the results are discussed in this section.

6.3.2.1 Stepwise regression

It was shown in previous sections that at least one of the predictors (i.e. pH) in the model might be insignificant. In order to more systematically look for the best model that provides the best combination of fit and number of predictors, stepwise regression analysis was performed on the data. Stepwise regression is a variable selection method. If there are p potential predictors, 2^p

models can be developed including the model with an intercept only. Stepwise regression investigates several possible models and selects the best combination based on a set criterion. It has three procedure: forward addition, backward elimination, or a combination of both [172]. A common forward addition operates as follows: Initially p-values for models built for each separate predictor are calculated. Predictor with the lowest p-value is selected e.g. X_1. In the next step, p-value is calculated for the models including X_1 and each of the remaining predictors. Then the two predictors with lowest p-value proceed to next round. This process continues only until the set criterion is improving. In this analysis Akaike Information Criterion (AIC) was chosen as the criterion. AIC for a Gaussian model is defined as AIC= nlog(RSS/n)+2p (RSS is sum of squared residuals and n is sample number). The goal is to minimize AIC. First term in AIC formula measures goodness of fit. Second term is added to penalize the model for adding unnecessary predictors. The stepwise regression continues as long as AIC can be reduced.

Results of stepwise regression for both LMR and LMLR showed that best fit includes all 6 predictors.

Considering the size of data set and number of predictors, it is possible to perform an exhaustive search on models built for all the possible subsets of predictors (2^p). Figure 6.17 shows top 5 models (based on R^2) for different subset sizes of variables (1 to 7). It can be observed how R^2 increases as more predictors are added into the model. It also shows R^2 for different combination of predictors.

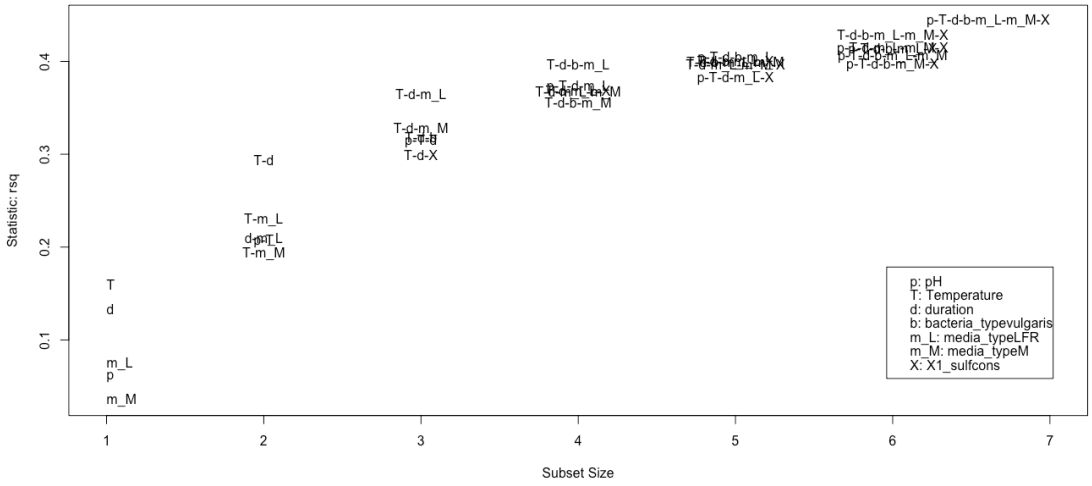

Figure 6.17- R^2 improvement during stepwise regression process for multiple linear regression model.

6.3.2.2 K-fold cross-validation

Errors obtained from a model that fits to all of the data do not give a realistic understanding of neither the error nor the R^2. Cross-validation technique provides a better evaluation of these two parameters. In k-fold cross-validation, data is divided into k subsets. The training is performed on k-1 subsets, and one subset is kept for validation of the fitted model. Then another subset is set aside and the other k-1 subsets are used to train the model. In each step, cross-validation is performed on the subsets not used in the training. This process is repeated k times and it gives a more realistic error of estimate.

A 10-fold cross validation was done on the data to gives a more realistic coefficient of determination R^2. A multiple linear regression and a logarithmic multiple linear regression were fitted to data applying cross validation method. Response values (mass loss) predicted from cross validation are plotted vs. response values obtained from previous models (MLR & LMLR) in Figure 6.18 and Figure 6.19. Data points in the testing subset are shown with larger symbols.

With a 10-fold cross validation, R^2 shrunk from 0.444 to 0.297 (34% decrease) for the linear model, while it shrunk from 0.5487 to 0.416 (25% decrease) for the logarithmic model (LMLR).

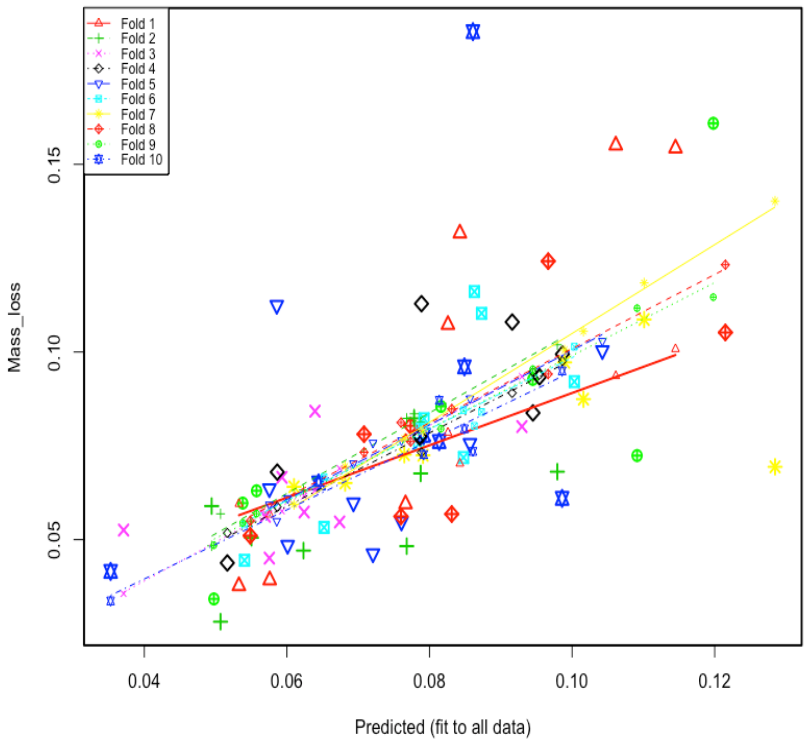

Figure 6.18-10-fold cross validation for multiple linear regression model (MLR)

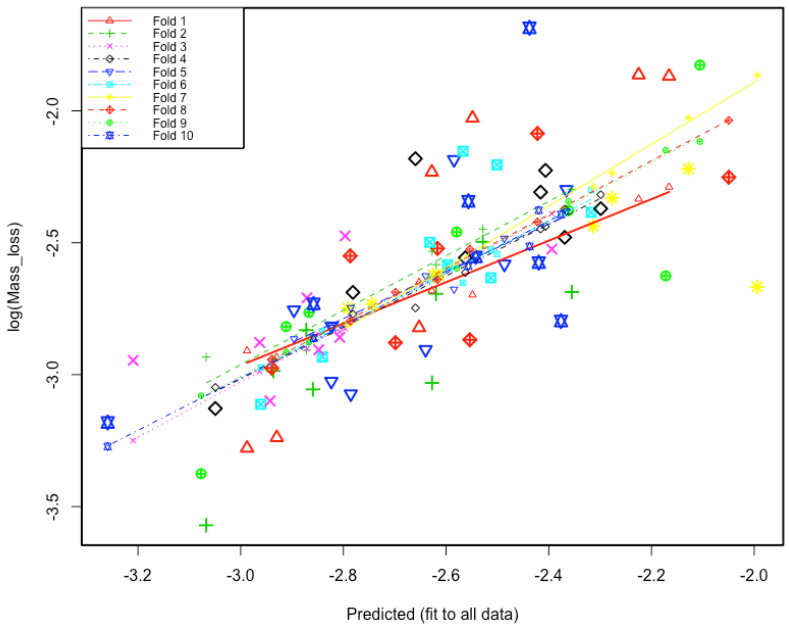

Figure 6.19-10-fold cross validation for logarithmic multiple linear regression model (LMLR)

6.3.3 Neural network modeling

Artificial Neural Network (ANN) is a modeling procedure inspired by human brain neural system. ANN is a powerful tool for modeling non-linear and complex systems. It is a super-regression technique [173]. Learning paradigms in ANN can be divided into two categories: supervised or unsupervised. In supervised learning a "teacher" provides additional input to assess how well the model is performing. As an example of supervised learning, actual values of a predicted output can be used to assess the accuracy of the output and train the network. On the other hand, in unsupervised learning there is no measure to evaluate performance of the model. Unsupervised learning is used in clustering and pattern recognition problems.

Several studies took advantage of ANN for corrosion modeling. Trasatti and Mazza (1996) implemented an ANN to predict crevice corrosion of alloys in chlorinated environments [174]. ANN was also used in another study to predict atmospheric corrosion of steel and zinc [173]. Rosen and Silverman (1991) developed a neural network that used potentiodynamic polarization scans as input to detect initiation of pitting and crevice corrosion [175]. In another study, ANN was constructed to assess risk of stress corrosion cracking (SCC) in stainless steel in chlorinated waters. The network incorporated temperature, chlorine concentration and oxygen as inputs to evaluate risk of SCC [176].

6.3.4 Neural network

Artificial neural network predicts an output based on complicated non-linear relations in the network. In Neural network algorithm information from inputs are transferred to processing elements and produce the outputs. ANN structure consists of multiple layers, each layer formed from a set of nodes called neurons. Nodes transfer information to each other through weighted connections. At each node, information coming from other nodes through weighted connections

is summed up and then an activation function is applied to this summation to produce the node's output. Schematic of this process is depicted in Figure 6.20. w_i represents weight coefficients of inputing neurons. Function f(.) is any arbitrary activation function applied to summation of weighted inputs [177]. The result is then transferred to other nodes through weighted connections.

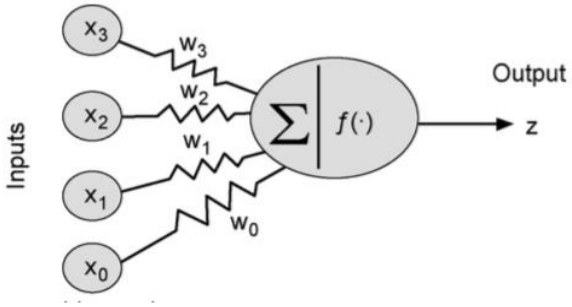

Figure 6.20-Schematic of inputs and outputs of a node in neural network [177].

Activation functions in neural networks are generally non-linear. A very popular activation function is the sigmoid function:

$$s(x)=\frac{1}{1+e^{-x}} \qquad \text{Eq. 6.4}$$

Output in Figure 6.20 upon application of sigmoid function would be:

$$z=\frac{1}{1+e^{-(\Sigma_i w_i x_i)}}=\frac{1}{1+e^{-(w_0x_0+w_1x_1+\cdots+w_3x_3)}} \qquad \text{Eq. 6.5}$$

Other common activation functions include hyperbolic tangent, linear threshold function, step function.

6.3.4.1 Feedforward neural network

Different training algorithms can be implemented in neural networks resulting in different architecture, function, and behavior. Neural networks can be divided into two categories

based on network architecture: feedforward and recurrent. Schematic of a feedforward model is depicted in Figure 6.21. This model consists of several hidden layers with arbitrary number of neurons. In this model, outputs from neurons in each layer only move forward, thus the connections between nodes do not form a cycle. In other words, network proceeds according to neurons layer numbering (k as in Figure 6.21). The activation function is applied to summation of weighted inputs to each neuron before the neurons in next layer are examined [178]. The designer can use any transfer function between layers. Multilayer perceptron (MLP) is a common network in feedforward architecture [179]. In contrast, networks that transfer neurons outputs to previous layer are called recurrent networks.

Backpropagation is a common training method in supervised learning. Since the network's outputs are dependent on connection weights between neurons, the weights need to be changed to produce outputs that are aligned with our measured (desired) values. Backpropagation provides a method for adjusting network's weights and biases. In backpropagation method after a calculation of ANN's output based on a data point (i.e. a forward pass), predicted outputs are compared to actual outputs. The weights are readjusted with the goal of decreasing the calculated error. For instance consider a loss function (C_0) that is used as training tool to calculate error in a neural network with L layers. This function can be expressed as:

$$C_0 = \sum_{j=0}^{n-1} (a_j^L - y_j)^2 \qquad \text{Eq. 6.6}$$

In this equation, j counts the number of nodes in a given layer. a_j^L is the activation output of node j in layer L. y_j is the actual (desired) value of node j. Therefore, the loss function calculates error by subtracting the desired output from the output attained from the network.

It was mentioned earlier that an activation function is applied to entries of a node. Thus the output of a node is a result of applying an activation function to input of that node. This relationship can be demonstrated as follows:

$$a_j^L = g^L(z_j^L)$$ Eq. 6.7

where, z_j^L is the input for node j in layer L. g^L is the activation function used for layer L. The whole equation represents: The output of node j is a result of activation function g applied to inputs of node j.

The input to a node is a result of weighted sum of activation outputs from previous layers. This can be expressed as:

$$z_j^L = \sum_{k=0}^{n-1} w_{jk}^L a_k^{L-1}$$ Eq. 6.8

where, k counts the number of nodes in layer L-1 (note that j was the counter of nodes in layer L while k is the counter of nodes in layer L-1). w_{jk}^L is the weight of the connection that connects each node k in layer L-1 to node j in layer L. a_k^{L-1} is the activation output node k in layer L-1. So, overall the equation shows input to node j is the weighted sum of the values coming from previous neurons.

Now, if to calculate gradient of loss for a weight in the network, it can be seen that loss function is not only a function of output value a_j^L:

$$C_{0j} = C_{0j}(a_j^L\left(z_j^L(w_j^L)\right))$$ Eq. 6.9

Chain rule can be applied to calculate the derivative of the loss function. This shows how backpropagation is used in supervised training. In this study a multi-layer feedforward ANN is trained using backpropagation.

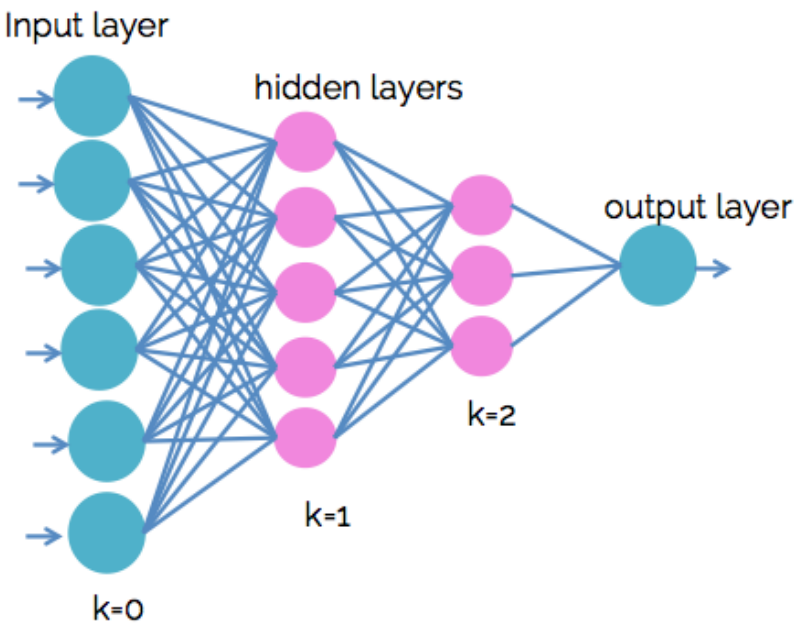

Figure 6.21- Schematic of a feedforward neural network with 2 hidden layers.

6.3.4.2 Neural network implementation

H_2O platform is used for building the neural networks in this study. There are multiple ANN characteristics and parameters that need to be selected before the training process begins. Important characteristics include activation function, number of hidden layers and number of nodes in each layer. H_2O provides an option for searching for the best ANN model in a grid of candidate models built with different structures. In this study, different number of hidden layers, different number of neurons in each of those layers, and different activation functions are used to build a grid of candidate networks. H_2O trains the networks and calculates errors for each of them. Three options for activation function are used in this study: rectifier, hyperbolic tangent, and maxout.

Rectifier function (ReLU) is represented as:

$$ReLU(x) = \begin{cases} 0, & x < 0 \\ x, & x \geq 0 \end{cases}$$ **Eq. 6.10**

This function has couple of advantages over the commonly-used functions in ANN (e.g. sigmoid): It is computationally inexpensive; and it does not suffer from vanishing gradient problem. It was shown in previous section that in order to calculate derivative of loss function for a specific weight a chain of derivatives must be multiplied. Vanishing gradient problem appears when there are numerous terms smaller than 1. Multiplication of these values approaches zero. Therefore weights in the network, especially ones in initial layers, are not modified very much. The downside of the rectifier model is that it can cause dead neurons in the network. For instance, if outputs of a neuron are always negative, the derivative of input to the following node with respect to weights remains zero ($\frac{\partial z_j^L}{\partial w_{jk}^L}$). Thus the weights are not updated. Despite the non-differentiability and non-linearity of rectifier function at zero, it is very useful for sparse data [180].

Hyperbolic tangent is another well-known activation function used in ANN. It is expressed as:

$$\tanh(x) = \frac{e^x - e^{-x}}{e^x + e^{-x}} \qquad \text{Eq. 6.11}$$

This function squashes entries in [-1,1] range. Its output is zero-centered which is an advantage over sigmoid function. However, it has the vanishing gradient problem.

Maxout function is expressed as:

$$maxout(x) = \max(z_{jk}) \qquad \text{Eq. 6.12}$$

Where $z_{ij} = x^T W_{\dots ij} + b_{ij}$ [181]. Its output is the maximum value of entering neurons.

A combination of different number of layers and number of nodes in each layer were tested in the architecture. Characteristics of ANN tested in this work are presented in Table 6.16.

Table 6.16-Features of ANN for MIC prediction

Description of ANN	Features

Number of input neurons in input layer	6
Number of neurons in output layer	1
Number of neurons in hidden layers	5 to 20
Number of hidden layers	1,2,3,4
Stop criterion	Cross Validation
Transfer function	Rectifier,Tanh, maxout

While the goal is to minimize the error of predictions vs. actuals, achieving minimum error does not always guarantee the best model. If the training of the ANN is continued until error is minimized, overfitting may occur. This means that the trained network has most accurate predictions for the training data, however, it might perform poorly when used for predicting output for new data, thus losing its generality. To avoid this problem cross validation technique is used during network training. In cross validation, part of the data is set aside as the cross-validation data and not used in network training and instead is used to validate the performance of the trained network after each training round (epoch). The training will stop when the prediction error on the cross-validation portion of the data increases.

In this study a k-fold (5-fold for the network developed herein) cross validation methodology is used. For 5-fold cross validation, dataset is randomly divided into 5 segments, with almost equal size. A total of 5+1 networks are trained for each ANN architecture, 5 for cross-validation folds and one general model trained on the complete dataset. For training of each of the 5 cross-validation networks, the associated cross-validation data is set aside and used for evaluation of the trained network. Mean squared error, coefficient of determination, and residual mean squared error for each fold were calculated.

Summary of top 5 fitted models are shown in Table 6.17. Mean squared error (MSE) was selected as the criteria for sorting the top model.

Table 6.17-ANN architecture for the top 5 models of MIC

Activation function	Hidden layers [number of nodes]	MSE
Tanh	[6,6]	3.66E-04
Rectifier	[7,7,7,7]	4.54E-04
Maxout	[10,10]	4.67E-04
Tanh	[12,12]	4.69E-04
Maxout	[6, 6]	5.04E-04

A 5-fold cross validation was performed on the best-fitted model represented in Table 6.17. The cross-validation method prevent overfitting the models and reveals how good the model can predict unseen data. Cross-validation error estimates the generality of the model. Figure 6.22-a shows the predicted vs. measured outputs of the general ANN model (model fitted to the complete dataset). It can be observed that most of the points fall on the bisector line, indicating a very good prediction of the model. The correlation coefficient of the best-fitted model was 0.948, an almost perfect prediction on the training set. Figure 6.22-b shows the prediction of the set-aside cross-validation data vs. their measured values. As expected, these points are farther from the bisector line since these points represent the prediction for data that was not used in training in the 5 cross-validation models. Correlation coefficient attained from 5-fold cross validation was 0.7854. This value, which is still high, gives a better prediction of networks performance on future new data. It must be noted that R^2 values are not usually reported for non-linear models. Because in non-linear models Total Variation (TV) is not equal to summation of Explained Bariation (EV) and Unexplained Variation (UV). Therefore R^2 is not square root of correlation coefficient. TV is the variation of measured points from the mean of y. EV is the variation of

predicted values about the mean of y. UV is the variation between measured and predicted values. Correlation coefficient is alternatively used.

Mean Average Error (MAE), Mean Squared Error (MSE), Root Mean Squared Error (RMSE), and Root Mean Squared Log Error (RMSLE) are calculated for each cross-validation fold and are represented in Table 6.18. There was not a significant difference among the statistical parameters of main model and models for cross-validation folds, indicating the generalized performance of the ANN.

a. b.

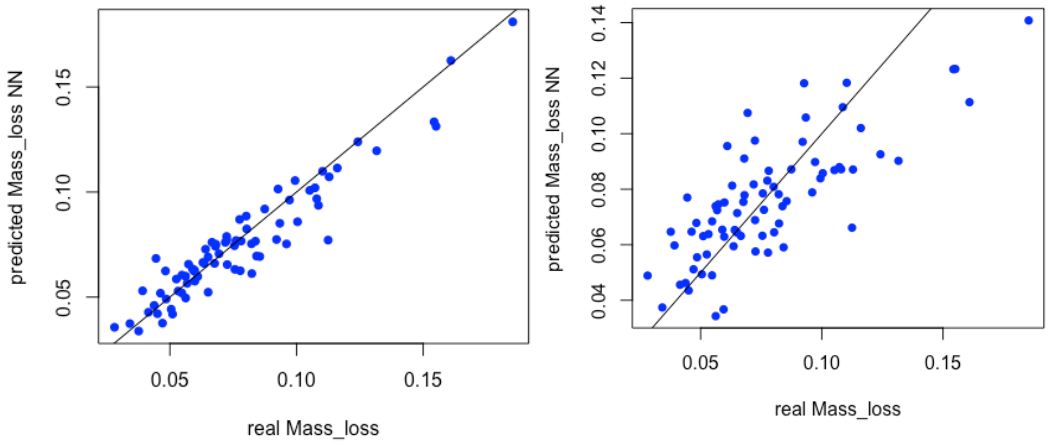

Figure 6.22-predicted values vs. measured values for bet-fitted ANN model (a) ANN trained on all data in the dataset (b) ANN trained via 5-fold cross validation.

Table 6.18- Statistical parameters obtained for different cross validation folds.

	Original Model	1st fold	2nd fold	3rd fold	4th fold	5th fold
MAE	0.01492	0.00246	0.0201	0.017905585	0.01161	0.01358
MSE	3.62E-04	1.02E-04	5.93E-04	4.53E-04	2.18E-04	3.36E-04
RMSE	0.01866	0.00266	0.0243	0.02127	0.014765	0.01832
RMSLE	0.01707	0.00234	0.02202	0.01934	0.01343	0.01692

Correlation coefficients (R) attained from ANN shows significant improvement over the regression models. Table 6.19 shows the correlation coefficients attained both for the model trained on the whole dataset and R for model attained from cross validation training. First set of R values are very high indicating good fit to the data. There was more than 100% increase in R for ANN compared to multiple regression models. Although there was a drop for cross-validation R values in comparison to the general ANN trained on complete dataset, they are still higher than cross-validation R from the regression. Cross-validation R values of ANN is also much higher than other corrosion models in literature [174][176][173].

Table 6.19- Correlation coefficient (R) attained for top 5 fitted ANN models

Model Ranking	Trained on all data	Cross validation training
1	0.949	0.785
2	0.931	0.722
3	0.973	0.710
4	0.963	0.713
5	0.964	0.695

Chapter 7 - Conclusions and future work

7.1 - Conclusions

The ultimate objective of this dissertation is to elucidate the mechanisms of the MIC caused by SRB. The corrosion mechanism induced by these microorganisms has not fully understood and changes dramatically under different conditions. Cathodic depolarization theory was known to be the main MIC mechanism for decades. As mentioned earlier this theory states that SRB accelerate corrosion by removing the adsorbed hydrogen on the surface of the metal. SRB utilize the adsorbed hydrogen for their sulfate reduction metabolism. Recent studies on a few hydrogen-consuming SRB, methanogens, and acetogens isolated from oil facilities showed that hydrogen consumption of these microorganisms did not accelerate corrosion [7]. Advent of molecular techniques helped better interpretation of underlying mechanisms and identifying responsible microorganisms for MIC. Theory of direct electron uptake was suggested in 2004 in a novel research study. This theory suggests that SRB can liberate electrons from the metal through direct and indirect pathways. Non- MIC related studies showed that iron oxidation can be an alternate source of energy for microorganisms in absence of organic electron donors [183–186]. Little experimental evidence is provided for this theory so far. A great deal of experimental proof is provided for newly isolated SRB strains from corroding environments. This research study provided further proof of direct electron uptake for common SRB strains. Understanding how these microorganisms induce corrosion helps eradicating microbial corrosion in oil pipelines. By shedding light on how SRB corrode metal, appropriate mitigative measures can be taken to reduce MIC rates and protect the environment.

7.2 - Contribution to science

Two common SRB strains were selected for MIC studies, D. vulgaris and D. bastinii. This work has shown that both SRB strains inherit direct electron uptake capabilities. This shows

that direct electron uptake can be a main MIC mechanism because not only newly isolated microorganisms possess such capability, but also other common SRB demonstrate such capabilities as well. Numerous evidences of direct electron uptake were provided for both strains in this PhD work.

Electrochemical measurements performed in this work, further corroborated SRB flow of electrons from the metal to the cell, complementing the missing experimental proof for D. vulgaris in direct electron uptake theory. Evidences of direct-electron uptake by means of electrochemical measurements were also provided for D. bastinii, which was not previously been subjected to these measurements before. These evidences are introduced for the first time.

Other achievement in this work is the demonstration that MIC patterns depend strongly on the environmental conditions. In addition, models were developed to predict MIC based on environmental conditions. These models demonstrated higher correlation coefficients than reported models in the literature. Combination of revealed mechanisms for MIC and predictive models in this study can be used to prevent MIC in oil and gas industry.

7.2.1 Elucidation of direct-electron uptake mechanism in MIC by D. vulgaris

D. vulgaris was subjected to corrosion studies in three different media: 1249, 1249-LF, and 1249-LFR. Starvation conditions in 1249-LF media altered the sulfate consumption patterns for this strain. In the original media most of the sulfate is consumed within the first couple of days. However by elimination of lactate, two distinctive slopes were observed in the sulfate consumption curve. Later analysis showed that sulfate consumption follows a pseudo-first order reaction kinetics with two different half-lives; A larger half life followed by a smaller one. This was attributed to the fact that SRB in absence of organic electron donor needs to exploit electrons directly from the metal. In order to do that SRB needs to be close to the metal surface. Hence, metabolic activity of SRB accelerates after establishment of biofilm. As a consequence, this starvation condition not only did not decelerate the corrosion rate but also increased the weight

loss of carbon steel coupons in the cultures. This was due to the fact that D. vulgaris exploit Fe^0 as the sole electron donor. If chemical corrosion (due to presence of H_2S) was the main mechanism of MIC, mass loss should have been decreased under starvation conditions in comparison with full-nutrient media. Because during starvation the SRB population are suppressed, and consequently less H_2S is produced. MIC is mainly happening through SRB gaining electrons directly from the metal surface in starvation conditions. Cultivating SRB in the absence of both carbon steel coupons and organic electron donors showed no SRB metabolizing activity. This further confirmed that SRB survival is dependent on the presence of metallic iron.

This work has also shown that corrosion rate increases with increasing temperatures in the original growth media with full nutrients. However, the elimination of lactate changes this pattern. There was not a significant difference in mass loss between 35˚C and 45˚C.

As another evidence of direct electron uptake, carbon steel coupons were analyzed by SEM. These analysis showed deeper pits were present on the surface of coupons in absence of organic electron donors. In fact, the absence of organic electron donors triggered SRB to attack the iron for electron utilization. Deep pits are more dangerous than shallow pits and finally perforate the material and cause failure. This shows how nutrient availability can change MIC patterns. It also shows how nutrients content can affect MIC. And abundance of nutrients for SRB does not necessarily lead to higher corrosion rates and failure. It was shown that elimination of lactate triggered a more aggressive attack on carbon steel coupons by SRB.

Direct-electron uptake through mediator compounds was studied by addition of riboflavin. The presence of riboflavin vitamins as potential mediator compounds did not enhance MIC. The inefficacy of these compounds can be related to impermeability of D. vulgaris cell wall to theses compounds. Besides, these compounds can go through numerous redox pathway that each is dependent on environmental conditions and is hard to assess.

Electrochemical results have corroborated direct electron uptake in D. vulgaris cultures. Polarization resistance curves showed significant drop in Rp in the presence of SRB cells. This was due to the electron transfer from metal to SRB cells.

Electron transfer from solid to SRB cytoplasm is postulated to be enhanced through cell-membrane bound proteins like c-type cytochrome or conductive nanowires in SRB [103]. C-type cytochromes operate at specific potentials (-0.120 to -320 V vs. SHE).The carbon steel electrodes were polarized to optimal potentials for these proteins and the cathodic current density was measured. The observed increased currents at these potentials demonstrated the enhancement of electron transfer via cytochrome c. In these experiments, the attained current densities were more than two orders of magnitude higher than the abiotic (control) system.

Corrosion potential measurements have also provided more insight into electron transfer mechanisms. The corrosion potential shifted towards more positive values in the presence of SRB. This process is called ennoblement. This showed SRB promoted redox quality of the aqueous solution. Carbon steel coupons were subjected to the electrochemical measurements after the inactivation of SRB cells by glutaraldehyde. Results of this experiment showed that the shift in the corrosion potential was merely due to the presence of SRB cells.

7.2.2 Elucidation of direct-electron uptake mechanism in MIC by D. bastinii

D. bastinii is a common SRB strain in oil pipelines that was never subjected to MIC studies. This strain was subjected to corrosion immersion tests in presence and absence of organic electron donors like D. vulgaris. It was also subjected to electrochemical measurements. Experiments showed that this SRB strain could oxidize metallic iron, as well.

Long-term starvation induced more mass loss in the SRB cultures. Intuitively the elimination of lactate, a vital nutrient for SRB growth, should decrease mass loss due to suppression of SRB. However, this was not the case. Corrosion rate did not decrease in absence of organic electron donors. D. bastinii showed that they can replace lactate by iron and thrive.

This survival strategy taken by SRB leads to more corrosion because the SRB utilize electrons from the metal surface (oxidation) leading to more iron ions dissolution into the aqueous phase .

The SEM analysis showed extensive biofilm coverage on the surface of carbon steel coupons under starvation conditions. If the direct-electron uptake happens through direct pathways (not through mediator compounds), it requires SRB cells to be close to the metal surface to transfer the electron into the cell. This electron transfer happens either through proteins in the SRB membrane or through bacterial nanowires known as pili. Colonization of SRB on metal surface in the absence of organic electron donors demonstrated that SRB attacked the metal for their survival.

Electrochemical techniques provided more evidence of direct-electron uptake. Electron transfer can be vividly depicted through electrochemical measurements. Polarization resistance measurements revealed that as soon as the SRB establish biofilm on the metal surface, the electrode polarization resistance drops significantly. It should be mentioned that the corrosion rate is inversely proportional to the polarization resistance.

The measurements of the cathodic current density showed significant increase in the current, in the presence of SRB. This is an indication of electron transfer from the metal to the cells.

Corrosion potential monitoring over a 2-week period showed ennoblement happens in D. bastinii cultures like D. vulgaris.

7.2.3 Predictive models

A large database of corrosion loss at different environmental conditions was gathered as a result of this PhD work. The experimental data obtained in this PhD work were compared with the field data. This comparison howed agreement of the lab and field data. Therefore, the experimental results can be used to build valid models that can predict MIC.

In this work, the database was initially subjected to regression analysis to better understand the cause and effect relationship of environmental parameters and corrosion rate. Correlation of different parameters and mass loss were calculated. These parameters included: temperature, media type, bacteria type, immersion duration, sulfate consumption rate, and pH. Initially a linear multiple regression model was developed. Log-log transformation of the data improved coefficient of determination from 0.444 to 0.5487. Multiple regression analysis helped revealing important parameters in corrosion analysis.

In this dissertation, artificial neural network was used as the final modeling tool to predict MIC. Numerous ANNs with different characteristic were trained to attain optimal network architecture. k-fold cross validation was used as a tool to assess how well the models can generalize. 5-fold cross-validation on the data did not reduce correlation coefficient significantly. It confirmed that the model can generalize very well when unseen data is input. Correlation coefficients attained for ANN were higher than those previously reported in literature for general corrosion prediction. Correlation coefficients for top 5 ANN models ranged from 0.931-0.973, while the cross validation correlation coefficients ranged from 0.695-0.785. The cross-validation correlation coefficients were still high nd comparable to the values reported in the literature for general corrosion prediction.

7.3 - Future works

Revealing evidence of direct-electron uptake for D.bastinii opened a novel path to look at MIC with a different perspective. With this new perspective more appropriate mitigative approaches can be devised to prevent MIC. These evidences also opened the path that other formerly isolated SRB strains to be subjected to electrochemical test for identification of the electrogenic capabilities.

The mechanisms of direct-electron uptake can be further elucidated. Cell membrane structure of SRB can be studied for further insight into the electron transfer mechanism. It was

suggested in the literature that cyctochrome c is responsible for electron transfer through SRB membrane. This protein can be quantified and characterized to determine the pathway of the electron transfer.

Other mediator compounds can be analyzed for possibility of electron transfer. Also efficacy of riboflavin as electron shuttle can be investigated for other SRB strains.

This area of research can further be expanded into microbial fuel cells. Microbial fuel cells use bacteria as biocatalysts that can provide bioelectricity for the cell. Fuel cells mainly use bacteria in anode for electron production. However, in the last decade development of biocathodes gained a lot of attention [187]. Biocathods can enhance performance of fuel cells by providing higher electron transfer than abiotic cathodes. SRB strains in this work induced high cathodic current that can be utilized in biocathodes.

There is always room for improvement in the modeling. More data can be collected to reach this purpose. For instance, the experiments executed in this work can be extended to higher temperatures. Other SRB strains known as MIC culprits can be subjected to corrosion testing. Additional parameters can be added to the model. For instance MIC can be studied under different flow regimens. Pitting data obtained in this study can be quantified and used as another input to the model.

References

[1] G. H. Koch, *HISTORIC CONGRESSIONAL STUDY: CORROSION COSTS AND PREVENTIVE STRATEGIES IN THE UNITED STATES.*, 2002.

[2] R. Javaherdashti, 1999, "A review of some characteristics of MIC caused by sulfate-reducing bacteria: past, present and future.," *Anti-corrosion methods and materials*. vol. 46, no. 3, pp. 173–180.

[3] Y. Chen, Q. Tang, J. M. Senko, et al., 2015, "Long-term survival of Desulfovibrio vulgaris on carbon steel and associated pitting corrosion.," *Corrosion Science*. vol. 90, pp. 89–100.

[4] C. A. C. Sequeira and A. K. Tiller, "Microbial corrosion-1.," In: *European Federation of Corrosion Workshop on Microbial Corrosion 1988: Sintra, Portugal). Sole distributor in the USA and Canada, Elsevier Science Pub. Co.* (1988).

[5] W. A. Hamilton, 1985, "Sulphate-reducing bacteria and anaerobic corrosion.," *Annual Reviews in Microbiology*. vol. 39, no. 1, pp. 195–217.

[6] W. Lee, Z. Lewandowski, P. H. Nielsen, and W. A. Hamilton, 1995, "Role of sulfate-reducing bacteria in corrosion of mild steel: A review.," *Biofouling*. vol. 8, no. 3, pp. 165–194.

[7] K. Mori, H. Tsurumaru, and S. Harayama, 2010, "Iron corrosion activity of anaerobic hydrogen-consuming microorganisms isolated from oil facilities.," *Journal of bioscience and bioengineering*. vol. 110, no. 4, pp. 426–430.

[8] M. G. Fontana, *Corrosion engineering*. *Tata McGraw-Hill Education*, 2005.

[9] J. O. Bockris and A. K. N. Reddy, *Modern electrochemistry: an introduction to an interdisciplinary area [by] John O'M. Bockris and Amulya KN Reddy*. *Plenum Publishing Corporation*, 1970.

[10] H. A. Videla, 2001, "Microbially induced corrosion: an updated overview.," *International*

biodeterioration & biodegradation. vol. 48, no. 1–4, pp. 176–201.

[11] R. A. Buchanan, 2000, "EE Stansbury.," p.

[12] S. J. Yuan, A. M. F. Choong, and S. O. Pehkonen, 2007, "The influence of the marine aerobic Pseudomonas strain on the corrosion of 70/30 Cu–Ni alloy.," *Corrosion Science*. vol. 49, no. 12, pp. 4352–4385.

[13] S. J. Yuan and S. O. Pehkonen, 2007, "Microbiologically influenced corrosion of 304 stainless steel by aerobic Pseudomonas NCIMB 2021 bacteria: AFM and XPS study.," *Colloids and Surfaces B: Biointerfaces*. vol. 59, no. 1, pp. 87–99.

[14] R. I. Ray, J. S. Lee, B. J. Little, and T. L. Gerke, 2010, "The anatomy of tubercles: A corrosion study in a fresh water estuary.," *Materials and Corrosion*. vol. 61, no. 12, pp. 993–999.

[15] S. Borenstein, *Microbiologically influenced corrosion handbook*. *Elsevier*, 1994.

[16] W. Sand, 1987, "Importance of hydrogen sulfide, thiosulfate, and methylmercaptan for growth of thiobacilli during simulation of concrete corrosion.," *Appl. Environ. Microbiol.* vol. 53, no. 7, pp. 1645–1648.

[17] H. Tributsch, J. A. Rojas-Chapana, C. C. Bartels, A. Ennaoui, and W. Hofmann, 1998, "Role of transient iron sulfide films in microbial corrosion of steel.," *Corrosion*. vol. 54, no. 3, pp. 216–227.

[18] D. R. Cullimore and A. E. McCANN, 1977, "The identification, cultivation and control of iron bacteria in ground water.," *Aquatic microbiology*. pp. 219–261.

[19] E. G. Pringsheim, 1949, "Iron bacteria.," *Biological Reviews*. vol. 24, no. 2, pp. 200–245.

[20] B. Little and P. Wagner, 1997, "Myths related to microbiologically influenced corrosion.," *Materials performance*. vol. 36, no. 6, p.

[21] D. Starosvetsky, R. Armon, J. Yahalom, and J. Starosvetsky, 2001, "Pitting corrosion of carbon steel caused by iron bacteria.," *International biodeterioration & biodegradation*. vol. 47, no. 2, pp. 79–87.

[22] H.-C. Flemming, 1995, “Eating away at the infrastructure-the heavy cost of microbial corrosion.,” *Water Quality International*. no. 4, pp. 16–19.

[23] J. Starosvetsky, R. Armon, D. Starosvetsky, and A. Groysman, 1999, “Fouling of carbon steel heat exchanger caused by iron bacteria.,” *Materials performance*. vol. 38, no. 1, p.

[24] H. L. Ehrlich, 1996, “Geomicrobiology Marcel Dekker.,” *Inc. New York*. pp. 578–614.

[25] M. Wilimzig and E. Bock, 1996, “21 Attack of Mortar by Bacteria and Fungi.,” *Microbially Influenced Corrosion of Materials: Scientific and Engineering Aspects*. p. 311.

[26] R. M. Atlas, 1981, “Microbial degradation of petroleum hydrocarbons: an environmental perspective.,” *Microbiological reviews*. vol. 45, no. 1, p. 180.

[27] B. Little, R. Staehle, and R. Davis, 2001, “Fungal influenced corrosion of post-tensioned cables.,” *International biodeterioration & biodegradation*. vol. 47, no. 2, pp. 71–77.

[28] R. Javaherdashti, H. Nikraz, M. Borowitzka, N. Moheimani, and M. Olivia, 2009, “On the impact of Algae on accelerating the biodeterioration/biocorrosion of reinforced concrete: A mechanistic review.,” *European Journal of Scientific Research*. vol. 36, no. 3, pp. 394–406.

[29] N. E. Tolbert and L. P. Zill, 1956, “Excretion of glycolic acid by algae during photosynthesis.,” *Journal of Biological Chemistry*. vol. 222, no. 2, pp. 895–906.

[30] F. Widdel and F. Bak, “Gram-negative mesophilic sulfate-reducing bacteria.,” In: *The prokaryotes*. pp. 3352–3378. *Springer* (1992).

[31] H. F. Castro, N. H. Williams, and A. Ogram, 2000, “Phylogeny of sulfate-reducing bacteria.,” *FEMS Microbiology Ecology*. vol. 31, no. 1, pp. 1–9.

[32] E. A. Henry, R. Devereux, J. S. Maki, et al., 1994, “Characterization of a new thermophilic sulfate-reducing bacterium.,” *Archives of Microbiology*. vol. 161, no. 1, pp. 62–69.

[33] A. Volbeda, M.-H. Charon, C. Piras, E. C. Hatchikian, M. Frey, and J. C. Fontecilla-

Camps, 1995, “Crystal structure of the nickel–iron hydrogenase from Desulfovibrio gigas.,” *Nature*. vol. 373, no. 6515, p. 580.

[34] J. C. Fontecilla-Camps, M. Frey, E. Garcin, et al., 1997, “Hydrogenase: a hydrogen-metabolizing enzyme. What do the crystal structures tell us about its mode of action?,” *Biochimie*. vol. 79, no. 11, pp. 661–666.

[35] G. Voordouw, V. Niviere, F. G. Ferris, P. M. Fedorak, and D. W. S. Westlake, 1990, “Distribution of hydrogenase genes in Desulfovibrio spp. and their use in identification of species from the oil field environment.,” *Applied and environmental microbiology*. vol. 56, no. 12, pp. 3748–3754.

[36] W. Badzjong and R. K. Thauer, 1980, “Vectorial electron transport in Degulfovibrio vulgaris (Marburg) growing on hydrogen plus sulfate as sole energy source.,” *Archives of Microbiology*. vol. 125, no. 1–2, pp. 167–174.

[37] M. T. Madigan, J. M. Martinko, and J. Parker, *Brock biology of microorganisms*. *Prentice hall Upper Saddle River, NJ*, 1997.

[38] R. H. Gaines, 1910, “Bacterial Activity as a Corrosive Influence in the Soil.,” *Industrial & Engineering Chemistry*. vol. 2, no. 4, pp. 128–130.

[39] C. A. H. von Wolzogen Kuehr and L. S. Van der Vlugt, *Graphitization of cast iron as an electrobiochemical process in anaerobic soils*. *ARMY BIOLOGICAL LABS FREDERICK MD*, 1964.

[40] A. K. Tiller and G. H. Booth, 1962, “Polarization studies of mild steel in cultures of sulphate-reducing bacteria. Part 2.—Thermophilic organisms.,” *Transactions of the Faraday Society*. vol. 58, pp. 110–115.

[41] G. H. Booth and A. K. Tiller, 1962, “Polarization studies of mild steel in cultures of sulphate-reducing bacteria. Part 3.—Halophilic organisms.,” *Transactions of the Faraday Society*. vol. 58, pp. 2510–2516.

[42] H. Venzlaff, D. Enning, J. Srinivasan, et al., 2013, “Accelerated cathodic reaction in

microbial corrosion of iron due to direct electron uptake by sulfate-reducing bacteria.," *Corrosion Science*. vol. 66, pp. 88–96.

[43] D. Enning and J. Garrelfs, 2013, "Corrosion of iron by sulfate-reducing bacteria–new views of an old problem.," *Applied and environmental microbiology*. p. AEM-02848.

[44] J. A. Costello, 1975, "The mechanism of cathodic depolarization exhibited by sulphate-reducing bacteria during metallic corrosion processes.," p.

[45] J. A. Hardy, 1983, "Utilisation of cathodic hydrogen by sulphate-reducing bacteria.," *British Corrosion Journal*. vol. 18, no. 4, pp. 190–193.

[46] R. Jia, J. L. Tan, P. Jin, D. J. Blackwood, D. Xu, and T. Gu, 2018, "Effects of biogenic H2S on the microbiologically influenced corrosion of C1018 carbon steel by sulfate reducing Desulfovibrio vulgaris biofilm.," *Corrosion Science*. vol. 130, pp. 1–11.

[47] K.-Y. Chan, L.-C. Xu, and H. H. P. Fang, 2002, "Anaerobic electrochemical corrosion of mild steel in the presence of extracellular polymeric substances produced by a culture enriched in sulfate-reducing bacteria.," *Environmental science & technology*. vol. 36, no. 8, pp. 1720–1727.

[48] J. W. Sowards and E. Mansfield, 2014, "Corrosion of copper and steel alloys in a simulated underground storage-tank sump environment containing acid-producing bacteria.," *Corrosion Science*. vol. 87, pp. 460–471.

[49] D. T. Hang, 2003, "Microbiological study of the anaerobic corrosion of iron.," *Trabajo de Grado para el titulo de Doctor en Ciencias Naturales. Universidad de Bremen, Alemania*. p.

[50] H. T. Dinh, J. Kuever, M. Mußmann, A. W. Hassel, M. Stratmann, and F. Widdel, 2004, "Iron corrosion by novel anaerobic microorganisms.," *Nature*. vol. 427, no. 6977, p. 829.

[51] D. Enning, H. Venzlaff, J. Garrelfs, et al., 2012, "Marine sulfate-reducing bacteria cause serious corrosion of iron under electroconductive biogenic mineral crust.," *Environmental*

microbiology. vol. 14, no. 7, pp. 1772–1787.

[52] S. Kato, 2016, “Microbial extracellular electron transfer and its relevance to iron corrosion.,” *Microbial biotechnology*. vol. 9, no. 2, pp. 141–148.

[53] P. Zhang, D. Xu, Y. Li, K. Yang, and T. Gu, 2015, “Electron mediators accelerate the microbiologically influenced corrosion of 304 stainless steel by the Desulfovibrio vulgaris biofilm.,” *Bioelectrochemistry*. vol. 101, pp. 14–21.

[54] T. Uchiyama, K. Ito, K. Mori, H. Tsurumaru, and S. Harayama, 2010, “Iron-corroding methanogen isolated from a crude-oil storage tank.,” *Applied and environmental microbiology*. vol. 76, no. 6, pp. 1783–1788.

[55] S. Kato, I. Yumoto, and Y. Kamagata, 2014, “Isolation of acetogenic bacteria that induce biocorrosion by utilizing metallic iron as the sole electron donor.,” *Applied and environmental microbiology*. p. AEM-02767.

[56] Z. M. Summers, H. E. Fogarty, C. Leang, A. E. Franks, N. S. Malvankar, and D. R. Lovley, 2010, “Direct exchange of electrons within aggregates of an evolved syntrophic coculture of anaerobic bacteria.,” *Science*. vol. 330, no. 6009, pp. 1413–1415.

[57] R. P. Frankenthal and P. C. Milner, 1986, “Hydrogen evolution kinetics on a high-carbon steel and on tin in seawater.,” *Corrosion*. vol. 42, no. 1, pp. 51–53.

[58] S. Deckena and K.-H. Blotevogel, 1990, “Growth of methanogenic and sulfate-reducing bacteria with cathodic hydrogen.,” *Biotechnology Letters*. vol. 12, no. 8, pp. 615–620.

[59] M. Siegert, X.-F. Li, M. D. Yates, and B. E. Logan, 2015, “The presence of hydrogenotrophic methanogens in the inoculum improves methane gas production in microbial electrolysis cells.,” *Frontiers in microbiology*. vol. 5, p. 778.

[60] J. Mand, H. S. Park, C. Okoro, et al., 2016, “Microbial methane production associated with carbon steel corrosion in a Nigerian oil field.,” *Frontiers in microbiology*. vol. 6, p. 1538.

[61] T. Zhang, H. H. P. Fang, and B. C. B. Ko, 2003, “Methanogen population in a marine

biofilm corrosive to mild steel.," *Applied microbiology and biotechnology*. vol. 63, no. 1, pp. 101–106.

[62] J. Mand, H. S. Park, T. R. Jack, and G. Voordouw, 2014, "The role of acetogens in microbially influenced corrosion of steel.," *Frontiers in microbiology*. vol. 5, p. 268.

[63] J. M. Suflita, T. J. Phelps, and B. Little, 2008, "Carbon dioxide corrosion and acetate: a hypothesis on the influence of microorganisms.," *Corrosion*. vol. 64, no. 11, pp. 854–859.

[64] N. J. E. Dowling, S. A. Brooks, T. J. Phelps, and D. C. White, 1992, "Effects of selection and fate of substrates supplied to anaerobic bacteria involved in the corrosion of pipe-line steel.," *Journal of industrial microbiology*. vol. 10, no. 3–4, pp. 207–215.

[65] C. W. Marshall, D. E. Ross, E. B. Fichot, R. S. Norman, and H. D. May, 2013, "Long-term operation of microbial electrosynthesis systems improves acetate production by autotrophic microbiomes.," *Environmental science & technology*. vol. 47, no. 11, pp. 6023–6029.

[66] H. A. Videla, S. Le Borgne, C. Panter, and R. K. Singh Raman, "MIC of steels by iron reducing bacteria.," In: *CORROSION 2008*. *NACE International* (2008).

[67] L. K. Herrera and H. A. Videla, 2009, "Role of iron-reducing bacteria in corrosion and protection of carbon steel.," *International biodeterioration & biodegradation*. vol. 63, no. 7, pp. 891–895.

[68] B. Little, P. Wagner, K. Hart, et al., "The role of metal-reducing bacteria in microbiologically influenced corrosion.," In: *Corrosion97*. *NACE International* (1997).

[69] C. O. Obuekwe, D. W. S. Westlake, F. D. Cook, and J. W. Costerton, 1981, "Surface changes in mild steel coupons from the action of corrosion-causing bacteria.," *Appl. Environ. Microbiol.* vol. 41, no. 3, pp. 766–774.

[70] A. K. Lee and D. K. Newman, 2003, "Microbial iron respiration: impacts on corrosion processes.," *Applied microbiology and biotechnology*. vol. 62, no. 2–3, pp. 134–139.

[71] G. S. Frankel, 1998, "Pitting corrosion of metals a review of the critical factors.," *Journal*

of the Electrochemical Society. vol. 145, no. 6, pp. 2186–2198.

[72] B. D. Craig, *Fundamental aspects of corrosion films in corrosion science*. *Springer Science & Business Media*, 2013.

[73] A. V Levy, *Solid particle erosion and erosion-corrosion of materials*. *Asm International*, 1995.

[74] A. V Levy, 1995, "Erosion and erosion-corrosion of metals.," *Corrosion*. vol. 51, no. 11, pp. 872–883.

[75] B. S. McLaury and S. A. Shirazi, 2000, "An alternate method to API RP 14E for predicting solids erosion in multiphase flow.," *Journal of energy resources technology*. vol. 122, no. 3, pp. 115–122.

[76] R. J. K. Wood, 2006, "Erosion–corrosion interactions and their effect on marine and offshore materials.," *Wear*. vol. 261, no. 9, pp. 1012–1023.

[77] T. E. Cloete, L. Jacobs, and V. S. Brözel, 1998, "The chemical control of biofouling in industrial water systems.," *Biodegradation*. vol. 9, no. 1, pp. 23–37.

[78] M. K. Sztyler, "Molecular analysis of microbial communities from oil industry environments," (2014).

[79] H. A. Videla and L. K. Herrera, 2007, "Biocorrosion in oil recovery systems. Prevention and protection. An update.," *Edición Especial*. vol. 30, pp. 272–279.

[80] L. R. Gardner and P. S. Stewart, 2002, "Action of glutaraldehyde and nitrite against sulfate-reducing bacterial biofilms.," *Journal of Industrial Microbiology and Biotechnology*. vol. 29, no. 6, pp. 354–360.

[81] C. Hubert and G. Voordouw, 2007, "Oil field souring control by nitrate-reducing Sulfurospirillum spp. that outcompete sulfate-reducing bacteria for organic electron donors.," *Appl. Environ. Microbiol.* vol. 73, no. 8, pp. 2644–2652.

[82] R. E. Eckford and P. M. Fedorak, 2002, "Chemical and microbiological changes in laboratory incubations of nitrate amendment 'sour' produced waters from three western

Canadian oil fields,." *Journal of Industrial Microbiology and Biotechnology*. vol. 29, no. 5, pp. 243–254.

[83] A. Gittel, K. B. Sørensen, T. L. Skovhus, K. Ingvorsen, and A. Schramm, 2009, "Prokaryotic community structure and sulfate reducer activity in water from high-temperature oil reservoirs with and without nitrate treatment.," *Appl. Environ. Microbiol.* vol. 75, no. 22, pp. 7086–7096.

[84] C. U. Schwermer, G. Lavik, R. M. M. Abed, et al., 2008, "Impact of nitrate on the structure and function of bacterial biofilm communities in pipelines used for injection of seawater into oil fields.," *Applied and environmental microbiology*. vol. 74, no. 9, pp. 2841–2851.

[85] R. K. Thauer, K. Jungermann, and K. Decker, 1977, "Energy conservation in chemotrophic anaerobic bacteria.," *Bacteriological reviews*. vol. 41, no. 1, p. 100.

[86] T. Thorstenson, E. Sunde, G. Bodtker, B.-L. Lillebo, T. Torsvik, and J. Beeder, "Biocide replacement by nitrate in sea water injection systems.," In: *CORROSION 2002*. *NACE International* (2002).

[87] G. E. Jenneman, P. D. Moffitt, G. A. Baja, and R. H. Webb, "Field demonstration of sulfide removal in reservoir brine by bacteria indigenous to a Canadian reservoir.," In: *SPE Annual Technical Conference and Exhibition*. *Society of Petroleum Engineers* (1997).

[88] C. Pillay and J. Lin, 2014, "The impact of additional nitrates in mild steel corrosion in a seawater/sediment system.," *Corrosion Science*. vol. 80, pp. 416–426.

[89] S. Myhr, B.-L. Lillebø, E. Sunde, J. Beeder, and T. Torsvik, 2002, "Inhibition of microbial H 2 S production in an oil reservoir model column by nitrate injection.," *Applied microbiology and biotechnology*. vol. 58, no. 3, pp. 400–408.

[90] M. A. Reinsel, J. T. Sears, P. S. Stewart, and M. J. McInerney, 1996, "Control of microbial souring by nitrate, nitrite or glutaraldehyde injection in a sandstone column.,"

Journal of industrial microbiology. vol. 17, no. 2, pp. 128–136.

[91] J. Larsen, M. H. Rod, and S. Zwolle, "Prevention of reservoir souring in the Halfdan field by nitrate injection.," In: *CORROSION 2004*. *NACE International* (2004).

[92] J. Larsen, "Downhole nitrate applications to control sulfate reducing bacteria activity and reservoir souring.," In: *CORROSION 2002*. *NACE International* (2002).

[93] A. J. Telang, S. Ebert, J. M. Foght, et al., 1997, "Effect of nitrate injection on the microbial community in an oil field as monitored by reverse sample genome probing.," *Appl. Environ. Microbiol.* vol. 63, no. 5, pp. 1785–1793.

[94] J. Quarini and S. Shire, 2007, "A review of fluid-driven pipeline pigs and their applications.," *Proceedings of the Institution of Mechanical Engineers, Part E: Journal of Process Mechanical Engineering*. vol. 221, no. 1, pp. 1–10.

[95] A. Standard, 2011, "Standard practice for preparing, cleaning, and evaluating corrosion test specimens.," *American Society for Testing and Materials G1-03*. p.

[96] E. Principles and P. Polarization, 1980, "Application Note CORR-1 Basics of Corrosion Measurements.," *Princeton Applied Research*. p.

[97] M. Stern and A. L. Geary, 1957, "Electrochemical polarization I. A theoretical analysis of the shape of polarization curves.," *Journal of the electrochemical society*. vol. 104, no. 1, pp. 56–63.

[98] H. A. Videla and L. K. Herrera, 2005, "Microbiologically influenced corrosion: looking to the future.," *International microbiology*. vol. 8, no. 3, p. 169.

[99] J. Duan, S. Wu, X. Zhang, G. Huang, M. Du, and B. Hou, 2008, "Corrosion of carbon steel influenced by anaerobic biofilm in natural seawater.," *Electrochimica Acta*. vol. 54, no. 1, pp. 22–28.

[100] G. Muyzer and A. J. M. Stams, 2008, "The ecology and biotechnology of sulphate-reducing bacteria.," *Nature Reviews Microbiology*. vol. 6, p. 441.

[101] J. R. Postgate, *The sulphate-reducing bacteria*. *CUP Archive*, 1979.

[102] A. T. Vasilaki, D. C. McMillan, J. Kinsella, A. Duncan, D. S. J. O'Reilly, and D. Talwar, 2010, "Relation between riboflavin, flavin mononucleotide and flavin adenine dinucleotide concentrations in plasma and red cells in patients with critical illness.," *Clinica Chimica Acta*. vol. 411, no. 21–22, pp. 1750–1755.

[103] D. Xu and T. Gu, 2014, "Carbon source starvation triggered more aggressive corrosion against carbon steel by the Desulfovibrio vulgaris biofilm.," *International Biodeterioration & Biodegradation*. vol. 91, pp. 74–81.

[104] W. Dou, R. Jia, P. Jin, J. Liu, S. Chen, and T. Gu, 2018, "Investigation of the mechanism and characteristics of copper corrosion by sulfate reducing bacteria.," *Corrosion Science*. vol. 144, pp. 237–248.

[105] R. Jia, D. Yang, Y. Li, D. Xu, and T. Gu, 2017, "Mitigation of the Desulfovibrio vulgaris biofilm using alkyldimethylbenzylammonium chloride enhanced by D-amino acids.," *International Biodeterioration & Biodegradation*. vol. 117, pp. 97–104.

[106] M. Cable and E. T. Smith, 2005, "Identifying the n= 2 reaction mechanism of FAD through voltammetric simulations.," *Analytica chimica acta*. vol. 537, no. 1–2, pp. 299–306.

[107] E. Marsili, D. B. Baron, I. D. Shikhare, D. Coursolle, J. A. Gralnick, and D. R. Bond, 2008, "Shewanella secretes flavins that mediate extracellular electron transfer.," *Proceedings of the National Academy of Sciences*. vol. 105, no. 10, pp. 3968–3973.

[108] S. L. J. Tan and R. D. Webster, 2012, "Electrochemically induced chemically reversible proton-coupled electron transfer reactions of riboflavin (vitamin B2).," *Journal of the American Chemical Society*. vol. 134, no. 13, pp. 5954–5964.

[109] H. Von Canstein, J. Ogawa, S. Shimizu, and J. R. Lloyd, 2008, "Secretion of flavins by Shewanella species and their role in extracellular electron transfer.," *Appl. Environ. Microbiol.* vol. 74, no. 3, pp. 615–623.

[110] D. Coursolle, D. B. Baron, D. R. Bond, and J. A. Gralnick, 2010, "The Mtr respiratory

pathway is essential for reducing flavins and electrodes in Shewanella oneidensis.," *Journal of bacteriology*. vol. 192, no. 2, pp. 467–474.

[111] F. P. Van der Zee and F. J. Cervantes, 2009, "Impact and application of electron shuttles on the redox (bio) transformation of contaminants: a review.," *Biotechnology advances*. vol. 27, no. 3, pp. 256–277.

[112] A. B. dos Santos, I. A. E. Bisschops, F. J. Cervantes, and J. B. van Lier, 2004, "Effect of different redox mediators during thermophilic azo dye reduction by anaerobic granular sludge and comparative study between mesophilic (30 C) and thermophilic (55 C) treatments for decolourisation of textile wastewaters.," *Chemosphere*. vol. 55, no. 9, pp. 1149–1157.

[113] A. L. Demain, 1972, "Riboflavin oversynthesis.," *Annual Reviews in Microbiology*. vol. 26, no. 1, pp. 369–388.

[114] D. W. Shoesmith, P. Taylor, M. G. Bailey, and D. G. Owen, 1980, "The formation of ferrous monosulfide polymorphs during the corrosion of iron by aqueous hydrogen sulfide at 21 C.," *Journal of the Electrochemical Society*. vol. 127, no. 5, pp. 1007–1015.

[115] B. W. A. Sherar, I. M. Power, P. G. Keech, S. Mitlin, G. Southam, and D. W. Shoesmith, 2011, "Characterizing the effect of carbon steel exposure in sulfide containing solutions to microbially induced corrosion.," *Corrosion Science*. vol. 53, no. 3, pp. 955–960.

[116] S. W. Poulton, M. D. Krom, and R. Raiswell, 2004, "A revised scheme for the reactivity of iron (oxyhydr) oxide minerals towards dissolved sulfide.," *Geochimica et cosmochimica acta*. vol. 68, no. 18, pp. 3703–3715.

[117] L. Zhou, J. Liu, and F. Dong, 2017, "Spectroscopic study on biological mackinawite (FeS) synthesized by ferric reducing bacteria (FRB) and sulfate reducing bacteria (SRB): Implications for in-situ remediation of acid mine drainage.," *Spectrochimica Acta Part A: Molecular and Biomolecular Spectroscopy*. vol. 173, pp. 544–548.

[118] V. Rouchon, H. Badet, O. Belhadj, et al., 2012, "Raman and FTIR spectroscopy applied to

the conservation report of paleontological collections: identification of Raman and FTIR signatures of several iron sulfate species such as ferrinatrite and sideronatrite.," *Journal of Raman Spectroscopy*. vol. 43, no. 9, pp. 1265–1274.

[119] C. M. Eggleston, J.-J. Ehrhardt, and W. Stumm, 1996, "Surface structural controls on pyrite oxidation kinetics: An XPS-UPS, STM, and modeling study.," *American Mineralogist*. vol. 81, no. 9–10, pp. 1036–1056.

[120] M. Khabbaz and M. H. Entezari, 2016, "Simple and versatile one-step synthesis of FeS2 nanoparticles by ultrasonic irradiation.," *Journal of colloid and interface science*. vol. 470, pp. 204–210.

[121] R. K. Rath, S. Subramanian, and T. Pradeep, 2000, "Surface chemical studies on pyrite in the presence of polysaccharide-based flotation depressants.," *Journal of Colloid and Interface Science*. vol. 229, no. 1, pp. 82–91.

[122] S. Fathinia, M. Fathinia, A. A. Rahmani, and A. Khataee, 2015, "Preparation of natural pyrite nanoparticles by high energy planetary ball milling as a nanocatalyst for heterogeneous Fenton process.," *Applied Surface Science*. vol. 327, pp. 190–200.

[123] M. Gotić and S. Musić, 2007, "Mössbauer, FT-IR and FE SEM investigation of iron oxides precipitated from FeSO4 solutions.," *Journal of Molecular Structure*. vol. 834, pp. 445–453.

[124] F. M. AlAbbas, C. Williamson, S. M. Bhola, et al., 2013, "Influence of sulfate reducing bacterial biofilm on corrosion behavior of low-alloy, high-strength steel (API-5L X80).," *International Biodeterioration & Biodegradation*. vol. 78, pp. 34–42.

[125] H. Castaneda and X. D. Benetton, 2008, "SRB-biofilm influence in active corrosion sites formed at the steel-electrolyte interface when exposed to artificial seawater conditions.," *Corrosion Science*. vol. 50, no. 4, pp. 1169–1183.

[126] I. B. Beech and J. Sunner, 2004, "Biocorrosion: towards understanding interactions between biofilms and metals.," *Current opinion in Biotechnology*. vol. 15, no. 3, pp. 181–

186.

[127] Y. M. Zeng, J. L. Luo, and P. R. Norton, 2004, “Initiation and propagation of pitting and crevice corrosion of hydrogen-containing passive films on X70 micro-alloyed steel.,” *Electrochimica acta*. vol. 49, no. 5, pp. 703–714.

[128] R. N. Iyer and H. W. Pickering, 1990, “Mechanism and kinetics of electrochemical hydrogen entry and degradation of metallic systems.,” *Annual Review of Materials Science*. vol. 20, no. 1, pp. 299–338.

[129] M. Rosenbaum, F. Aulenta, M. Villano, and L. T. Angenent, 2011, “Cathodes as electron donors for microbial metabolism: which extracellular electron transfer mechanisms are involved?,” *Bioresource technology*. vol. 102, no. 1, pp. 324–333.

[130] F. V. O. Kloeke, R. D. Bryant, and E. J. Laishley, 1995, “Localization of cytochromes in the outer membrane of Desulfovibrio vulgaris (Hildenborough) and their role in anaerobic biocorrosion.,” *Anaerobe*. vol. 1, no. 6, pp. 351–358.

[131] M. Bruschi, M. Loutfi, P. Bianco, and J. Haladjian, 1984, “Correlations studies between structural and redox properties of cytochromes C3.,” *Biochemical and biophysical research communications*. vol. 120, no. 2, pp. 384–389.

[132] V. Niviere, E. C. Hatchikian, P. Bianco, and J. Haladjian, 1988, “Kinetic studies of electron transfer between hydrogenase and cytochrome c3 from Desulfovibrio gigas. Electrochemical properties of cytochrome c3.,” *Biochimica et Biophysica Acta (BBA)-Bioenergetics*. vol. 935, no. 1, pp. 34–40.

[133] J. Haladjian, P. Bianco, F. Guerlesquin, and M. Bruschi, 1987, “Electrochemical study of the electron exchange between cytochrome c3 and hydrogenase from Desulfovibrio desulfuricans Norway.,” *Biochemical and biophysical research communications*. vol. 147, no. 3, pp. 1289–1294.

[134] R. Rabus, T. A. Hansen, and F. Widdel, 2013, “Dissimilatory sulfate-and sulfur-reducing prokaryotes.,” *The Prokaryotes: Prokaryotic Physiology and Biochemistry*. pp. 309–404.

[135] P. F. Beese-Vasbender, S. Nayak, A. Erbe, M. Stratmann, and K. J. J. Mayrhofer, 2015, "Electrochemical characterization of direct electron uptake in electrical microbially influenced corrosion of iron by the lithoautotrophic SRB Desulfopila corrodens strain IS4.," *Electrochimica Acta*. vol. 167, pp. 321–329.

[136] B. J. Little and J. S. Lee, *Microbiologically influenced corrosion*. *John Wiley & Sons*, 2007.

[137] B. J. Little, J. S. Lee, and R. I. Ray, 2008, "The influence of marine biofilms on corrosion: a concise review.," *Electrochimica Acta*. vol. 54, no. 1, pp. 2–7.

[138] B. Little, J. Lee, and R. Ray, *Microbiologically influenced corrosion: global phenomena, local mechanisms*. *NAVAL RESEARCH LAB STENNIS SPACE CENTER MS OCEANOGRAPHY DIV*, 2011.

[139] E. Huttunen-Saarivirta, P. Rajala, M. Marja-Aho, J. Maukonen, E. Sohlberg, and L. Carpen, 2018, "Ennoblement, corrosion, and biofouling in brackish seawater: Comparison between six stainless steel grades.," *Bioelectrochemistry*. vol. 120, pp. 27–42.

[140] A. Mollica, 1992, "Biofilm and corrosion on active-passive alloys in seawater.," *International biodeterioration & biodegradation*. vol. 29, no. 3–4, pp. 213–229.

[141] H.-J. Zhang and S. C. Dexter, 1995, "Effect of biofilms on crevice corrosion of stainless steels in coastal seawater.," *Corrosion*. vol. 51, no. 1, pp. 56–66.

[142] R. Holthe, 1988, "The time dependence of cathodic properties of stainless steels, titanium, platinum and 90/10 CuNi in seawater.," *R. Holthe, et. al. Corrosion 88/393, NACE, Houston, TX. Per Copy$ 4*. p.

[143] T. A. N. J. I. E. L. KENNETH, "THE ROLE OF METHANOGENS IN MICROBIOLOGICALLY INFLUENCED CORROSION," (2017).

[144] B. Janik and P. J. Elving, 1968, "Polarographic behavior of nucleosides and nucleotides of purines, pyrimidines, pyridines, and flavines.," *Chemical reviews*. vol. 68, no. 3, pp. 295–319.

[145] H. Wei and S. Omanovic, 2008, “Interaction of flavin adenine dinucleotide (FAD) with a glassy carbon electrode surface.,” *Chemistry & biodiversity*. vol. 5, no. 8, pp. 1622–1639.

[146] J. W. Morse, F. J. Millero, J. C. Cornwell, and D. Rickard, 1987, “The chemistry of the hydrogen sulfide and iron sulfide systems in natural waters.,” *Earth-science reviews*. vol. 24, no. 1, pp. 1–42.

[147] A. Jayaraman, D. Ornek, D. A. Duarte, C.-C. Lee, F. B. Mansfeld, and T. K. Wood, 1999, “Axenic aerobic biofilms inhibit corrosion of copper and aluminum.,” *Applied microbiology and biotechnology*. vol. 52, no. 6, pp. 787–790.

[148] D. Ren, J. J. Sims, and T. K. Wood, 2002, “Inhibition of biofilm formation and swarming of Bacillus subtilis by (5Z)-4-bromo-5-(bromomethylene)-3-butyl-2 (5H)-furanone.,” *Letters in applied microbiology*. vol. 34, no. 4, pp. 293–299.

[149] A. Nagiub and F. Mansfeld, 2002, “Evaluation of microbiologically influenced corrosion inhibition (MICI) with EIS and ENA.,” *Electrochimica Acta*. vol. 47, no. 13–14, pp. 2319–2333.

[150] D. Örnek, T. K. Wood, C. H. Hsu, and F. Mansfeld, 2002, “Corrosion control using regenerative biofilms (CCURB) on brass in different media.,” *Corrosion science*. vol. 44, no. 10, pp. 2291–2302.

[151] A. Jayaraman, J. C. Earthman, and T. K. Wood, 1997, “Corrosion inhibition by aerobic biofilms on SAE 1018 steel.,” *Applied microbiology and biotechnology*. vol. 47, no. 1, pp. 62–68.

[152] A. Jayaraman, F. B. Mansfeld, and T. K. Wood, 1999, “Inhibiting sulfate-reducing bacteria in biofilms by expressing the antimicrobial peptides indolicidin and bactenecin.,” *Journal of Industrial Microbiology and Biotechnology*. vol. 22, no. 3, pp. 167–175.

[153] Y. El Mendili, A. Abdelouas, and J.-F. Bardeau, 2013, “Insight into the mechanism of carbon steel corrosion under aerobic and anaerobic conditions.,” *Physical Chemistry*

Chemical Physics. vol. 15, no. 23, pp. 9197–9204.

[154] R. E. Melchers and T. Wells, 2006, "Models for the anaerobic phases of marine immersion corrosion.," *Corrosion Science*. vol. 48, no. 7, pp. 1791–1811.

[155] R. Singleton, "The sulfate-reducing bacteria: an overview.," In: *The sulfate-reducing bacteria: contemporary perspectives*. pp. 1–20. *Springer* (1993).

[156] R. E. Melchers, 2003, "Modeling of Marine Immersion Corrosion for Mild and Low-Alloy Steels—Part 2: Uncertainty Estimation.," *Corrosion*. vol. 59, no. 4, pp. 335–344.

[157] G. G. Koshelev and I. L. Rozenfel'd, *Corrosion Stability of Low-Carbon and Low-Alloy Steels in Sea Water*. *FOREIGN TECHNOLOGY DIV WRIGHT-PATTERSON AFB OH*, 1963.

[158] F. Blekkenhorst, G. M. Ferrari, C. J. Van Der Wekken, and F. P. IJsseling, 1986, "Development of high strength low alloy steels for marine applications: Part 1: Results of long term exposure tests on commercially available and experimental steels.," *British corrosion journal*. vol. 21, no. 3, pp. 163–176.

[159] R. E. Melchers, 2004, "Effect of small compositional changes on marine immersion corrosion of low alloy steels.," *Corrosion Science*. vol. 46, no. 7, pp. 1669–1691.

[160] C. R. Southwell and A. L. Alexander, 1970, "Corrosion of metals in tropical waters, structural ferrous metals.," *Materials Protection*. vol. 9, no. 1, p.

[161] C. R. Southwell, J. D. Bultman, and A. L. Alexander, 1976, "Corrosion of metals in tropical environments. Final report of 16-year exposures.," *Materials Performance (MP)*. vol. 15, no. 7, p.

[162] R. E. Melchers, 2003, "Effect on marine immersion corrosion of carbon content of low alloy steels.," *Corrosion Science*. vol. 45, no. 11, pp. 2609–2625.

[163] C. P. Larrabee, 1945, "Corrosion of steels in marine atmospheres and in sea water.," *Transactions of the Electrochemical Society*. vol. 87, no. 1, pp. 161–182.

[164] C. P. Larrabee, 1953, "Corrosion resistance of high-strength low-alloy steels as influenced

by composition and environment.," *Corrosion*. vol. 9, no. 8, pp. 259–271.

[165] B. W. Forgeson, C. R. Southwell, and A. L. Alexander, 1960, "Corrosion of metals in tropical environments—Part 3—Underwater corrosion of ten structural steels.," *Corrosion*. vol. 16, no. 3, pp. 87–96.

[166] J. C. Hudson and J. F. Stanners, 1955, "The corrosion resistance of low alloy steels.," *J. of the Iron and Steel Inst*. vol. 180, pp. 271–284.

[167] R. Jeffrey and R. E. Melchers, *Corrosion tests of mild steel in temperate seawater*. *Department of Civil, Surveying and Environmental Engineering, University of …*, 2001.

[168] H. Liu, L. Huang, Z. Huang, and J. Zheng, 2007, "Specification of sulfate reducing bacteria biofilms accumulation effects on corrosion initiation.," *Materials and Corrosion*. vol. 58, no. 1, pp. 44–48.

[169] M. H. Peterson and L. J. WALDRON, 1961, "Investigation of mild steel corrosion rate in San Diego harbor.," *Corrosion*. vol. 17, no. 4, p. 188t–190t.

[170] R. E. Melchers, 2003, "Modeling of marine immersion corrosion for mild and low-alloy steels—Part 1: Phenomenological model.," *Corrosion*. vol. 59, no. 4, pp. 319–334.

[171] I. Pardoe, *Applied regression modeling: a business approach*. *John Wiley & Sons*, 2012.

[172] X. Yan and X. Su, *Linear regression analysis: theory and computing*. *World Scientific*, 2009.

[173] J. Cai, R. A. Cottis, and S. B. Lyon, 1999, "Phenomenological modelling of atmospheric corrosion using an artificial neural network.," *Corrosion Science*. vol. 41, no. 10, pp. 2001–2030.

[174] S. P. Trasatti and F. Mazza, 1996, "Crevice corrosion: a neural network approach.," *British Corrosion Journal*. vol. 31, no. 2, pp. 105–112.

[175] E. M. Rosen and D. C. Silverman, 1992, "Corrosion prediction from polarization scans using an artificial neural network integrated with an expert system.," *Corrosion*. vol. 48, no. 9, pp. 734–745.

[176] H. M. G. Smets and W. F. L. Bogaerts, 1992, “SCC analysis of austenitic stainless steels in chloride-bearing water by neural network techniques.,” *Corrosion*. vol. 48, no. 8, pp. 618–623.

[177] K. L. Priddy and P. E. Keller, *Artificial neural networks: an introduction*. *SPIE press*, 2005.

[178] S. I. Gallant and S. I. Gallant, *Neural network learning and expert systems*. *MIT press*, 1993.

[179] A. K. Jain, J. Mao, and K. M. Mohiuddin, 1996, “Artificial neural networks: A tutorial.,” *Computer*. vol. 29, no. 3, pp. 31–44.

[180] X. Glorot, A. Bordes, and Y. Bengio, “Deep sparse rectifier neural networks.,” In: *Proceedings of the fourteenth international conference on artificial intelligence and statistics*. pp. 315–323 (2011).

[181] I. J. Goodfellow, D. Warde-Farley, M. Mirza, A. Courville, and Y. Bengio, 2013, “Maxout networks.,” *arXiv preprint arXiv:1302.4389*. p.

[182] C. J. P. Spruit and J. N. Wanklyn, 1951, “Iron/sulphide ratios in corrosion by sulphate-reducing bacteria.,” *Nature*. vol. 168, no. 4283, p. 951.

[183] D. Xu, Y. Li, F. Song, and T. Gu, 2013, “Laboratory investigation of microbiologically influenced corrosion of C1018 carbon steel by nitrate reducing bacterium Bacillus licheniformis.,” *Corrosion Science*. vol. 77, pp. 385–390.

[184] B. K. Chastain and T. A. Kral, 2010, “Zero-valent iron on Mars: An alternative energy source for methanogens.,” *Icarus*. vol. 208, no. 1, pp. 198–201.

[185] J. L. Ginner, P. J. J. Alvarez, S. L. Smith, and M. M. Scherer, 2004, “Nitrate and nitrite reduction by Fe0: influence of mass transport, temperature, and denitrifying microbes.,” *Environmental engineering science*. vol. 21, no. 2, pp. 219–229.

[186] S. Biswas and P. Bose, 2005, “Zero-valent iron-assisted autotrophic denitrification.,” *Journal of Environmental Engineering*. vol. 131, no. 8, pp. 1212–1220.

[187] Z. He and L. T. Angenent, 2006, “Application of bacterial biocathodes in microbial fuel cells.,” *Electroanalysis: An International Journal Devoted to Fundamental and Practical Aspects of Electroanalysis*. vol. 18, no. 19-20, pp. 2009–2015.